

Summer 2024

Adopt: An Environmentally-Friendly System for Alerting Drivers to Occluded Pedestrians Traffic

Abrar Abdulrahman Alali
Old Dominion University, ab.alali@hotmail.com

Follow this and additional works at: https://digitalcommons.odu.edu/computerscience_etds



Part of the [Computer Sciences Commons](#), [Environmental Engineering Commons](#), [Transportation Commons](#), and the [Transportation Engineering Commons](#)

Recommended Citation

Alali, Abrar A.. "Adopt: An Environmentally-Friendly System for Alerting Drivers to Occluded Pedestrians Traffic" (2024). Doctor of Philosophy (PhD), Dissertation, Computer Science, Old Dominion University, DOI: 10.25777/4wnq-ha20
https://digitalcommons.odu.edu/computerscience_etds/177

This Dissertation is brought to you for free and open access by the Computer Science at ODU Digital Commons. It has been accepted for inclusion in Computer Science Theses & Dissertations by an authorized administrator of ODU Digital Commons. For more information, please contact digitalcommons@odu.edu.

**ADOPT: AN ENVIRONMENTALLY-FRIENDLY SYSTEM FOR ALERTING DRIVERS
TO OCCLUDED PEDESTRIANS TRAFFIC**

by

Abrar Abdulrahman Alali
B.S. May 2006, Taibah University, Saudi Arabia
M.S. May 2013, California Lutheran University

A Dissertation Submitted to the Faculty of
Old Dominion University in Partial Fulfillment of the
Requirements for the Degree of

DOCTOR OF PHILOSOPHY

COMPUTER SCIENCE

OLD DOMINION UNIVERSITY

August 2024

Approved by:

Stephan Olariu (Director)

Ravi Mukkamala (Member)

Michele C. Weigle (Member)

Shubham Jain (Member)

ABSTRACT

ADOPT: AN ENVIRONMENTALLY-FRIENDLY SYSTEM FOR ALERTING DRIVERS TO OCCLUDED PEDESTRIANS TRAFFIC

Abrar Abdulrahman Alali
Old Dominion University, 2024
Director: Dr. Stephan Olariu

The emergence of sensing technologies and vehicular communications has brought significant opportunities for enhancing pedestrian safety on city streets. However, existing solutions rely on costly technologies such as computer vision and trajectory prediction to detect crossing pedestrians, while they have limits in detecting pedestrians who are occluded by parked cars. Despite the presence of collaborative perception by surrounding vehicles and infrastructure, there is a notable absence of incorporating existing parked cars themselves due to their insufficiency in detecting pedestrians and communicating with other cars while they are turned off. Furthermore, accommodating pedestrians on streets has been linked to an additional cost to the environment. This cost is due to the fluctuations in the speed of the car to avoid collisions with pedestrians, which increases fuel consumption and CO₂.

We first propose to enlist the help of cars parked along the sidewalk to detect and protect crossing pedestrians. In support of this goal, we propose ADOPT: an Environmentally-friendly system for Alerting Drivers to Occluded Pedestrian Traffic. ADOPT lays the theoretical foundations of a system to use parked cars to detect and protect occluded pedestrians. We cope with the resource constraints in parked cars by utilizing short-range and low-power radio frequency sensors to detect pedestrians who also transmit radio signals from energy-harvesting wearables.

To estimate fuel consumption and CO₂ of cars, we found that the existing estimating ap-

proaches for user-specific requirements are not suitable for our goal. We overcome this limitation by using a simple version of the energy demand model knowing the most suitable powertrain efficiency. Thus, in this dissertation, we evaluate the vehicle energy demand model by testing several powertrain efficiencies. This allows us to accomplish our next task in this dissertation.

Next, we propose speed reduction schemes based on studying possible scenarios for midblock crossing. In these scenarios, the approaching car receives, in advance, caution messages about crossing pedestrians from ADOPT system. We show that these schemes reduce the fuel consumption and CO₂ emissions of approaching cars. With this, we show how ADOPT is an environmentally friendly system without compromising the safety of midblock pedestrians by utilizing parked cars along the street.

Copyright, 2024, by Abrar Abdulrahman Alali, All Rights Reserved.

To my parents, for their sacrifices, generosity and prayers, which have been the primary reason, after Allah, for my achievements today. Thank you for everything I have now because of both of you.

To my husband, Meshari Aljohani, who has been my rock and stood by me through every moment, despite being busy with his own PhD thesis. His unwavering support and presence have been constant sources of strength and encouragement. Thank you for your endless patience and for always being there for me.

To my sons, Mohamed and Abdulrahman, for their help to both me and their father. Their dedication to their studies and their excellence have been sources of pride and motivation for us. Thank you, my dear sons, for your hard work and for being such an inspiration. And to my lovely twins, Ziad and Moath, for the joy and happiness they brought into my life during this journey. Your laughter and energy have been a constant source of light and have made this experience all the more special. Thank you for filling my days with smiles and love.

To my sisters, for sharing in both my worries and my joys. Thank you for being there for me through thick and thin. And to my brothers, for their support and constant encouragement. Thank you for always standing by my side and for your endless motivation.

To everyone who prayed for me and wished me luck along the way, thank you all.

ACKNOWLEDGMENTS

All praise and thanks are due to Allah, who provided me with the strength, patience, and perseverance to complete this dissertation.

Then, I would like to thank my academic supervisor, Dr. Stephan Olariu, whose unwavering support and abundant knowledge have been instrumental in completing this dissertation. His mentorship not only improved my academic skills but also enriched my personal growth. I consider myself incredibly fortunate to have had the opportunity to be under the supervision of such a distinguished scholar.

Furthermore, I am deeply appreciative of the invaluable contributions from the esteemed members of my committee, Dr. Ravi Mukkamala, Dr. Michele Weigle, and Dr. Shubham Jain. Their insightful and thoughtful feedback provided me with valuable ideas on how to improve my work and enhance the quality of my dissertation. Their dedication and commitment to excellence have been sources of great inspiration for me.

I would like to express my special thanks to Dr. Shubham Jain for her invaluable support at the beginning of my research. Her guidance and expertise have been instrumental in my learning process, and I gained a valuable experience from the opportunities she offered to me.

I would also like to specifically thank Dr. Michele Weigle for her detailed comments and comprehensive feedback on my dissertation, which were particularly beneficial to refine my work.

Finally, I would like to thank the Saudi Electronic University for granting me this scholarship to complete my graduate studies and for generously funding my research.

TABLE OF CONTENTS

	Page
LIST OF TABLES.....	ix
LIST OF FIGURES	x
 Chapter	
1. INTRODUCTION	1
1.1 MOTIVATION	1
1.2 PROBLEM.....	2
1.3 TECHNICAL BACKGROUND	8
1.4 RESEARCH QUESTIONS	17
1.5 CONTRIBUTIONS.....	18
1.6 THESIS ORGANIZATION.....	19
 2. RELATED WORK.....	 21
2.1 PEDESTRIAN DETECTION SYSTEMS	21
2.2 ESTIMATING FUEL CONSUMPTION AND CO ₂	25
2.3 REDUCING FUEL CONSUMPTION AND EMISSIONS USING VANET	27
2.4 SUMMARY	28
 3. ADOPT: ALERTING DRIVERS TO OCCLUDED PEDESTRIAN TRAFFIC.....	 30
3.1 SYSTEM ASSUMPTIONS	30
3.2 PEDESTRIAN CLASSIFICATION AND LOCALIZATION	34
3.3 ESTIMATING THE TIME TO CROSS	41
3.4 SAFETY ZONE AND MESSAGE PROPAGATION	44
3.5 HOW APPROACHING CARS DETERMINE A SAFE SPEED.....	47
3.6 SIMULATION	50
3.7 EVALUATION.....	57
3.8 CONCLUDING REMARKS.....	82
 4. EVALUATING THE ENERGY DEMAND MODEL FOR ESTIMATING FUEL CON- SUMPTION AND CO ₂ EMISSIONS.....	 87
4.1 METHODOLOGY.....	87
4.2 RESULTS AND ANALYSIS.....	96
4.3 CONCLUDING REMARKS.....	114
 5. REDUCING THE ENVIRONMENTAL IMPACT OF CROSSING PEDESTRIANS	 115
5.1 FUEL CONSUMPTION AND EMISSION ESTIMATION MODEL	115
5.2 THE ALERT SYSTEM MODEL	116
5.3 SPEED REDUCTION SCHEMES	118
5.4 SIMULATION AND RESULTS	125

	Page
5.5 CONCLUDING REMARKS.....	132
6. CONCLUSION.....	133
6.1 CONTRIBUTION	135
6.2 LIMITATIONS AND FUTURE WORK	136
REFERENCES	138
APPENDICES	
A. TIME-SPACE DIAGRAM OF A CROSSING COHORT	156
B. EPA TEST CAR DATA	158
VITA	159

LIST OF TABLES

Table	Page
1. Power consumption of sensors and CPU used in autonomous cars	14
2. Examples of low-power and short-range RF Sensors.....	15
3. A summary of simulation parameters	52
4. Overall Accuracy of Pedestrian Classification (Noise-Free Mode)	58
5. Overall Accuracy of Pedestrian Classification (Noisy Mode)	59
6. Overall RMSE of ADOPT Estimations	61
7. Specifications and calculated ratios for Device A and Device B.....	82
8. Driving cycles details.....	93
9. Car specifications as obtained from EPA test car data (with unit conversion).	95
10. Estimated η for the selected cars.	98
11. $RMSE_{Fuel}$ [gal/sec] for the selected cars.....	100
12. $RMSE_{CO_2}$ [grams/sec] for the selected cars.	102
13. RSE_{Fuel} [gal/mile] of the selected cars.	105
14. RSE_{CO_2} [grams/mile] of the selected cars.....	106
15. Comparisons of car specifications used in this study and in [13].	109
16. Speed statistics and duration of driving modes in the evaluated scenarios	130
16. Speed statistics and duration of driving modes in the evaluated scenarios (Continued).....	131
17. List of used fields from EPA test car aggregated data and their usage.....	158

LIST OF FIGURES

Figure	Page
1. Illustrating the time-space diagram	16
2. Examples of ambient energy that can be harvested to operate car's sensors	32
3. Illustrating ADOPT	33
4. Illustrating the proof of Lemma 3.2.1.	36
5. Illustrating the notation for the proof of Lemma 3.2.3.	39
6. Message propagation by parked cars	46
7. Delivering the caution message if a gap exist in the chain	47
8. Illustrating the computation of the safe average speed in the case of two crossing cohorts. .	48
9. An instance of the ADOPT simulation model.	51
10. Absolute error of estimated distances.....	55
11. Effect of noise on $c(\Gamma)$	56
12. Aggregated classification accuracy.....	62
13. Detailed classification accuracy based on $c(\Gamma)$ and $c(\Gamma)'$	63
14. Detailed classification accuracy.....	64
15. FPPL and FNPL in horizontal locations	65
16. The effect of simultaneous transmission by pedestrians on the classification accuracy.	66
17. Distribution of localization error against the actual location.....	67
18. Distribution of localization error against the actual location.....	69
19. ECDF of remaining crossing time.....	71
20. ECDF of propagation distance	73
21. Correlation between the estimation error of D and Δ	75
22. Approaching cars maintained safe speeds.	77

Figure	Page
23. Moving vehicle reduces its speed upon receiving "Caution" message.....	79
24. The expected number of missing pedestrians per second.	80
25. The expected number of detected pedestrians versus several sampling rates	81
26. The average processing time for different ADOPT calculations.	83
27. Methodology overview.....	92
28. Speed profile for the driving cycles used.	94
29. Instantaneous fuel consumption for CAMRY XLE/XSE.	99
30. Instantaneous CO ₂ emissions for TOYOTA CAMRY XLE/XSE.	101
31. Total fuel consumption and CO ₂ for selected cars.....	104
32. RSS_{Fuel} and RSS_{CO_2} for all cars under various values of η	107
33. Results of applying the energy demand model on EUDC driving cycle.	110
34. Sensitivity analysis of RSS_{Fuel} against used parameters.	111
35. Sensitivity analysis of RSS_{Fuel} against used parameters from EPA aggregated data.	113
36. A generic alert system model.	117
37. Trajectory of a car receiving one alert message about midblock crossing	119
38. Trajectory of a car receiving two alert messages about midblock crossing.....	119
39. Evaluated scenarios of vehicle trajectory when receiving three alert messages.	122
40. The increase of fuel consumed for all the trajectories.	126
41. The increase of emitted CO ₂ for all the trajectories.	127
42. The reduction of fuel consumed for all the trajectories.....	128
43. The reduction of emitted CO ₂	128
44. Illustrating the time-space diagram of a crossing pedestrian.....	156

CHAPTER 1

INTRODUCTION

1.1 MOTIVATION

The current trends in pedestrian fatalities in the United States show that the number of pedestrians killed by U.S. drivers has remained high over the past few years, as reported by the Governor Highway Safety Association [23]. A closer look into the location of these fatalities shows that 75% of these fatalities occur at non-intersectional or midblock locations [50]. These statistics motivate us to look into the aspects that are related to pedestrian safety at midblock. At midblock, parked cars create a visual obstruction, impeding the driver's view of pedestrians attempting to cross. This is a well known issue in pedestrians safety research. Recent studies [19], [106] concluded that one of the main causes of crashes involving pedestrians is occlusion: the driver is unaware of the presence of pedestrians because some objects partially or fully occlude them. The issue continues to endure during the advancement of Autonomous Vehicles (AVs) [99] when the on-board sensors fail to detect pedestrians because of occlusion. Therefore, detecting occluded pedestrians reliably and in a timely manner is key to promoting pedestrian safety [48].

The second problem related to the midblock crossing, is the additional environmental cost that is elevated because of accommodating pedestrians at midblock. A study in [41] showed that the fuel consumption of a car increased incrementally as the number of pedestrians increased. Consequently, the CO₂ emission was also increased in streets. This increase has been linked to the change in the car's speed to avoid collisions with pedestrians. In fact, the continuous change

of driving modes (i.e., cruising, acceleration, and deceleration) increases fuel consumption and pollution, which is measured by elevated CO₂ levels in the environment.

1.2 PROBLEM

In this section, we introduce the research problems that we intend to tackle in this dissertation. We first discuss the problems related to the safety of occluded pedestrians in Section 1.2.1. Next, as we are interested in solving the problem of the increase of the environmental impact of accommodating crossing pedestrians, we discuss the problem of the current methods to estimate fuel consumption and CO₂ in Section 1.2.2. Then, we discuss the problem of reducing the environmental impact of accommodating midblock crossing pedestrians in Section 1.2.3.

1.2.1 Occluded Pedestrian Detection

The emergence of sensing technologies and wireless communication capabilities is being leveraged to increase pedestrian safety. Modern cars are equipped with on-board sensors such as cameras, laser devices, and Light Detection and Ranging (LiDAR) are part of the arsenal of local sensors employed to detect pedestrians [22]. One common characteristic of these sensors is that they require a clear Line-of-Sight (LoS) to be able to detect pedestrians [52]. Because of this, occluded pedestrians are not detected when some objects block the line of sight of these sensors [111]. In addition, weather and lighting conditions (e.g., glinting sun or other reduced visibility conditions) are apt to thwart the ability of on-board sensors to detect pedestrians [15], [82].

To overcome the limitations of local LoS sensors, wireless communications and collaborative perception have been leveraged to increase road safety. Wireless communications have enabled Vehicles-to-Pedestrians (V2P) communications [72] where drivers are alerted to the presence of

pedestrians by sending safety messages from their hand-held devices (usually smartphones) to an On-Board Unit (OBU) in the vehicle or to the driver's smartphone. However, V2P involves several challenges in order to work effectively. One challenge is the lack of an effective direct communication channel between pedestrians and cars. WiFi is a communication channel that was utilized, but it has its own constraints that limit its usage in the fast mobility of cars [36]. Similarly, Zigbee and Bluetooth have scalability issues in terms of the number of paired devices [45]. Dedicated Short Range Communication (DSRC) is prominent in Vehicle-to-Everything (V2X) communications, but pedestrians' smartphones are not equipped with it yet. Several researchers proposed the use of cellular V2X (C-V2X) to enable the communications of cars and pedestrians. This approach is feasible, but the expenses of using it are high, and there are privacy issues that remain unsolved for the pedestrian side [104]. Furthermore, the major limitation in the pedestrian side is the potential high power consumption of the pedestrian devices [66]. Not to mention the inaccurate localization of GPS, which is still within a few meters [97] which is critical for crossing pedestrians. In addition, smartphone privacy and security may be violated since these communications require accessing sensitive information such as the Media Access Control (MAC) address in order to route messages, and it can be used by attackers.

Another promising approach to tackle the occlusion issue is adopting the *Collaborative Perception* to share detection information of the surrounding pedestrians among moving vehicles and/or Roads-Side Units (RSU)[72]. Collaborative perception is enabled among vehicles through Vehicle-to-Vehicle (V2V) communications, where a moving vehicle that has a LoS connection to a group of pedestrians alerts neighboring vehicles. Sharing information among moving cars about surrounding pedestrians [81] overcomes the occlusion that is caused by other moving cars. However, the problem remains in the case of occlusion that is caused by parked cars. Alternatively, a number

of researchers have suggested supplementing the data collected by local LoS sensors with information collected by pre-deployed roadside infrastructure [24] through Vehicle-to-Infrastructure (V2I) communications. This approach is done by installing sensors, cameras, and communication units on existing roadside infrastructure, such as light poles, or by installing them on additional infrastructure, such as RSU to detect pedestrians and alert approaching cars [113]. Although this approach improves the detection of occluded pedestrians, it focuses on signalized intersections, while most pedestrian accidents tend to occur midblock [42], [87], [108]. Moreover, this approach is problematic since roadside infrastructure may not be available at midblock [15]. While collaborative perception mitigates the LoS challenge, it has serious scalability problems since it mostly relies on DSRC to disseminate the alert messages. Indeed, reporting pedestrians within a large radio coverage area tends to be unreliable due to known impairments of radio transmission, various forms of interference, message propagation delays, and security concerns [68].

In business and residential areas, the coexistence of parked cars and pedestrians is inevitable. However, the current approaches of addressing pedestrian occlusion because of parked cars along streets have neglected the role of parked cars themselves. The existence of parked cars could be taken positively by utilizing them as alternative infrastructure units to detect midblock crossing pedestrians. Several researchers have recognized the potential of using parked vehicles as an alternative road-side infrastructure in support of sensing and networking. For example, parked cars can be used as relaying nodes in the network to retransmit the received messages to the incoming cars to enhance the connectivity in VANET [18], [76].

In this dissertation, we enlist parked cars to detect pedestrians and alert approaching cars, thereby avoiding collisions. We consider the low-power constraints of parked cars in which they are not operated, and they can consume a small amount of their batteries to operate low-power devices

in the car, such as the clock and the alarm. In addition, our system uses sensing technologies that can cope with the constraints of pedestrian devices in terms of power usage and privacy. Also, our system utilizes an accurate localization approach to accurately determine whether pedestrians are crossing or walking along the sidewalk. Moreover, our sensing service provides messages that are informative and accurate to the AVs or the drivers. Information such as the location and the time of crossing is provided while preserving the privacy of pedestrians.

1.2.2 Estimating Fuel Consumption and CO₂

Researchers involved in the study of the environmental impact of transportation often need to estimate instantaneous fuel consumption and CO₂ emissions, given driving cycles¹ and the car specifications of interest. To accomplish this, several approaches may be contemplated.

One natural approach is to conduct real-world experiments to record measured fuel consumption and emissions using specialized equipment [37]. The collected data can then be used to develop statistical models (i.e., data-driven models), such as linear regression models, to predict fuel consumption and emissions for user-defined driving cycles and car-specific characteristics. This approach is challenging to apply because real-world experiments are expensive to carry out and require specialized equipment to measure fuel and emissions. Alternatively, researchers can use the data-driven models that are developed based on the data collected in the field by applying them either directly (with the required model calibrations) [67] or by utilizing simulation tools that embed them to predict fuel and emissions in simulation environments. This approach has its shortcomings: (1) Choosing a suitable data-driven model can be challenging due to differences between the conditions under which the models were developed and the user-defined cycles they are aiming

¹That is, the data points represent the speed of a driven vehicle over time for a typical driving pattern) [2]

to study; and, (2) Data-driven models derived from real-world experiments contain constant coefficients that may be hard to understand by users [117].

On the other hand, fuel consumption and emissions can be estimated using physics-based models [26], [35]. To predict the energy needed by a car to complete a given driving cycle, these models use speed profiles and car specifications as input parameters. This allows the model to be generalized to various driving patterns and car models. Moreover, physics-based models provide an intuitive way to understand the relationships between inputs and outputs, making the model understandable to researchers. However, the complexity of these models may vary depending on the input parameters. Considering more related inputs might increase the accuracy of the estimations, while considering fewer inputs might decrease it [3]. These types of models can be applied using specific software such as MOtor Vehicle Emission Simulator (MOVES) [96]. However, this software cannot be used to obtain real-time data during driving when needed, such as in fuel optimization algorithms. Therefore, researchers need a simple fuel consumption model that considers available data as parameters and produces accurate and explainable results in real time.

One of the simplest physics-based models used directly to estimate fuel consumption is the *energy demand* model that was used in [13], [26], [35]. The energy demand model utilizes variable parameters determined by the speed profile and the specifications of the vehicle. The EPA provides car test datasets that contain these specifications [91]. This, in turn, makes the car specifications that were used for official car tests available to be used in the model. Additionally, the efficiency of a car to convert fuel to mechanical energy can be determined using the measurements of the fuel expended and the estimated power demand [35], [88]. This efficiency value can be used to estimate fuel consumption accurately if the correct powertrain efficiency is known. One of the advantages of this model is that it can capture the instantaneous changes in fuel consumption based on the car

dynamics, determined using the speed profile and the specifications of the car. The output of this model can be easily explained and understood by researchers. Although the energy demand model offers a simple way to estimate fuel consumption for any driving cycle, at the moment there is a lack of studies that assess the quality of the estimates it produces using publicly available data.

In this dissertation, we evaluate the fuel consumption and CO₂ emission estimates produced by the energy demand model and compare them to official measurements published by the EPA. Then, we demonstrate the ability of the energy demand model to be generalized to various driving cycles, including user-defined driving cycles and a variety of car models.

1.2.3 Reducing the Impacts of Midblock Crossing Pedestrians

Recent statistics revealed that midblock crossing, including jaywalking, is a ubiquitous societal phenomenon that is here to stay [32], [87]. Further studies have confirmed that accommodating pedestrians who cross midblock increases fuel consumption, CO₂ emissions, and the average trip time [9], [41], [64]. In order to avoid crashing into pedestrians crossing midblock, cars must reduce their speed and then accelerate to resume their cruising speed. Unfortunately, these avoidance maneuvers significantly increase fuel consumption and emissions [75].

The common approach taken by researchers to contain the increase in fuel consumption due to promoting pedestrian safety at controlled intersections involves using vehicular communications, such as V2I communications (e.g., intersection management system) and/or V2V communications [6], [47], [98], [101].

If pedestrians are detected at intersections managed by traffic systems, the approaching cars react according to the scheduling scheme sent by the traffic management system. However, pedestrians who cross midblock can be detected using on-board pedestrian detection systems [60] or

by collaborative perception from surrounding cars and/or infrastructure [4], [53], [109]. Virtually all studies on reducing the environmental impact of promoting road safety have focused on communication between intersection management systems and vehicles to optimize fuel consumption. However, as previously mentioned, cars can now receive alerts about midblock crossings. Therefore, it is necessary to develop methods to efficiently reduce the speed based on the received alert messages while considering the environmental impact.

In this dissertation, we fill this research gap by providing schemes for adjusting the speed of the car after receiving midblock crossing alerts, considering the environmental impacts. While the environmental impacts of midblock crossing have been explored, there is a glaring lack of effort to reduce these impacts. We propose two schemes for maintaining a safe speed to avoid collisions with pedestrians crossing at several different locations, without the need for the cars to stop. The first scheme is to immediately reduce the speed to a safe speed that minimizes fuel consumption and reduces emissions. The second scheme is to defer the deceleration if the car is already responding to a previous alert until it reaches the crossing area. Our simulation results show that the timely dissemination of pedestrian crossing information to approaching cars can reduce fuel consumption and emissions by up to 16.7%.

1.3 TECHNICAL BACKGROUND

1.3.1 Energy Harvesting Wearables

Body-energy harvesting devices represent a paradigm shift in wearable technologies. These intelligent clothing and accessories replaced traditional battery-powered electronics by exploiting human motion and thermal energy as alternative energy sources. These wearables transform ki-

netic energy from footsteps, friction-induced charges from fabric contacts, and internal body heat into usable power by integrating piezoelectric, triboelectric, or thermoelectric components. This technique enables a wide range of applications, such as motion detection, health monitoring and remote health diagnostics in resource-constrained environments [118]. Recent studies have explored the use of piezoelectric elements to provide power to communication modules. [30] developed a shoe module that can communicate with a smartphone held by the user. Their work showed that the power produced by a single shoe is sufficient to transmit data from a Bluetooth module to a hand-held smartphone. Such a module can be used to enable pedestrians to generate signals to be received by nearby receivers that operate on the same frequency. Most importantly, they can transmit signals while harvesting power from their own motion rather than from external batteries.

Similarly, ambient energy, such as solar energy and radio frequency energy, has been harvested to power wearables. For example, [34] designed a wristband to harvest solar energy. A single flexible solar panel in their design can harvest up to 16 mW of power in outdoor environment. Similarly, [58] designed a wristband prototype consisting of a solar energy harvester and a Bluetooth Low Energy (BLE) module with a battery to conserve the harvested energy. Both solar and RF harvested energy were also combined to power wearable devices. [105] designed a hybrid RF-solar system to power wearable electronic devices.

1.3.2 RSS-Based Ranging

Received Signal Strength (RSS) ranging is commonly used approach in wireless localization due to its simplicity and energy efficiency in estimating distances between transmitters and receivers [107]. This approach depends on the fact that the power of a transmitted signal diminishes with distance when calculating the range between devices. RSS measures the power level received

by a radio receiver, and it can be obtained by the Free-space propagation model given by Equation.

1.3.2.

$$P_r = P_t \left(\frac{G_t G_r \lambda^2}{(4\pi d)^2} \right),$$

where²:

- P_r : Received power in mW,
- P_t : Transmitted power in mW,
- G_t : Gain of the transmitting antenna,
- G_r : Gain of the receiving antenna,
- λ : Wavelength of the signal,
- d : Distance between the transmitter and the receiver.

Because of its limited accuracy in long-range communication, RSS-based ranging is used mostly as a coarse-grain indicator. However, this approach achieves higher accuracy in short-range (within 1-5 meters) localization [80].

1.3.3 Controller Area Network (CAN Bus)

Controller Area Network (CAN) is an in-vehicle network employed in the automotive industry to facilitate real-time communication among various electronic control units within a vehicle. CAN enables high-speed and reliable communication, supporting multiple nodes on the same network. It is suitable for applications where timely and accurate data exchange is critical.

²The parameter names listed here may be re-defined in the other sections.

1.3.4 Vehicular Ad-Hoc Networks (VANET)

Vehicular Ad-hoc Network (VANET) is a special type of Mobile Ad-hoc Networks which enables modern cars to communicate directly with the surrounding infrastructure, vehicles and pedestrians to exchange traffic information [57]. These communications are categorized into three types: 1) Vehicle to Infrastructure (V2I) which enable the communication between the vehicle and surrounding lights such as traffic lights and road side units; 2) Vehicle-to-Vehicle (V2V) which enables the communication among vehicles; 3) Vehicle-to-Pedestrians which enables the vehicles to exchange traffic information with surrounding pedestrians and other vulnerable road users. These combined communications are described as Vehicle-to-Everything (V2X) in a broader term. These types of communications are enabled by equipping the modern cars with communication devices to send and receive information. There are two types of communication technologies that enable VANET: 1) Dedicated Short-Range Communications (DSRC), that is a wireless communication protocol designed for use by vehicles; 2) Cellular V2X (C-V2X) [77] in which the cellular networks are used to support wide range and reliable V2X communications.

1.3.5 Modern Cars On-Board Equipment for Pedestrian Detection

Modern cars are equipped with a variety of on-board sensors and devices that are used for pedestrian detection as part of advanced driver assistance systems (ADAS) and autonomous driving technologies. Here are some of the commonly used on-board sensors for pedestrian detection:

- **Camera Systems**

Cameras capture visual information to identify and analyze objects. They are crucial for pedestrian detection by recognizing shapes, patterns, and movements. They are often used

in conjunction with image processing algorithms.

- **Radar Sensors**

Radar sensors use radio waves to detect objects around the vehicle. It is effective in detecting pedestrians, especially in adverse weather conditions. It can provide information about the distance, speed, and direction of pedestrians.

- **Light Detection and Ranging (LiDAR)**

LiDAR sensors use laser beams to create a detailed 3D map of the surroundings. It is capable of providing precise information about the shape and position of objects, including pedestrians. It is effective in various lighting conditions.

- **Ultrasonic Sensors**

Ultrasonic sensors use sound waves to detect objects in close proximity. These sensors are often used for detecting obstacles, including pedestrians, at low speeds or during parking maneuvers.

- **Infrared Sensors**

Infrared sensors detect heat emitted by objects. They can be useful for pedestrian detection, especially in low-light conditions, by recognizing the heat emitted by human bodies.

- **Global Positioning System (GPS)**

GPS provides the vehicle's location and helps in understanding the context of the surroundings. While not directly used for pedestrian detection, GPS can complement other sensor data to enhance overall situational awareness.

- **On-Board Unit for V2X Communication**

Modern vehicles are also equipped with On-board Unit (OBU) to enable V2X communications. These types of communications are used in the collaborative perception approach to increase the situational awareness about pedestrians. Pedestrian information from V2X communication can be valuable for anticipating and reacting to pedestrians' presence.

The central processing unit (CPU) is crucial for processing data from various sensors to identify and track pedestrians in real-time. The CPU runs advanced algorithms to analyze sensor data, make decisions to avoid collisions, and ensure pedestrian safety. It integrates data from different subsystems, manages communication with other vehicles and infrastructure, and supports the vehicle's ability to anticipate and react to pedestrian movements.

Understanding the power requirements is crucial for assessing the energy efficiency and operational costs of these systems. Table 1 shows the power consumption for each sensor type as well as the central processing unit (CPU) [21].

1.3.6 Low-Power RF Sensors

Low-power Radio Frequency (RF) sensors are crucial components for applications requiring energy efficiency and short ranges operations. These sensors, are typically designed to consume minimal power, extending the battery life of electronic devices. Despite their limited range, often extending up to a few hundred meters in LOS cases, these sensors provide reliable and efficient data transmission, making them suitable for detecting and communicating with devices in the surrounding areas. Their compact size and low energy consumption make them highly effective for applications where both size and power constraints are important. In Table 2, we list examples of these sensors. The data in the table is derived from the manufacturer's websites [29], [55], [86].

Table 1. Power consumption of sensors and CPU used in autonomous cars

Device/Sensor	Model	Power Usage (W)
Camera	Pt. Gray Dragonfly2	2.1
Radar	Bosch LRR3	4
Sonar	Bosch Ultrasonic	0.13
Large LiDAR	Velodyne HDL-64E	60
Small LiDAR	Velodyne VLP-16	8
GPS/INS	NovAtel PwrPak7	2
CPU	Nvidia Drive PX2	96

1.3.7 Parked Cars in VANET

Parked cars have been used in VANET to relay safety message dissemination in areas with low traffic density. As an example, [43] proposed the idea of using parked cars as RSUs to improve VANET connectivity. Similarly, [18] showed that parked cars are useful to work as relay nodes in support of VANET communications. To increase road safety, [76] proposed that parked cars communicate with their moving counterparts as relay nodes to increase safety in low-density areas by multi-hopping the cooperative awareness messages. Due to the vast panoply of their on-board sensors, parked cars can also be used as a sensing resource to alternate additional road-side units. [1] showed that parked cars can be used as sensing resources, and the CAN bus, which is used to connect in-vehicle devices, can also be used to provide power to the sensors while the car is

Table 2. Examples of low-power and short-range RF Sensors

Sensor Model	Manufacturer	Approximate Price \$	Frequency Range (GHz)	Power Usage (mW)
NRF24L01+	Nordic Semiconductor	1.50 to 2.00	2.400 - 2.525	< 13
CC2500	Texas Instruments	4.00 to 6.00	2.400 - 2.4835	< 15
RFM75	HopeRF	1.50 to 2.50	2.400 - 2.4835	< 12

stopped. Alternatively, parked car sensors can be powered by harvesting ambient-energy such as solar and wind energy.

1.3.8 Harvesting Ambient Energy

Harvesting ambient-energy is the process of extracting naturally occurring energy from the environment and converting it into usable electrical energy. This technique uses a variety of sources, such as solar radiation, wind, temperature gradients, and motion. The generated energy is used to power small, low-energy devices such as sensors and wearable electronics. This reduces the dependency on traditional batteries and extends the operational life of these devices. Leveraging ambient energy sources supports the development of sustainable and self-sufficient systems.

1.3.9 Time-Space Diagram

One of the basic tools in the toolbox of traffic engineers is the *time-space diagram* that allows one to plot the trajectories of vehicles as curves in a Cartesian plane with axes labeled “time” and “space”. Referring to Figure 1, the vehicle’s coordinates at time t are (t, s) . The projection of this

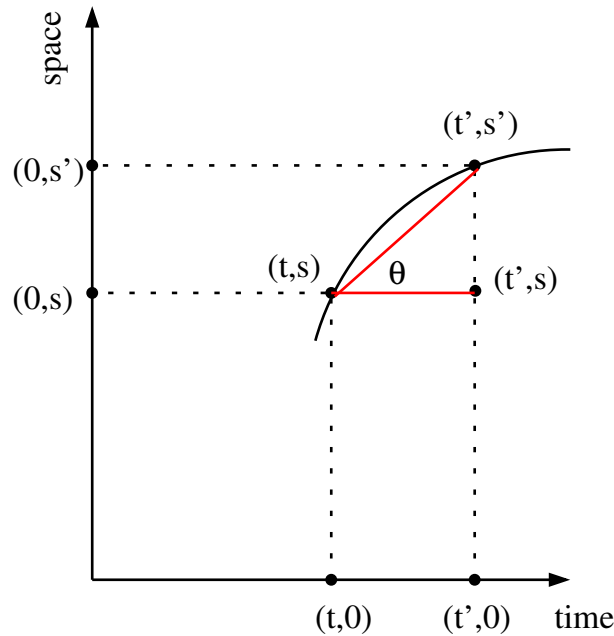


Figure 1. Illustrating the time-space diagram: The vehicle's coordinates at time t are (t, s) . The vehicle has continued moving along its trajectory in such a way that at time t' , ($t' > t$), its coordinates are (t', s') . In the time interval $[t, t']$, the vehicle has moved along the space axis from location $(0, s)$ to location $(0, s')$. The average speed is $\tan(\theta)$, where θ is the angle determined by the line segment connecting the points of coordinates (t, s) and (t', s') and the positive direction of the time axis.

point on the vertical axis, $(0, s)$, indicates the position, at time t , of a vehicle that moves along the space axis North-bound (i.e. from bottom to top).

Assume that the same vehicle has continued moving along its trajectory in such a way that at time t' , ($t' > t$), its coordinates in the time-space coordinate system are (t', s') . Equivalently, in the time interval $[t, t']$, the vehicle has moved along the space axis from location $(0, s)$ to location $(0, s')$.

One of the nice features of the time-space diagram is that it allows one to compute and to *visualize* the average speed of the vehicle. Indeed, referring again to Figure 1, elementary physics indicate that the average speed, v_{avg} , of the vehicle in the time interval $[t, t']$ is the ratio

$$v_{avg} = \frac{s' - s}{t' - t}. \quad (1)$$

This is the same as the *slope* of the line segment connecting the points of coordinates (t, s) and (t', s') . Equivalently, the average speed v_{avg} is $\tan(\theta)$, where θ is the angle determined by the line segment connecting the points of coordinates (t, s) and (t', s') and the positive direction of the time axis.

Finally, it is not hard to see that the *instantaneous speed* of the vehicle at an arbitrary time τ , ($t \leq \tau \leq t'$) turns out to be the slope of the tangent to the trajectory at time τ . In particular, if the trajectory happens to be a straight line, then the average speed matches the instantaneous speed, as expected.

1.4 RESEARCH QUESTIONS

We recognize the challenges and limitations of the existing driver's alert systems to occluded pedestrians and the fuel's cost of avoiding collisions with pedestrians. Thus, we aim to answer the main research question: Can we utilize parked cars to protect occluded pedestrians and reduce the environmental impact of accommodating pedestrians? In this dissertation, we split this question into three questions to organize this work. The three questions are as follows:

- **RQ1:** Can we utilize parked cars to protect occluded pedestrians and alert approaching cars?
- **RQ2:** Can we accurately estimate the instantaneous fuel consumption and CO₂ emissions using the energy demand model?

- **RQ3:** Can the alert messages about crossing pedestrians reduce the environmental impact of midblock crossing?

Each of these research questions will be tackled in a separate chapter in this dissertation.

1.5 CONTRIBUTIONS

We recognize the challenges that need to be overcome in order to achieve improved pedestrian safety while reducing fuel consumption and CO₂ emissions to avoid pedestrians. Ultimately, our work aims to build upon existing knowledge and make a contribution to fill the following research gaps: 1) Although parked cars are one of the major causes of pedestrian occlusion, they have not been leveraged to support occluded pedestrian detection; 2) Reducing fuel consumption due to midblock pedestrian accommodation has not been investigated in pedestrian safety systems; and 3) Researchers interested in environment and transportation need an accurate and straightforward model to estimate fuel consumption for their driving cycles and car specifications.

This dissertation contributes to improving the safety of occluded pedestrians and reducing the environmental impact of midblock crossing through the following key contributions:

1. Providing the theoretical foundations of a low-power and infrastructure-free occluded pedestrian detection system (Chapter 3);
2. Introducing a novel criterion for the *binary* classification of pedestrians as “on the sidewalk” or “in the street” (Chapter 3);
3. Offers a scheme for estimating the expected time it takes a crossing cohort to clear the street(Chapter 3);

4. Providing an algorithm that allows approaching cars to adjust their speed dynamically, given several simultaneous crossing locations (Chapter 3);
5. Estimating fuel consumption and CO₂ emissions for driving cycles resulting from adopting ADOPT suggested speed using more realistic parameters (Chapter 3);
6. Providing a scheme for cars to choose the speed that reduces the elevated fuel consumption and CO₂ emissions while avoiding colliding with pedestrians (Chapter 3);
7. Applying the energy demand model for fuel consumption estimation, including instantaneous and average speed for user-defined driving cycles;
8. Comparing the computed fuel consumption with real-world data from several driving cycles and evaluating the accuracy of the energy demand approach (Chapter 4);
9. Providing a simple approach for cross-disciplinary researchers to implement the model directly, given publicly available data related to car specifications (Chapter 4);
10. Providing schemes to reduce speed appropriately based on alert messages sent to approaching cars along the street about midblock crossing. The proposed scheme showed a reduction in fuel consumption and CO₂ compared to sudden stop (Chapter 5).

1.6 THESIS ORGANIZATION

The rest of this dissertation is organized as follows:

- Chapter 2: We present the related work;

- Chapter 3: We present our work *ADOPT*: a system for alerting drivers to occluded pedestrian traffic. This chapter is designated to answer the first research question **RQ1**.
- Chapter 4: We present our work to evaluate the energy demand model for estimating fuel consumption and CO₂ emissions. This chapter is designated to answer the second research question **RQ2**.
- Chapter 5: We present our work to reduce the environmental impact of midblock crossing pedestrians using the alert messages from *ADOPT*. This chapter is designated to answer the third research question **RQ3**.
- Chapter 6: We conclude our work in this dissertation by summarizing the main components of this dissertation, revisiting the key contributions and listing the possible future work.

CHAPTER 2

RELATED WORK

In this chapter, we review the literature on the three topics of this dissertation. In Section 2.1, we present the related work of pedestrian detection systems, including occluded pedestrians. Then, in Section 2.2, we offer a succinct review of relevant literature on estimating fuel consumption and emissions for various user-defined driving cycles and car models. Lastly, in Section 2.3, we review the related work on reducing fuel consumption and emissions using vehicular communications.

2.1 PEDESTRIAN DETECTION SYSTEMS

In this section, we focus on presenting the research related to detecting pedestrians in roads in order to alert drivers or autonomous vehicles. This has been done by utilizing 1) on-board system of the moving vehicle itself; 2) collaborative perception that is enabled through different types of vehicular communications; and 3) parked cars that have been used to detect a particular type of individuals.

2.1.1 Detecting Pedestrians Using On-Board Sensors

The literature on pedestrian detection by vehicle's local Line of Sight (LoS) on-board sensors, such as various camera technologies, LiDAR, and laser, is quite vast. LoS sensors can detect pedestrians directly if they fully appear in the view. Brehar, Muresan, Marița, Vancea, Negru, and Nedevschi [11], used an on-board infrared camera to detect pedestrians on the street. To overcome the camera's limitations in low-light conditions, De Nicolao, Ferrara, and Giacomini [16] fused

the laser sensor with the camera to detect pedestrians and calculate their speed. Similarly, Chen and Huang [14] fused thermal sensors with the stereo camera to detect pedestrians in low-visibility conditions.

If pedestrians are partially occluded, additional effort is needed to recognize them by an on-board camera utilizing deep learning and conventional networks [27], [61], [112], [116]. In addition, sensor fusion approaches have been leveraged to detect partially occluded pedestrians. Palffy, Kooij, and Gavrilă [59] used on-board thermal infrared sensors to detect pedestrians partially occluded by parked cars. Kwon, Hyun, Lee, Lee, and Son [39] suggested fusing on-board LiDAR and radar to detect partially occluded pedestrians. Recently, Palffy, Kooij, and Gavrilă [60] proposed an occlusion-aware fusion of stereo cameras and radar to detect partially occluded pedestrians earlier than using the camera alone for detection. While sophisticated LoS sensors can detect partially occluded pedestrians, fully occluded pedestrians cannot be detected using the same sensors. Furthermore, relying on LoS sensors for occluded pedestrian detection must involve extensive vision algorithms that may not perform the task in a timely manner.

2.1.2 Detecting Pedestrians Using Collaborative Perception

Collaborative perception in VANET is used in pedestrian safety systems when a moving car fails to detect pedestrians using its local LoS sensors and relies on remote sensors such as other cars' on-board cameras or street monitoring cameras to provide additional perception.

V2V Communications

Sun and Boukerche [81] proposed a collaborative system that shares the location of the pedestrians when they are detected by another car's camera. The detecting car exchanges pedestrian

location and speed with the blinded car that fails to detect low-visible pedestrians. Their system has the advantage of enabling collaboration between cars to prevent pedestrian/car collisions. Ngo, Fang, and Wang [51] addressed the issue of occlusion in autonomous vehicles by proposing a real-time collaborative vehicular communication method using a bird's-eye-view map, which contains depth information and allows efficient data transmission between autonomous vehicles.

V2V communications improve driver's awareness about surrounding pedestrians when they are blocked by another moving car. However, when pedestrians attempt to cross between two parked cars, all the moving cars may fail in detecting them.

V2I Communications

Several projects attempt to enhance pedestrian detection at intersections by installing cameras and ranging sensors on light poles or RSUs. Once pedestrians are detected, approaching vehicles are alerted to their presence. For example, Ben Khalifa, Alouani, Mahjoub, and Rivenq [10], Islam, Rahman, Chowdhury, Comert, Sood, and Apon [33], and Noh and Yeo [54] installed a camera in an RSU to detect pedestrians and alert approaching vehicles. Larson, Wyman, Hurwitz, Dorado, Quayle, and Shetler [40] and Zhao, Xu, Liu, Wu, Zheng, and Wu [115] suggested fusing the input from installed cameras with thermal and LiDAR sensors to detect pedestrians at day and night. In a lower cost mechanism, Pereira, Sampaio, Chaves, Correia, Luís, Sargento, Jordão, Almeida, Senna, Oliveira, *et al.* [63] installed piezoelectric elements at the beginning and end of crossing lines to detect pedestrians and alert approaching vehicles through RSUs.

The aforementioned approaches are expensive to deploy, and, municipalities usually do not have the resources to install them at all locations. In addition, they only cover controlled intersections, while many pedestrians are known to cross roads midblock. Additionally, the alert messages

are exchanged between RSU and approaching vehicles via DSRC which covers a large area, causing network load and impairments of radio transmissions, various forms of interference, message propagation delays, and security concerns.

V2P Communications

In order to mitigate the problem of occluded pedestrian detection with LoS sensors, Vehicle-to-Pedestrians (V2P) wireless communication was leveraged to detect the presence of pedestrians. WiFi, Zigbee, and Ultra-Wideband (UWB) were used in Dhondge, Song, Choi, and Park [17], Ho and Chen [28], Wang, Zhou, and Ding [102], and Zhang, Song, Jaiprakash, Talty, Alanazi, Alghafis, Biyabani, and Ozan Tonguz [110] for V2P communication and alerting either drivers or pedestrians about anticipated collisions. Tahmasbi-Sarvestani, Nourkhiz Mahjoub, Fallah, Moradi-Pari, and Abuchaar [83] have proposed a framework for V2P communications via DSRC units with the goal of alerting both the pedestrians and the vehicle to a possible collision. The fusion of the car's perception and V2P communications were leveraged by Merdrignac, Shagdar, and Nashashibi [49]. Their solution relies on recognizing the occlusion by a moving vehicle and sending an alert to both the approaching car and the pedestrian's device if detected via V2P communications. Shahriar, Kale, and Chang [73] considered pedestrian equipment battery limitations. The study established a practical method that effectively decreases collision rates by nearly 20% and conserves battery usage through reduced beaconing.

Although V2P communications enhance the safety of occluded pedestrians by improving the detection rate, their main drawback is that they are usually apt to drain the battery of the pedestrian's device if used for extended periods of time. Yet another drawback is that V2P communications rely on inaccurate GPS readings to determine the distance between the pedestrian and

approaching vehicles. Additionally, V2P communications do not scale well when multiple pedestrians are found in the street. In addition, most of the proposed methods rely on using cellular network communications that require additional costs to operate.

2.1.3 Detecting Pedestrians Using Parked Cars

Parked cars have been used for detecting individuals in need of special care who are at risk of becoming lost Griggs, Verago, Naoum-Sawaya, Ordóñez-Hurtado, Gilmore, and Shorten [25]. In this system, parked cars are instrumented with Radio-Frequency Identification (RFID) readers to detect tags attached to the person of interest. The detection information is then shared with administrative centers. Implementing RFID in parked cars to detect pedestrians has several drawbacks:

- Implementing RFID infrastructure, including readers, antennas, and tags, can be costly. The expenses associated with deploying and maintaining a large-scale RFID system might be a significant consideration.
- RFID systems can be vulnerable to security threats, such as unauthorized access and data interception.
- RFID technology raises privacy concerns as it involves tracking and identifying individuals.

2.2 ESTIMATING FUEL CONSUMPTION AND CO₂

Wang, Fu, Zhou, and Li [100] investigated fuel consumption for passenger cars for their user-defined driving cycle using a portable emissions measurement system (PEMS) to collect real-time data on driving parameters, fuel consumption rates, and emissions. The authors also used the vehicle specific power (VSP)-based model United States Environmental Protection Agency [96] to

validate their estimated fuel consumption. Their results showed that the model can predict fuel consumption to within 15% to 20% of the measured values. However, their model relies on using constant coefficients based on the specific data and conditions of the study. Applying them to different scenarios or vehicle models led to less accurate fuel consumption estimates. Chaim and Shmerling [13] utilized an energy-demand model that considers engine-specific parameters and the average speed of the driving cycle. The results of their estimation were reasonably accurate compared to the fuel consumption data they obtained from field test measurements. Engine-specific parameters determine powertrain loss and lead to an accurate estimate of fuel consumption. However, those parameters are not publicly available from official sources. Thus, it is challenging for researchers to adapt the model of Chaim and Shmerling [13] for their purposes. Weng, Liang, Qiao, Chen, and Rong [103] conducted a real-world experiment with four driving cycles (cruising, acceleration and deceleration, and composite) to obtain vehicle fuel consumption and emissions data using a vehicle emissions testing system. By analyzing the second-by-second data collected during the experiment, the authors developed a model to estimate taxi fuel consumption and emissions based on the reconstruction of driving trajectories using GPS data. Shaw, Hou, Zhong, Sun, Guan, and Su [74] conducted a field test to evaluate two fuel consumption models: the powertrain-based model and the vehicle dynamics-based model. The powertrain-based model estimates fuel consumption based on the engine's fuel injection rate, while the vehicle dynamics-based model (i.e., physics-based model) considers the mechanical work applied to the vehicle. The constant coefficients of the models were determined during model calibration using the measured data collected in the field test.

Perugu [65] estimated the emissions of light-duty vehicles in Hyderabad, India, using the default emission rates from MOVES model. The model incorporated parameters such as local mete-

orological conditions, vehicle age, and fuel data to generate base emission rates and deterioration factors for older vehicles. They used VSP model in emission rate calculations. VSP is one of the parameters that is used as input in MOVES lookup tables. In order to obtain the corresponding rate for the VSP, MOVES lookup tables need to be accessed, which makes the application of this method to real-time applications awkward, if not impossible.

Other researchers interested in studying the environmental impacts of intelligent transportation systems have used several models to estimate fuel consumption and emissions. For example, Alsabaan, Naik, and Khalifa [6] and Lu, Xu, Ding, and Lu [47] used the Virginia Tech Microscopic (VT-Micro) model to estimate instantaneous fuel consumption and emissions for the vehicle. The VT-Micro model was developed based on testing data collected at Oak Ridge National Laboratory and the U.S. EPA, incorporating fuel consumption and emission rate measurements as functions of vehicle speed and acceleration levels. The model was applied to a user-defined driving cycle using constant coefficients established by the regression model. This model uses instantaneous speed, acceleration and several regression coefficients.

More recently, Wang, Wen, and Chao [101] used the SUMO simulator to measure fuel consumption as part of their evaluation of their autonomous intersection management system. SUMO also uses a data-driven model with several constant coefficients that must be adjusted for use with different cars.

2.3 REDUCING FUEL CONSUMPTION AND EMISSIONS USING VANET

The transportation sector has been a major contributor to air pollution [95]. Therefore, a number of researchers have utilized information exchanged through vehicular networks to reduce the environmental impact of transportation systems.

Alsabaan, Naik, and Khalifa [6] introduced a comprehensive optimization model involving both V2V and traffic-light-signal-to-vehicle (TLS2V) communications. Through V2V and V2I communications, cars approaching a traffic light signal receive information to adjust their speed to a recommended value, aiming to minimize fuel consumption and emissions.

Similarly, Wan, Vahidi, and Luckow [98] proposed a speed advisory system for connected vehicles to enhance fuel efficiency and comfort by managing speed in advance based on upcoming traffic signal information.

Furthermore, Lu, Xu, Ding, and Lu [47] introduced advanced speed control at successive signalized intersections to mitigate fuel consumption and emissions, leveraging V2I and V2V technologies. Car speed was optimized by utilizing real-time traffic signal phasing, timing information, and vehicle queue data. The method notably reduced fuel consumption and CO₂ emissions by over 18%.

In addition, pedestrians who cross intersections were accommodated in a traffic management system proposed by Wang, Wen, and Chao [101]. They introduced Roadrunner+, a cooperative autonomous intersection management system designed for connected autonomous vehicles. This work addressed the challenges posed by pedestrian crossings at intersections and scheduled traffic, which resulted in efficiently reducing fuel consumption by up to 7.64%.

The aforementioned efforts focused in reducing the environmental impact of regulating traffic at intersections. Although the environmental impact of midblock crossing has been identified in many studies, there is a lack of proposed approaches to reduce this effect using vehicular networks.

2.4 SUMMARY

In this section, we provided an overview of the research related to detecting occluded pedes-

trians. From this overview, we conclude that detecting pedestrians who are occluded by parked cars along a street remains a challenging problem. After that, we showed the research related to estimating fuel consumption and emissions. This review showed that there is a lack of evaluation studies that assess the ability of the simple physics-based power demand model to estimate the instantaneous fuel consumption and CO₂ emissions. Finally, we presented an overview of the research related to reducing the environmental impact of transportation using vehicular networks. This overview showed that although the increase of the environmental impact due to midblock crossing has been identified, this issue has been overlooked by researchers in the domain of vehicular communications.

CHAPTER 3

ADOPT: ALERTING DRIVERS TO OCCLUDED PEDESTRIAN TRAFFIC

In this chapter, we aim to answer our first research question **RQ1**: Can we utilize parked cars to protect occluded pedestrians and alert approaching cars?.

This chapter presents our work that was previously published by [4]. The structure of this chapter is as follows: Section 3.1 establishes terminology and discusses system assumptions. A detailed discussion of how ADOPT works can be found in Sections 3.2–3.5. Specifically, Section 3.2 offers the details of pedestrian classification and localization. Section 3.3 offers the details of the way ADOPT estimates the time it takes a cohort to cross the street. Next, Section 3.4 discusses the details of propagating the alert message to the approaching cars. In Section 3.5 we present an algorithm that can be used by approaching cars to adjust their speed as a result of receiving information about one or several crossing cohorts. The empirical evaluation of ADOPT spans Sections 3.6 and 3.7. Specifically, Section 3.6 introduces the simulation model and the noise model assumed. Our comprehensive simulation results are presented and discussed in Section 3.7. Finally, Section 3.8 offers concluding remarks and maps out directions for future work.

3.1 SYSTEM ASSUMPTIONS

The main goal of this section is to spell out the basic system assumptions that underlie ADOPT. ADOPT relies on detecting radio frequency (RF) signals transmitted at each step while a pedestrian is walking. Many *wearable devices*, including smartphones, wristbands, and shoes, can detect human steps [71]. Since we aim to design a low-power and low-cost system, we focus on lever-

aging wearables that harvest energy from body motion. Specifically, we assume that pedestrians (who could be children) wear shoes equipped with piezoelectric elements that provide a robust, lightweight and inexpensive source of power for an in-shoe, battery-free power generator [30], [114]. As already mentioned, when pedestrian shoes touch the ground, a circuit is closed, and a rudimentary transmitter embedded in the pedestrian's shoe is activated for a fraction of a second. Although the transmission range depends on the amount of power generated by the piezoelectric elements, the transmission range in this work is assumed to be up to 4 meters.

We assume that the parked cars know their exact geographic location by interfacing with a digital map. In support of detecting the presence of pedestrians, cars are fitted with four low-power radio transceivers placed at the front and rear axles on each side of the car. These transceivers detect and measure the strength of RF signals transmitted by pedestrian shoes. Although the detection range of a transceiver depend on its sensitivity, and it is a device-specific, we assume the detection range of each transceiver to be up to 4 meters in this work. Recall that the four transceivers mentioned above are integrated into, powered by, and synchronized to the intra-vehicle CAN bus [78]. Nevertheless, the transceivers are assumed to be powered alternatively by harvesting ambient-energy as we show in Figure 2.

The cars parked along the sidewalk are assumed to be aware of the distance between their right transceivers and the sidewalk. This distance can be estimated by using any on-board proximity sensor before stopping. The cars are assumed to be parked parallel to the sidewalk. This is assumed for convenience only. Indeed, if the cars are parked orthogonally to the sidewalk, they are assumed to be aware of the distance between their front or rear transceivers and the sidewalk. Notice that a car can detect its orientation with respect to the sidewalk using any rudimentary on-board navigation system or its inertial sensors.

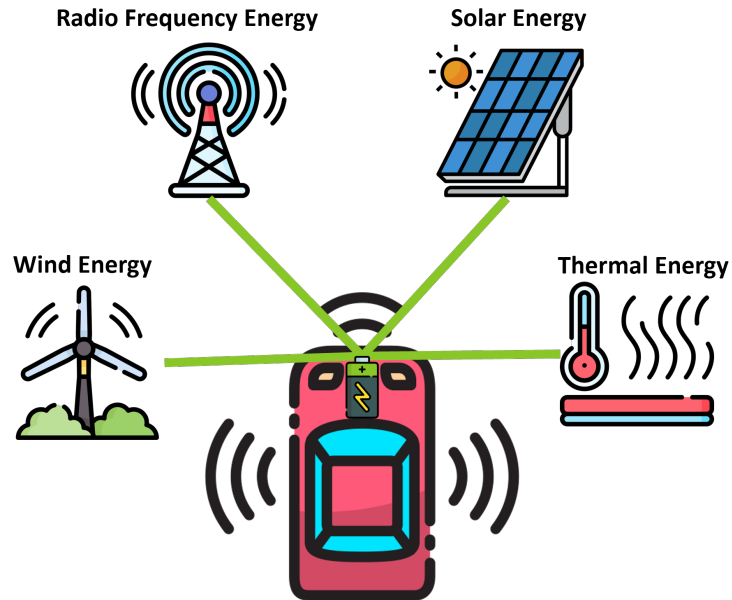


Figure 2. Examples of ambient energy that can be harvested to operate car’s sensors.

The cars parked along the sidewalk self-organize into a linear vehicular network [89] within one block in urban areas. Since we target a midblock crossing, we assume that traffic lights are far away from parked cars and should not affect ADOPT work. If a traffic light exists, we assume that parked cars are connected to the traffic light system and break the communication chain if the traffic light is red. In this work, we refer to the resulting network as a *chain* of parked cars. Refer to Figure 3 for an illustration. By consulting its on-board digital map, each car in the chain determines the width of the street and the speed limit. It also identifies its position in the chain and the pseudonyms of its two adjacent neighbors. When a car leaves or joins the chain, a simple maintenance operation is performed to maintain the network [70].

It is important to note that since in an on-street parking situation, adjacent parked cars are, typically, a short distance away from each other [5], the tasks inherent to self-organization and

maintenance of the chain of parked cars can be performed at low power using a suitable subset of transceivers such as Bluetooth Low Energy (BLE) or Zigbee.

We assume that when ADOPT is booted, there are no pedestrians in the street – pedestrians, if any, are all on the sidewalk. This assumption is non-essential and is made for convenience only. Similarly, we assume that pedestrians step into the street from the sidewalk *in front* of a parked car. If the pedestrians step into the street behind a given parked car, but in front of the next parked car in the chain, the latter will be responsible for undertaking the alerting actions. If there is no car in the chain, the latter will be responsible for undertaking the alerting actions, as described in Section 3.4, using its rear transceivers instead of the front ones.

Alert messages indicating the presence of a crossing cohort are propagated backward along the chain of parked cars, as illustrated in Figure 3. As they pass cars in the chain of parked cars,

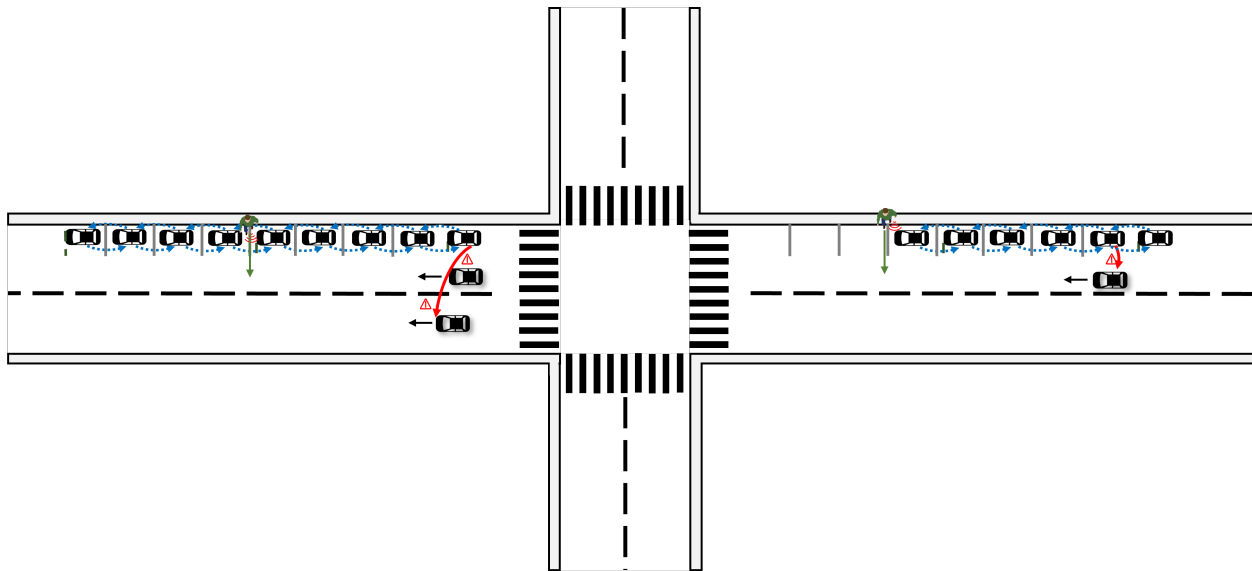


Figure 3. Illustrating ADOPT: Parked cars detect occluded crossing pedestrians and alert approaching cars.

approaching cars will be alerted, using low-power communications, to the reported location (or locations) of crossing pedestrians.

Although not specifically designed with self-driving cars in mind, ADOPT can be easily implemented to run on self-driving cars. When such a car receives an ADOPT “Caution – pedestrian in the street” message, it complies by reducing its speed without delay using a control system such as the system proposed by [69]. However, at the moment, self-driving cars are not very common, and so ADOPT alerts human drivers by displaying appropriate messages on a dashboard digital map, attempting to minimize distraction. For this purpose, we assume an ADOPT app that is running in approaching cars. The app determines the speed reduction necessary to avoid collision with the crossing cohorts and displays the suggested speed on the dashboard.

3.2 PEDESTRIAN CLASSIFICATION AND LOCALIZATION

The first task that parked cars need to undertake is to determine if there are pedestrians in the street. If there are no pedestrians in the street, all is well. Otherwise, pedestrians must be accurately localized and their crossing time estimated. Once this information is in hand, approaching cars are alerted to the presence of the crossing cohort. The main goal of this section is to provide the details of pedestrian classification and localization.

3.2.1 Pedestrian Detection

Recall that, as mentioned in Section 3.1, with each step the pedestrians’ shoes generate, for a fraction of a second, an RF signal with a known power T and a known frequency f [30]. When a pedestrian walks near a parked car, the transceivers in the car receive the signals generated by the pedestrian’s shoes. We calculate the Received Signal Strength $RSS(Rx)$ at a generic transceiver Rx

using the Free Space propagation model [44]:

$$RSS(Rx) = \frac{T\gamma}{\delta_{Rx}^2}, \quad (2)$$

where T is the power of the transmitted signal, γ is an environmental constant, and δ_{Rx} is the distance between the pedestrian who transmits the signal and the transceiver Rx . The pedestrian is assumed to be detected if her δ_{Rx} is less than or equal to the detection range of Rx .

3.2.2 Pedestrian Classification

An important task that ADOPT undertakes is the *binary* classification of detected pedestrians: *on the sidewalk or in the street*. We begin by stating and proving a technical result of an independent interest that provides a simple criterion for classifying pedestrians.

Lemma 3.2.1. *Consider two points L and R in the plane and assume that the line segment LR they determine has length $w > 0$. Let Γ be an arbitrary line perpendicular to LR . Γ is the locus of all the points P for which*

$$\delta_L^2(P) - \delta_R^2(P) = \text{constant}, \quad (3)$$

where $\delta_L(P)$ and $\delta_R(P)$ are, respectively, the distance from P to the endpoints of the segment LR .

Proof. Let Q be the intersection of the (infinite) line through L and R with Γ and refer to Figure 4. Assume, without loss of generality, that Q lies to the right of R . Denote by d the length of the segment PQ and by x the length of the segment RQ .

By applying the Pythagorean theorem to the LPQ and RPQ we write

$$\begin{cases} \delta_L^2(P) = (w+x)^2 + d^2 & \text{and} \\ \delta_R^2(P) = x^2 + d^2 \end{cases}$$

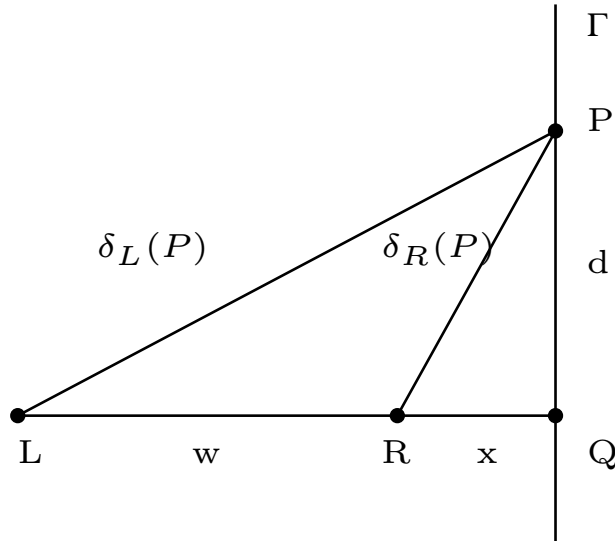


Figure 4. Illustrating the proof of Lemma 3.2.1.

and consequently,

$$\delta_L^2(P) - \delta_R^2(P) = (w+x)^2 + d^2 - x^2 - d^2 = w^2 + 2wx. \quad (4)$$

Observe that the line Γ determines *uniquely* x and conversely. Specifically, for a given line Γ , x is a constant (which depends on Γ), and so the expression $w^2 + 2wx$ is a constant implying that $\delta_L^2(P) - \delta_R^2(P)$ is itself a constant.

Conversely, assume that

$$\delta_L^2(P) - \delta_R^2(P) = c$$

for some constant c . By Equation 4, this implies that $w^2 + 2wx = c$ whereupon, solving for x yields

$$x = \frac{c - w^2}{2w}.$$

In turn, this uniquely determines the line Γ , and the proof of Lemma 3.2.1 is complete. \square

Lemma 3.2.1 justifies a simplification of notation. Specifically, when the line Γ is clear from the

context, the expression $\delta_L^2(P) - \delta_R^2(P)$ will be written, simply, as $\delta_L^2 - \delta_R^2$ as its value is independent of the choice of the point P on Γ .

We now state and prove an important consequence of Lemma 3.2.1 that will be used as a building block of our binary classification of pedestrians: *on the sidewalk* or *in the street*. In order to state our result, we find it convenient to inherit the notation of Lemma 3.2.1.

Theorem 3.2.2. *Consider an arbitrary line Γ and assume a transmitter placed at an arbitrary point P on Γ . Let $RSS(L)$ and $RSS(R)$ be, respectively, the Received Signal Strength received by two transceivers placed at L and R . Then, regardless of the location of P on Γ , we have*

$$\frac{1}{RSS(L)} - \frac{1}{RSS(R)} = c(\Gamma) \quad (5)$$

where $c(\Gamma)$ is a constant that depends on Γ .

Proof. By Equation 2, the Received Signal Strengths $RSS(L)$ and $RSS(R)$ received by two transceivers placed at L and R are, respectively,

$$RSS(L) = \frac{T\gamma}{\delta_L^2} \quad \text{and} \quad RSS(R) = \frac{T\gamma}{\delta_R^2}, \quad (6)$$

where T is the power of the transmitted signal and γ is an environmental constant.

Now, Equations 3 and 6, combined allow us to write

$$\begin{aligned} \frac{1}{RSS(L)} - \frac{1}{RSS(R)} &= \frac{\delta_L^2}{T\gamma} - \frac{\delta_R^2}{T\gamma} \\ &= \frac{\delta_L^2 - \delta_R^2}{T\gamma} \\ &= \frac{w^2 + 2wx}{T\gamma} \quad [\text{by Equation 4}] \\ &= c(\Gamma), \end{aligned} \quad (7)$$

where the last step of the derivation follows because there is a one-to-one correspondence between Γ and x . □

Discussion Assume a car parked parallel with the edge of the sidewalk. Theorem 3.2.2 establishes a one-to-one correspondence between a subset of real numbers and the set of lines in the plane parallel to the edge of the sidewalk. This is to say, to each line Γ in the plane parallel to the edge of the sidewalk, there corresponds a unique real number $c(\Gamma)$ and, conversely, to each real number there corresponds exactly one line in the plane parallel to the edge of the sidewalk. One of these lines is of a special interest: this is the edge of the sidewalk. As the next result shows, the resulting constant, c_0 acts as a discriminant between locations on the sidewalk and in the street.

Corollary 3.2.2.1. *Let the line Γ_0 coincide with the edge of sidewalk, assumed rectilinear. There is a unique constant c_0 such that the pedestrian (assumed to carry a transmitter) is on the sidewalk or in the street depending on whether $\frac{w^2+2wx}{T\gamma} > c_0$ or $\frac{w^2+2wx}{T\gamma} < c_0$.*

Proof. Let x_0 be the distance between R and the edge of the sidewalk and write

$$c_0 = \frac{w^2 + 2wx_0}{T\gamma} \quad (8)$$

Let Γ be a vertical line passing through an arbitrary point on the sidewalk and let x be the distance between R and the intersection point of the line LR with Γ . Clearly, $x > x_0$ and, consequently,

$$\frac{w^2 + 2wx}{T\gamma} > c_0.$$

Thus, for points on the sidewalk the expression $\frac{w^2+2wx}{T\gamma}$ is larger than c_0 . The proof is similar for points in the street. □

The one-to-one correspondence discussed above is a very useful property because in order to determine if a pedestrian is on the sidewalk, all we have to do is to evaluate the left-hand side of Equation 5 and to compare the result to the value of c_0 from Equation 8. This, in fact, is tantamount to a coarse-grain binary localization of pedestrians: on the sidewalk, or else in the street.

3.2.3 Pedestrian Localization

Pedestrians that are classified as *in the street* must be located more accurately, as we are about to explain. Referring to Figure 5, consider a pedestrian P and let point Q be the projection of P onto the line determined by L and R . We assume, without loss of generality, that Q lies between L and R . We assume that the pedestrian crosses the street by walking in a straight line parallel to the front of the parked car (i.e., perpendicular to the sidewalk). Let d be the length of the line segment PQ (that is, the vertical distance between the location of the pedestrian and the line LR). Further, let w be the width of the parked car, let x be the length of the line segment QR , let z be the distance from R to the sidewalk, and write $y = x + z$.

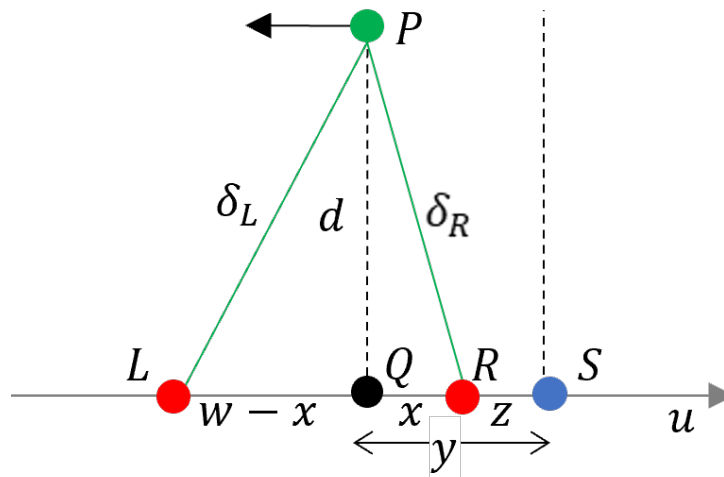


Figure 5. Illustrating the notation for the proof of Lemma 3.2.3.

Now, elementary geometry confirms that y has the following expression

Lemma 3.2.3.

$$y = \frac{w}{2} + z - \frac{T\gamma}{2w} \left[\frac{1}{RSS(L)} - \frac{1}{RSS(R)} \right]. \quad (9)$$

Proof. By using the Pythagorean theorem in the triangles PQL and PRQ we can write:

$$\begin{cases} \delta_L^2 = (w-x)^2 + d^2 & \text{and} \\ \delta_R^2 = x^2 + d^2 \end{cases}$$

and so:

$$\delta_L^2 - \delta_R^2 = (w-x)^2 - x^2 = w^2 - 2wx. \quad (10)$$

From Equation 2,

$$\begin{cases} \delta_L^2 = \frac{T\gamma}{RSS(L)} & \text{and} \\ \delta_R^2 = \frac{T\gamma}{RSS(R)} \end{cases}$$

by plugging these values into Equation 10, we obtain

$$\frac{T\gamma}{RSS(L)} - \frac{T\gamma}{RSS(R)} = w^2 - 2wx.$$

Solving for x yields

$$\begin{aligned} x &= \frac{w^2}{2w} - \frac{T\gamma}{2w} \left[\frac{1}{RSS(L)} - \frac{1}{RSS(R)} \right] \\ &= \frac{w}{2} - \frac{T\gamma}{2w} \left[\frac{1}{RSS(L)} - \frac{1}{RSS(R)} \right] \end{aligned} \quad (11)$$

Finally,

$$\begin{aligned} y &= x + z \\ &= \frac{w}{2} + z - \frac{T\gamma}{2w} \left[\frac{1}{RSS(L)} - \frac{1}{RSS(R)} \right]. \end{aligned} \quad (12)$$

as claimed. \square

Now, referring again to Figure 5, it is clear that since the pedestrians are crossing the street in a direction perpendicular to the sidewalk, in order to specify the location of a crossing pedestrian, it suffices to specify the value of y , as above, along with the value of d , the vertical distance to the front of the parked car.

In order to determine d , we compute the area of the triangle PLR in two different ways:

- First, evidently, $Area(PLR) = \frac{w \cdot d}{2}$;
- Second, writing $p = \frac{\delta_L + \delta_R + w}{2}$, the same area can be expressed as

$$Area(PLR) = \sqrt{p(p - \delta_R)(p - \delta_L)(p - w)}$$

Consequently,

$$\frac{w \cdot d}{2} = \sqrt{p(p - \delta_R)(p - \delta_L)(p - w)},$$

which, upon solving for d , yields:

$$d = \frac{2}{w} \sqrt{p(p - \delta_R)(p - \delta_L)(p - w)}. \quad (13)$$

3.3 ESTIMATING THE TIME TO CROSS

Recall that a crossing cohort is a group of pedestrians crossing together at the same location. Instead of dealing with each member of the cohort individually, we only concern ourselves with the *tail* of the cohort, defined as the last pedestrian in the cohort. It is clear that if the tail of the cohort has crossed safely, then all pedestrians in the cohort have crossed safely, too. It is important to note that ADOPT is *privacy-aware* as we are only interested in the location of the tail of the cohort, and not in the actual person that happens to be the last in the cohort.

We now define the tail of a crossing cohort more formally. Recall that the parameter y , defined in Lemma 3.2.3 keeps track of the current distance of a crossing pedestrian to the sidewalk she just departed. Formally, then, at each moment in time, the tail of the crossing cohort is the pedestrian with

$$\min\{y \mid \text{pedestrian classified as in the street}\}. \quad (14)$$

Notice that the tail may change dynamically, either because new pedestrians joined the cohort, a pedestrian turns back after starting crossing or, simply, because some folks in the cohort walk faster than others. ADOPT updates the tail of the crossing cohort every second.

To manage the tail of a cohort, ADOPT needs to process signals from several pedestrians simultaneously. To accomplish this, the transceivers in the parked car sample frequency f on which the pedestrians' shoes are transmitting signals, m times per second. Conceptually, this means that each second is partitioned into m slots. Assume that each pedestrian takes one step per second, and that each step generates one transmission. For all practical purposes, this transmission occurs, randomly, in one of the m slots discussed above. Now, suppose that there are k , ($k \geq 1$), pedestrians in the crossing cohort. We have just set up a "balls-into-bins" model involving k balls and m bins. If two or more pedestrians are transmitting in the same time slot, a collision occurs and the outcome cannot be disambiguated.

We are interested to assess the expected number of "clear" transmissions, where one single transmission occurs in a given time slot. For arbitrary i , ($1 \leq i \leq k$), let X_i be the indicator random variable that takes on the value 1 if, in a given second, slot i sees a clear transmission and 0 otherwise. It is easy to see that

$$\Pr[X_i = 1] = \left(1 - \frac{1}{m}\right)^{k-1}$$

and that the expected number, $E[M]$, of clear transmissions is

$$\begin{aligned} E[M] &= E[X_1 + X_2 + \cdots + X_k] \\ &= E[X_1] + E[X_2] + \cdots + E[X_k] \end{aligned} \quad (15)$$

$$= \Pr[X_1] + \Pr[X_2] + \cdots + \Pr[X_k] \quad (16)$$

$$= k \left(1 - \frac{1}{m}\right)^{k-1}. \quad (17)$$

As an illustration, if a given cohort were to contain $k = 8$ pedestrians, and assuming that frequency f is sampled 50 times per second, we would expect to see $E[M] = 8 \times \left(1 - \frac{1}{50}\right)^7 = 8 \times \left(\frac{49}{50}\right)^7 \approx 6.9$ clear transmissions each second.

With this in mind, consider the time ruled into seconds and assume that in second t , the tail of the current crossing cohort was located at $y(t)$ and its current speed, $v(t)$, has been estimated. The *remaining time to cross* at time t , $\Delta(t)$, can be estimated as

$$\Delta(t) = \frac{W - y(t)}{v(t)}, \quad (18)$$

where W is the width of the street that the pedestrians are crossing¹.

We need to show how these parameters are updated in the next second, $t + 1$. We begin by identifying all clear transmissions in second $t + 1$ and, using Equation 14, we obtain the location, $y(t + 1)$, of the current tail. We distinguish between the following cases:

Case 1: $y(t) < y(t + 1)$.

Evidently, in this case, the new tail is closer to the opposite sidewalk. It follows that no new pedestrian has joined the cohort in this second. In this case, it is natural to update the cohort

¹We assume here the real-time Δ is accurately estimated as long as the pedestrian's signal is detected by the right-front transceiver. If the signal is no longer detected and Δ is greater than zero, the Δ here is an estimation and could be not accurate if the pedestrian stays in street longer than the determined Δ .

parameters as follows:

- $v(t + 1) = y(t + 1) - y(t)$ m/s;
- $\Delta(t + 1) = \frac{W - y(t + 1)}{v(t + 1)}$.

Case 2: $y(t) > y(t + 1)$.

In this case, it is clear that one or more pedestrians have joined the cohort and, consequently, the new tail must be selected from among the pedestrians who have just joined the cohort. There is a complication: we cannot update the speed of the tail, because the tail is new. Instead, we assign to the new tail, tentatively, the average crossing speed. The cohort parameters are updated as follows:

- $v(t + 1) = v_0$, where v_0 is an estimate of the average pedestrian speed;
- $\Delta(t + 1) = \frac{W - y(t + 1)}{v(t + 1)}$.

3.4 SAFETY ZONE AND MESSAGE PROPAGATION

ADOPT involves two types of car-to-car messages, each with its own semantics:

- *Alert messages:* are sent by the parked car that detects a crossing cohort with the intention of establishing a *Safety Zone*, as we are about to describe;
- *Caution messages:* are messages sent by the parked cars in the *Safety Zone*² to alert approaching cars to the presence of crossing pedestrians.

²The safety zone here is assumed to be independent of the traffic light if exists. We are aware of the complications of the interference of traffic lights with ADOPT, and we will investigate this interference in the future work.

These two types of messages will be discussed in Sections 3.4.1 and 3.4.2, respectively.

3.4.1 Alert Messages

Referring to Figure 6, assume, without loss of generality, that car A detects a crossing cohort at time t . Proceeding as discussed in Section 3.3, car A estimates the remaining time, $\Delta(t)$ (see (18)), it takes the tail of the cohort to cross the street. Using this information, car A determines the distance, $D(t)$, the alert messages will have to be propagated along the chain as follows:

$$D(t) = [\Delta(t) + r] \cdot v_{max}, \quad (19)$$

where r is the *driver reaction* time, estimated to be between 1.24 seconds and 2 seconds [38]. If self-driving cars are considered, then r is set to zero, since the driver reaction time is a human factor and does not affect self-driving cars. Finally, car A propagates the alert message containing: its own location, $x(A)$, on the digital map, the current time, t , and the Distance-to-Live $D(t)$ of the alert message in meters.

Referring to Figure 6 again, the area of length $D(t)$, defined in Equation 19, starting at car A and running down the chain of parked cars is called the *Safety Zone* associated with the crossing cohort detected by car A. Each parked car in the chain of parked cars, upon receiving the alert message originated by car A, compares its own location with that of A and determines if the distance from A is smaller than or equal to $D(t)$. If so, it marks itself as being in the Safety Zone and propagates the alert message further along the chain. In the case that the distance between two consecutive cars is large, the low-power communication cannot be used to deliver the alert message. Instead, DSRC is assumed to deliver it to the next parked car.

As an illustration, in Figure 6, assume that car C has just received the alert message from

the previous car in the chain. Let $x(A)$ and $x(C)$ be the x-coordinates of A and C, respectively. If $|x(A) - x(C)| \leq D(t)$ then C remembers that it belongs to the Safety Zone and propagates the message further down the chain. Continuing in this way, the alert message will reach, eventually, car B. When car B receives the alert message, it finds that $|x(A) - x(B)| > D(t)$, and so it discards the message. As illustrated in Figure 6, car B is not in the Safety Zone.

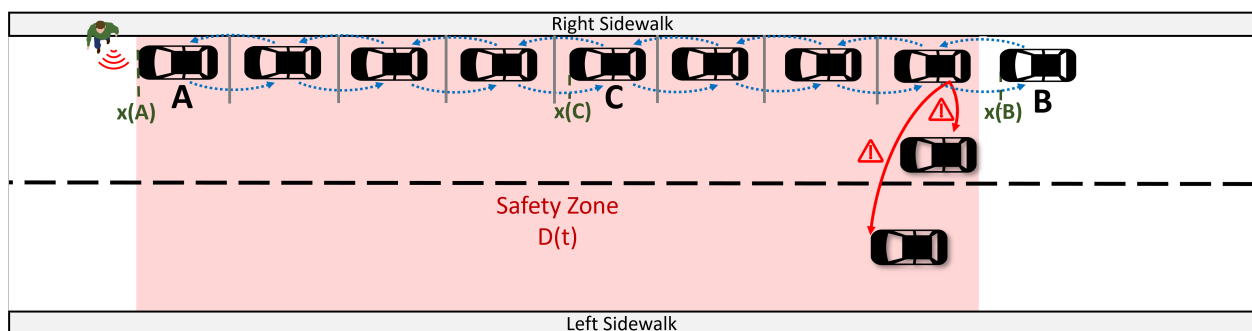


Figure 6. Parked cars in the Safety Zone propagate alert messages within the estimated propagation distance to alert approaching cars.

3.4.2 Caution Messages

Each parked car inside the Safety Zone is tasked with broadcasting a “Caution – pedestrians in the street” (Caution, for short) message to approaching cars. This broadcast must be done at low power, as illustrated in Figure 6, using BLE or Zigbee, as passing cars are a short distance away from parked cars. The Caution message contains:

- the location $x(A) + d$ of the crossing cohort, where d was computed in (13);

- the time, $t + \Delta(t)$, at which the cohort is expected to have crossed the street.
- the direction of the alert message indicated by one bit. By convention, if the alert message is intended for cars moving northbound, the direction bit will be set.

In the unlikely event where many cars in the chain of parked cars depart, leaving big gaps in the chain, as shown in Figure 7, the last car in the chain uses its DSRC transmitter to broadcast the Caution message to inform approaching cars of the location of the crossing cohort. As illustrated in Figure 7, car C with $|x(A) - x(C)| < D(t)$ does not detect any car behind it. Hence, car C will use its DSRC transmitter to broadcast the "Caution" message at a distance of $D(t) - x(C)$, where $x(C)$ is the location of C.

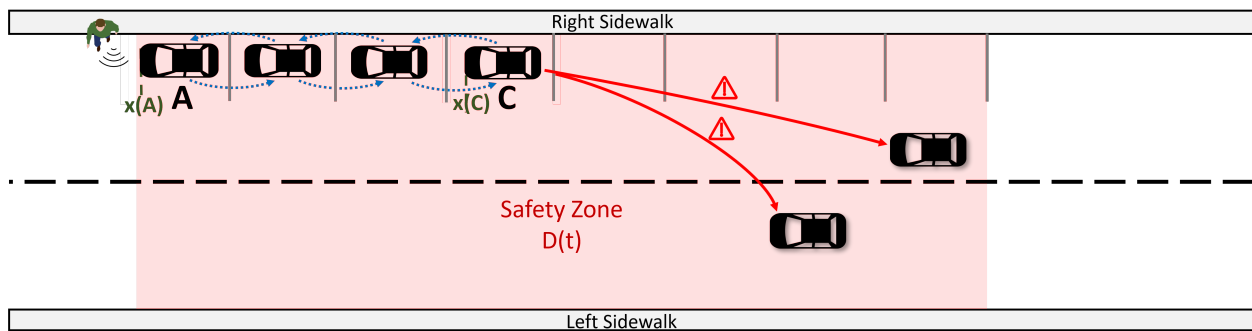


Figure 7. The last car in the chain delivers the caution message to the approaching car via DSRC if the chain length is less than $D(t)$.

In the next second, $t + 1$, a new estimate $D(t + 1)$ is made as discussed in Section 3.3. If $D(t + 1) > D(t)$ then an updated alert message is sent with Distance-to-Live $D(t + 1)$. Otherwise, no action is needed.

3.5 HOW APPROACHING CARS DETERMINE A SAFE SPEED

The main goal of this section is to show how approaching cars, alerted to the presence of crossing cohorts, adjust their speed in such a way that they avoid colliding with the crossing pedestrians.

Our approach is novel and is based of a new way of looking at the time-space diagram (see Section 1.3.9 for a refresher).

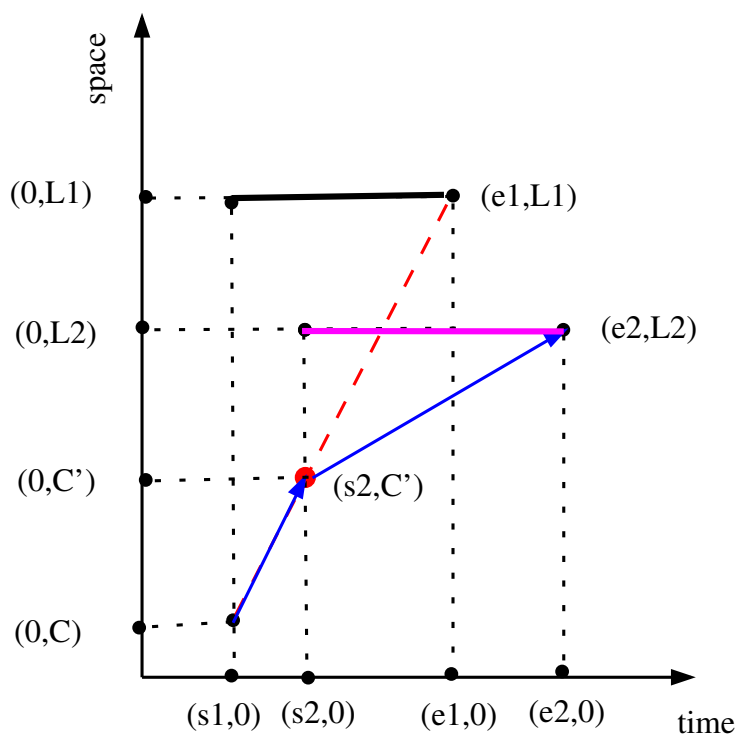


Figure 8. Illustrating the computation of the safe average speed in the case of two crossing cohorts.

Referring to Figure 8, consider a car moving North-bound along a street. At time s_1 , the car is inside the Safety Zone, and receives a “Caution – pedestrians in the street” message alerting it

to a crossing cohort at location $(0, L1)$. Upon receiving an alert message, the car will compare the direction bit with its actual direction of movement. If the car is moving South-bound, it will ignore the alert message. Assume that the location of the car at time $s1$ is $(s1, C)$ and that the cohort will finish crossing the street at time $e1$.

Proceeding as indicated in Appendix A, the approaching car computes the maximum safe speed:

$$v_{safe} = \min \left\{ v_{max}, \frac{L1 - C}{e1 - s1} \right\}, \quad (20)$$

where v_{max} is the speed limit along the street.

Traveling at this safe speed North-bound, the approaching car receives, at time $s2$, a second “Caution – pedestrians in the street” message alerting it to the presence of a second crossing cohort. This cohort crosses the street at location $(0, L2)$ and will finish crossing at time $e2$. How should the car change its speed to avoid an accident?

In order to answer this question, the first task is to determine the location, $(s2, C')$ of the car at time $s2$. This can be done by noting that v_{safe} in Equation 20 can be written as

$$\frac{L1 - C}{e1 - s1} = \frac{C' - C}{s2 - s1}.$$

Solving for C' yields:

$$C' = C + \frac{(L1 - C)(s2 - s1)}{e1 - s1}.$$

With C' firmly in hand, the car updates the current safe speed v_{safe} in (20) as follows:

$$\begin{aligned} v_{safe} &= \min \left\{ v_{safe}, \frac{L2 - C'}{e2 - s2} \right\} \\ &= \min \left\{ v_{max}, \frac{L1 - C}{e1 - s1}, \frac{L2 - C'}{e2 - s2} \right\}. \end{aligned} \quad (21)$$

The justification of (21) is simple. The car needs to select the largest average safe speed and this is the smallest of the slopes of the lines segments determined by the points $(s2, C')$ and $(e1, L1)$ on the one hand, and the points $(s2, C')$ and $(e2, L2)$ on the other.

At time $e1$, the car realizes that the first cohort has finished crossing the street and will adjust its speed again:

$$v_{safe} = \min \left\{ v_{max}, \frac{L2 - C'}{e2 - s2} \right\}. \quad (22)$$

In Figure 8,

$$\min \left\{ v_{max}, \frac{L1 - C}{e1 - s1}, \frac{L2 - C'}{e2 - s2} \right\} = \min \left\{ v_{max}, \frac{L2 - C'}{e2 - s2} \right\}$$

and, consequently, the car continues driving at the same speed.

Next, at time $e2$, the car realizes that the second cohort has finished crossing and so it will adjust its speed again:

$$v_{safe} = \min \{v_{max}\} = v_{max}, \quad (23)$$

essentially, reverting to the maximum allowed speed.

The same procedure is then continued, exactly as described, should other “Caution – pedestrians in the street” be received by the car in the future.

3.6 SIMULATION

In this section, we describe how ADOPT simulation model is developed and how we evaluated ADOPT performance.

3.6.1 Simulation Model

We validated the theoretical findings of ADOPT by testing them on simulated traffic data. For this purpose, we used Simulation of Urban MObility (SUMO) [46] to generate pedestrian and car traffic data for the ADOPT simulation model illustrated in Figure 9.

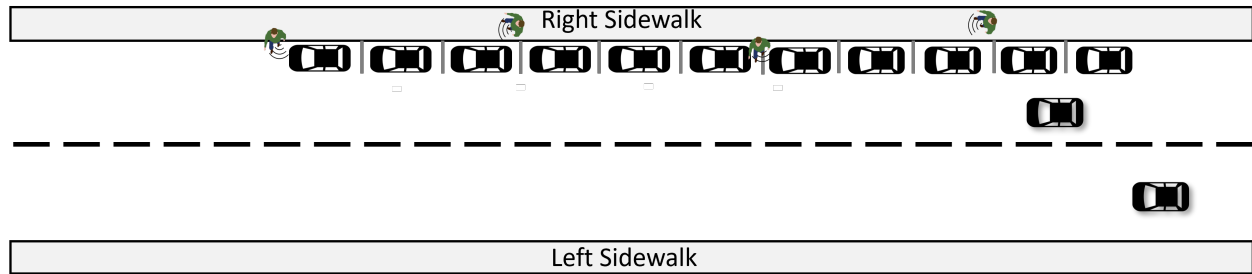


Figure 9. An instance of the ADOPT simulation model.

Our simulation model consists of a *one-way* street with a road-side parking lane on the right side of the street and sidewalks on both sides. Approaching cars enter at the end of the street and exit from the opposite end.

SUMO is also known as a microscopic simulation for pedestrian mobility. In our simulation model, the pedestrians are not restricted to crossing at intersections but, indeed, they may cross *midblock* a prevalent behavior Tezcan, Elmorssy, and Aksoy [87]. In SUMO, pedestrian are set by default to slowdown their speed before crossing to make sure the street is clear and stop if there passing cars. We enforced pedestrians to ignore the approaching cars. Hence, they do not stop or hesitate before crossing the street. By this setting, we collect more data when the car approaches while a pedestrian start crossing the street. Moreover, SUMO has implemented a collision avoidance model to force vehicles to reduce their speed if there are crossing pedestrians. We disabled

this mode before we generated the vehicular traffic to measure the effect of receiving the caution message correctly. For the reader's convenience, we summarize the simulation parameters in Table 3. Although the main goal of this simulation is to proof the concept of protecting pedestrians by parked cars, we tried to generate data that is close to real-world crossing data based on statistics of number of crossing pedestrian and crossing speed that has been collected by [20], [87].

Table 3. A summary of simulation parameters

Parameter	Value
RF Signal Frequency f	2.4 GHz
Transmission Power T	2 mW
Detection Range	4 meters
Street Width W	12.8 m
Distance From R Transceiver to the Sidewalk z	0.4 m
Number of Detected Pedestrians/sec $[\mu, \sigma]$	[1.8, 1.4]
Pedestrians Speeds $[\mu, \sigma]$	[1.15, 0.13] m/sec
Average Speed v_0	1.2 m/sec
Number of Crossing Pedestrians/sec $[\mu, \sigma]$	[0.11, 0.32]
Street Speed Limit v_{max}	15 m/sec
Simulation Step Length	1 sec
Simulation Duration	3600 sec (1 hour)

We modeled pedestrians' radio signals using Equation 2 by setting a constant transmission power equals to 2 mW transmitted from their actual locations. We then obtained the actual Euclidean distances δ_{Rx} between the pedestrian locations and the four transceivers located at the four corners of cars. We assumed that the pedestrian is detected by a transceiver if the distance between the transceiver and the pedestrian is less than or equal 3 meters.

For the communication between parked cars and approaching cars, we assume the cars are communicating using low-power communication modules such as BLE which has been proven to provide a reliable V2V communication [12]. Based on that, when the car enters the Safety Zone, we assume that it receives the "caution message" from the closest parked car.

The data we collected from SUMO are as follows: street and sidewalk dimensions, pedestrians' locations, pedestrians' speeds, parked cars' locations and dimensions, and approaching cars' speed and location at each time step. Data collected from SUMO is our ground truth, i.e., "actual", information about pedestrians and cars traffic.

3.6.2 Modeling RSS Noise

In real-life situations, RSS measurements experience random fluctuations due to hardware-based parameters such as thermal noise, or due to the natural behavior of the signal as it is reflected by the ground [79]. Being close to the ground, we assume that there are no obstacles between the pedestrians' shoes and the transceivers.

We modeled the uncertainty in the *RSS* produced by receiving either more or less power than the original *RSS* as a Gaussian random variable Φ_σ with zero mean and a standard deviation σ as follows:

$$RSS'(Rx) = RSS(Rx) + \Phi_\sigma$$

where RSS' is the noisy received signal strength at a generic transceiver Rx . We set σ to 0.3 mW since we only consider short transmission ranges and near-the-ground communication. The added noise affects the distance we estimate based on the RSS . We measured the impact of noise by calculating the absolute error ξ of the estimated distance at each transceiver $RSS(R)$ and $RSS(L)$ where $\xi_{\delta_R} = |\hat{\delta}_R - \delta_R|$ and $\xi_{\delta_L} = |\hat{\delta}_L - \delta_L|$. Figure 10 shows the distribution of the absolute errors in distance estimated from $RSS'(R)$ and $RSS'(L)$ plotted against the actual distances $\hat{\delta}_R$ in (a) and $\hat{\delta}_L$ in (b) obtained from SUMO. Note that the errors shown are observed at every 0.2-meters window.

Results showed that the added noise causes minor distance estimation errors in ranges near the transceivers, but the errors increase as the pedestrians move away from the transceivers.

As the noise affects the RSS at both transceivers, it also affects the result of Equation 7. Consequently, the noise impacts the one-to-one mapping, discussed in Section 3.2, between the set of lines parallel to the edge of the sidewalk and the $c(\Gamma)$ values as each line will have many $c(\Gamma)$ values. To determine the range of inaccuracy in $c(\Gamma)$, we defined a 0.2-meters window of the horizontal position before and after the sidewalk and aggregated the calculated noisy $c(\Gamma)$ from $RSS'(L)$ and $RSS'(R)$ at each window as we show in Figure 11A. To compare the noisy $c(\Gamma)$ with the noise-free $c(\Gamma)$, we show in the same figure the noise-free $c(\Gamma)$. The results showed that the noise impacts the $c(\Gamma)$ if pedestrians are far from the main axis of the car (i.e. middle of the LR line segment), while it has a lower impact near the LR midpoint the pedestrians are close to both transceivers and $c(\Gamma)$ is almost zero. This affected also the classification based on the threshold c_0 . Referring to Figure 11B, all $c(\Gamma)$ values of pedestrians walking on sidewalk are greater than c_0 . Similarly, all $c(\Gamma)$ values of pedestrians who are in the street are less than c_0 . The variation of $c(\Gamma)$ values shows that even though pedestrian location varies inside the sidewalk, they are identified to be inside the sidewalk as long as their $c(\Gamma)$ is greater than c_0 . This also proves that even though

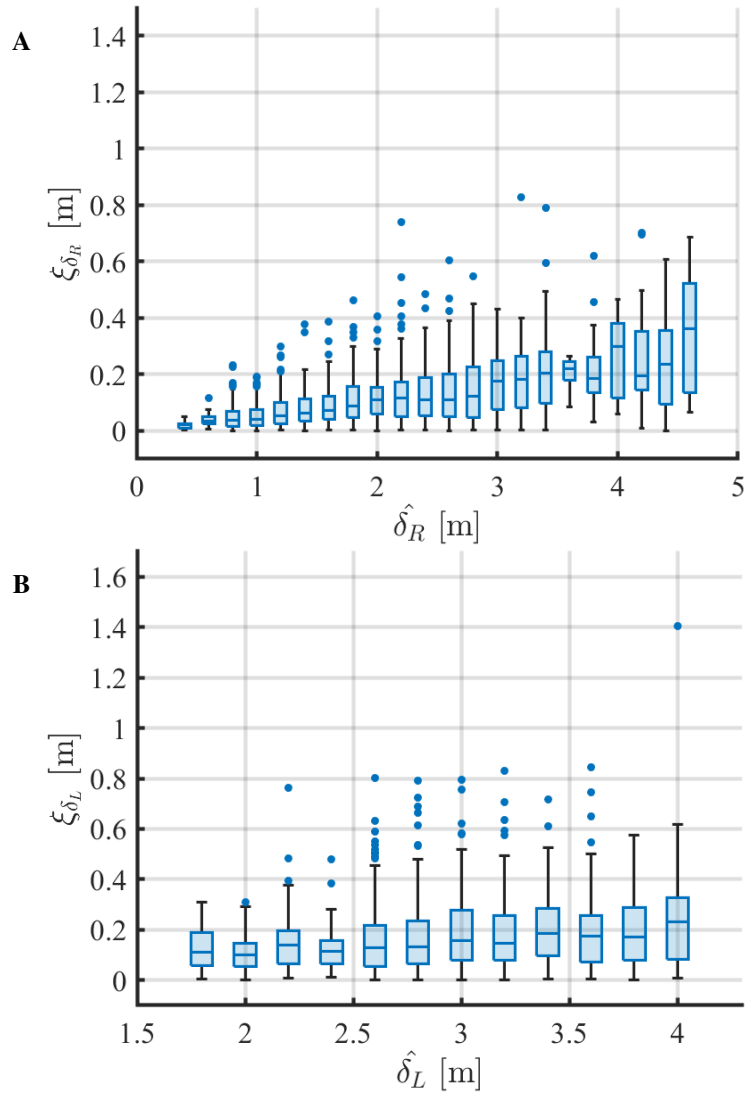


Figure 10. Absolute error of estimated distances (A) δ_R . (B) δ_L .

the pedestrian may not walk in straight lines, she will be classified correctly. On the other hand, with the noisy $c(\Gamma)$, several $c(\Gamma)$ values of pedestrians walking on the sidewalk are less than c_0 , and several $c(\Gamma)$ values of pedestrians walking in the street are greater than c_0 .

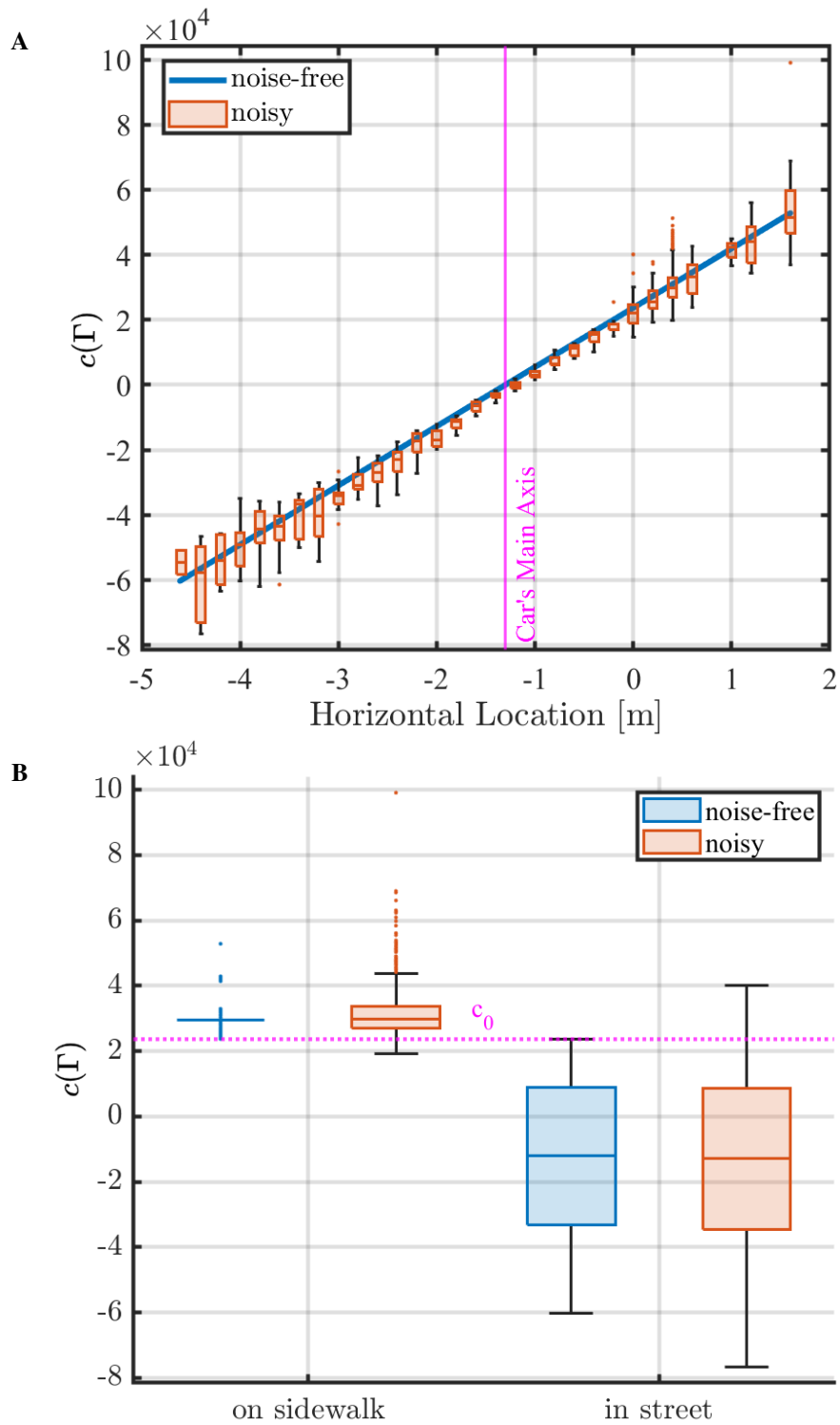


Figure 11. Effect of noise on $c(\Gamma)$ (A) The noise produces multiple $c(\Gamma)$ values for the same parallel line to the sidewalk while the actual $c(\Gamma)$ is unique for each line. (B) Distribution of $c(\Gamma)$ of pedestrians' signals per pedestrian's class (on the sidewalk and in the street).

3.7 EVALUATION

3.7.1 Evaluation Scenarios

We evaluated the performance of ADOPT in two scenarios:

- **Scenario 1 – Noise-free mode:** in which we performed pedestrian classification and crossing time estimation using the actual data generated by SUMO;
- **Scenario 2 – Noisy mode:** in which we performed pedestrian classification and crossing time estimation using noisy RSS to have a more realistic evaluation.

In the evaluation we assume that all pedestrians who transmit RF signals are detected by the parked car transceivers.

3.7.2 Overall Evaluation

We demonstrate the performance of ADOPT in both scenarios above. The overall performance of the pedestrian classification is shown in Table 4 and Table 5 for noise-free mode and noisy mode respectively. These statistics are for detecting pedestrians by two enabled cars in the simulation. We evaluated the accuracy of the pedestrian classification as *on the sidewalk* or *in the street* by using the following formula:

$$accuracy = \frac{TP + TN}{TP + TN + FP + FN} \times 100 \quad (24)$$

where

- TP (True Positive) is the total number of pedestrians that were correctly identified to be in the street;

- TN (True Negative) is the total number of pedestrians that were correctly identified to be on the sidewalk;
- FP (False Positive) is the total number of pedestrians incorrectly classified as in the street; and,
- FN (False Negative) is the total number of pedestrians incorrectly identified as on the sidewalk.

We obtained the ground truth of pedestrians classes directly from SUMO generated data. The accuracy of pedestrian classification in noise-free mode was 100% accuracy, while the accuracy dropped to 93.25% in noisy mode.

Table 4. Overall Accuracy of Pedestrian Classification (Noise-Free Mode)

Actual Class	Predicted Class (noise-free mode)	
	in street (positive)	on sidewalk (negative)
in street (positive)	340 (TP)	0 (FN)
on sidewalk (negative)	0 (FP)	1216 (TN)
Accuracy	100%	

The other metrics we use to empirically evaluate the performance of ADOPT are: the accuracy of pedestrian localization, the accuracy of crossing time estimation, the accuracy of the remaining

Table 5. Overall Accuracy of Pedestrian Classification (Noisy Mode)

Actual Class	Predicted Class (noisy mode)	
	in street (positive)	on sidewalk (negative)
in street (positive)	316 (TP)	24 (FN)
on sidewalk (negative)	81 (FP)	1135 (TN)
Accuracy	93.25%	

crossing time, as well as the accuracy of the Safety Zone size. We use Root Mean Squared Error (RMSE) to measure the accuracy of these estimations. To measure the overall accuracy of pedestrian localization, we evaluated E_d and E_y , where E_d is the RMSE of the location of pedestrians in front of the parked car (the vertical distance of the pedestrian) and E_y is the RMSE for estimating the distance of the pedestrian from the edge of the sidewalk (the horizontal distance of crossing pedestrians). We evaluated E_d as follows:

$$E_d = \sqrt{\frac{\sum_{j=1}^M (\hat{d}_j - d_j)^2}{M}} \quad (25)$$

where M is the total number of received signals and \hat{d}_j and d_j are, respectively, the actual and estimated vertical distances of the received signal. Similarly, we evaluated E_y as follows:

$$E_y = \sqrt{\frac{\sum_{j=1}^{M_s} (\hat{y}_j - y_j)^2}{M_s}} \quad (26)$$

where M_s is the total number of received signals that are actually detected in the street. \hat{y}_j and y_j are the actual and estimated horizontal distances. Recall that y is only calculated when a pedestrian

is classified as in the street. ADOPT estimation errors E_d and E_y were 0 meter in noise-free mode, and less than 0.3 meters in noisy mode as we show in Table 6.

We used RMSE to measure the overall accuracy of estimating the pedestrian's speed v as follows:

$$E_v = \sqrt{\frac{\sum_{i=1}^N (\hat{v}_i - v_i)^2}{N}} \quad (27)$$

where N is the total number of pedestrians generated in the simulation, and \hat{v}_i and v_i are, respectively, the actual and the estimated speed of each pedestrian who was actually in the street. We chose to average the speed of each pedestrian individually because one pedestrian may vary her speed in SUMO. The results shows that ADOPT RMSE in crossing speed estimation E_v was less than 1 meter/sec in noise-free mode while it has higher error in noisy mode. We used the same RMSE formula to measure the accuracy of the remaining crossing time:

$$E_\Delta = \sqrt{\frac{\sum_{i=1}^N (\hat{\Delta}_i - \Delta_i)^2}{N}} \quad (28)$$

where $\hat{\Delta}_i$ and Δ_i are, respectively, the actual and estimated remaining time to cross for each pedestrian. The results shows that ADOPT RMSE in crossing time estimation E_Δ was less than 1 sec in noise-free mode while it has higher error in noisy mode.

The RMSE of estimating the Safety Zone size, which is determined by the propagation distance $D(t)$, for each pedestrian is calculated as follows:

$$E_D = \sqrt{\frac{\sum_{i=1}^N (\hat{D}_i - D_i)^2}{N}} \quad (29)$$

where \hat{D}_i and D_i are, respectively, the actual and estimated propagation distances. \hat{D}_i is calculated based on the actual remaining time to cross $\hat{\Delta}_i$.

We show the overall result of the RMSE in Table 6. We notice here that the RMSE of ADOPT

Table 6. Overall RMSE of ADOPT Estimations

RMSE	noise-free mode	noisy mode
E_y	0.00 m	0.26 m
E_d	0.00 m	0.24 m
E_v	0.05 m/sec	0.11 m/sec
E_Δ	0.51 sec	1.21 sec
E_D	12.79 m	42.23 m

estimations in noise-free mode is low. However, in noisy mode the RMSE increases for all estimations. The details of the evaluation will be explained later in this section.

Next, we present the details of ADOPT evaluation and the results. Specifically, in Section 3.7.3 we discuss the accuracy of pedestrian classification; in Section 3.7.4 we discuss the accuracy of pedestrian localization, once they are in the street; the accuracy of pedestrian street traversal speed is discussed in Section 3.7.5; the accuracy of the remaining crossing time is discussed in Section 3.7.6; the accuracy of establishing the Safety Zone is discussed in Section 3.7.7. Finally, Section 3.7.8 offers an end-to-end evaluation of ADOPT. Furthermore, Section 3.7.9 shows the performance of the system under simultaneous transmission of pedestrian signals. Lastly, we measured the time performance of ADOPT computations in Section 3.7.10.

3.7.3 Accuracy of Pedestrian Classification

To investigate the impact of noise on the classification performance in noisy mode, in Figure 12

we plot the classification accuracy against the horizontal location (i.e the position of lines that are parallel to the edge of the sidewalk) of the transmitted signal from the edge of the sidewalk that is indicated with value 0. Locations with negative values are in the street while locations with positive values are on the sidewalk. We noticed that the classification accuracy only drops when the transmitted signal is within few decimeters away from the edge of the sidewalk (i.e. location 0).

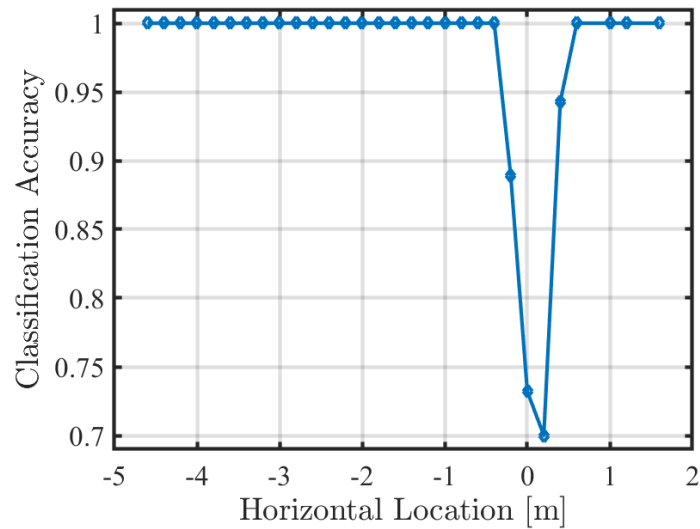


Figure 12. Aggregated classification accuracy at horizontal locations before and after the edge of the sidewalk.

To better understand why the accuracy drops around the horizontal location 0, we investigated the accuracy metrics TP, FP, TN, FN, defined above in more detail. Referring to Figure 13, the accuracy drops when we have FP and FN due to noisy $c(\Gamma)$ (denoted by $c(\Gamma)'$). We noticed that FP classification occurs if $c(\Gamma)$ is less than c_0 and, at the same time, $c(\Gamma)'$ is greater than c_0 . This

means we have FPs if the noise generates $c(\Gamma)$ above the threshold c_0 while the actual $c(\Gamma)$ is lower than the threshold. Similarly, FN classifications occur if $c(\Gamma)$ is greater than c_0 and, at the same time, $c(\Gamma)'$ is less than c_0 . This means we have FN if the noise generated $c(\Gamma)'$ below the threshold c_0 while the actual $c(\Gamma)$ is above the threshold. From the figure, we can see that this happens only in a limited area around c_0 .

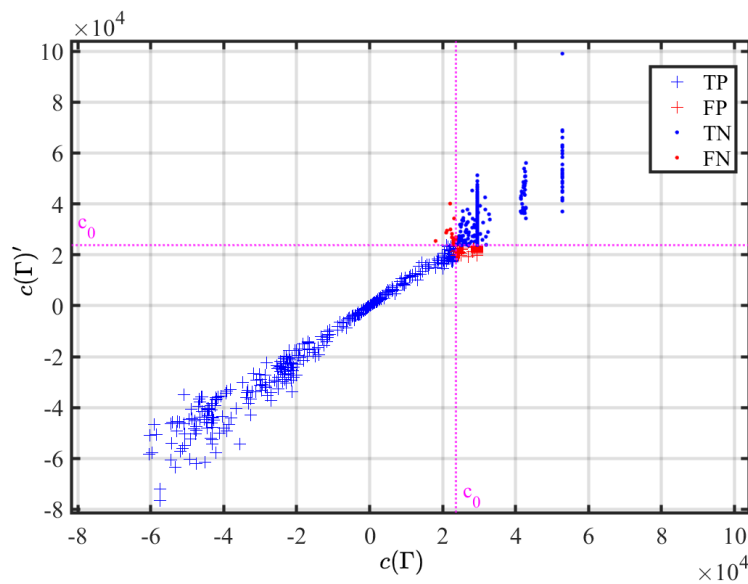


Figure 13. Detailed classification accuracy based on $c(\Gamma)$ and $c(\Gamma)'$

To translate this to spatial data, in Figure 14 we plotted $c(\Gamma)'$ corresponding to the horizontal location of the transmitted signal. Obviously, high FN puts pedestrians at the risk as they enter the street and ADOPT does not alert the approaching cars. On the other hand, high FP results in flooding the approaching vehicles with incorrect alert messages while the pedestrians are on the sidewalk. To assess where ADOPT has miss-classification, we define our metric False Positive Per

Location FPPL and False Negative Per Location FNPL where FPPL is the percentage of FP per horizontal location aggregated at each 0.2 meters, and FNPL is the percentage of FN per horizontal location aggregated at each 0.2 meters as well.

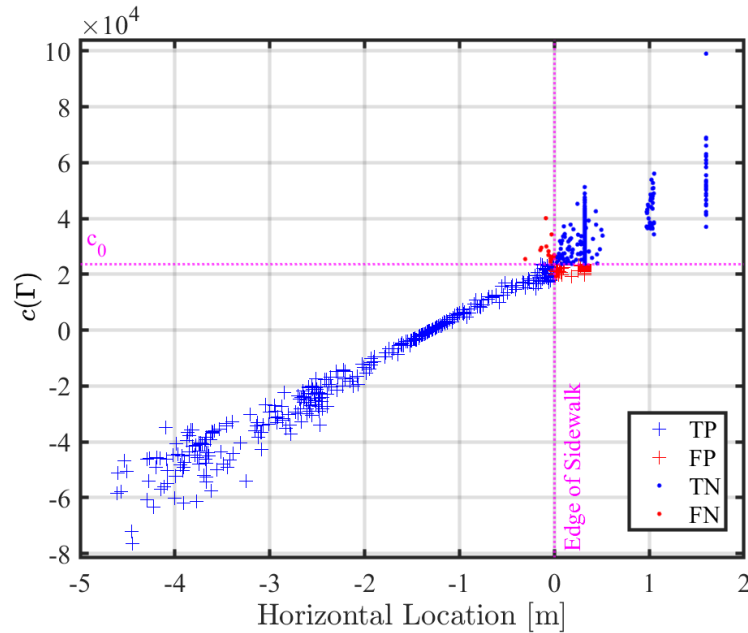


Figure 14. Detailed classification accuracy at horizontal locations before and after the edge of the sidewalk.

Figure 15 shows that FNPL is high only at locations situated a few decimeters away from the edge of the sidewalk. Moreover, ADOPT has higher FPPL a few decimeters away from the edge of the sidewalk. In conclusion, the ADOPT pedestrian classification scheme is able to classify pedestrians accurately even in the presence of noisy signals. Figure 16 shows the effectiveness of ADOPT in classifying pedestrians near the car in noisy mode by reporting the effect of simultaneous transmission by pedestrians on the classification accuracy.

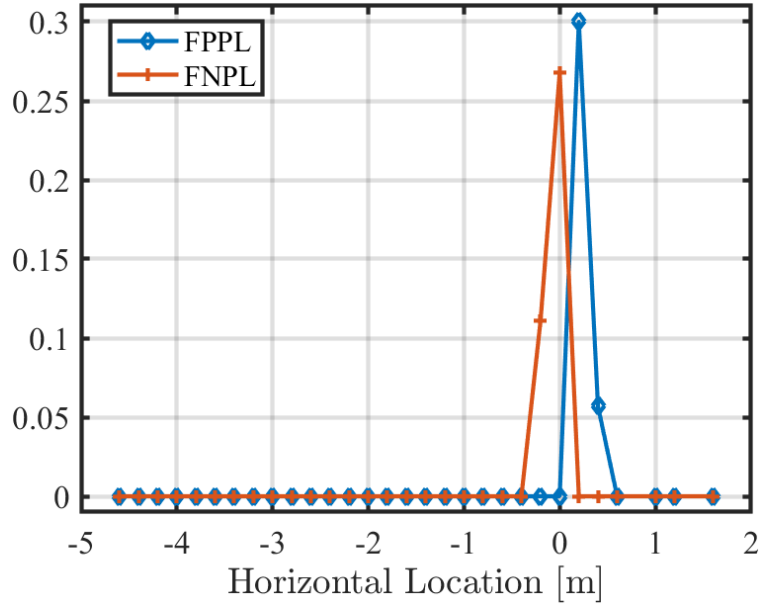


Figure 15. FPPL and FNPL are high only within 1 meter before and after the edge of the sidewalk with noisy signals.

3.7.4 Accuracy of Pedestrian Localization

To show the result in detail, we determined a 0.2-meters window of \hat{d} . Figure 17A shows that the aggregated absolute error $\xi_d = |\hat{d} - d|$ is zero in noise-free mode and does not exceed 1.5 meters in noisy mode.

Similarly, we determined a 0.2-meters window of \hat{y} to observe the absolute error at each window. The absolute error of y is $\xi_y = |\hat{y} - y|$. Figure 17B shows that the estimation of y in noise-free mode is accurate since we have zero aggregated error. However, the aggregated error increases in noisy mode. The errors are lower as pedestrians start crossing the street because they are closer to the main axis of the car (i.e. around $y = 1.3$) and the noise is low in this area as we showed previously in Figure 11A.

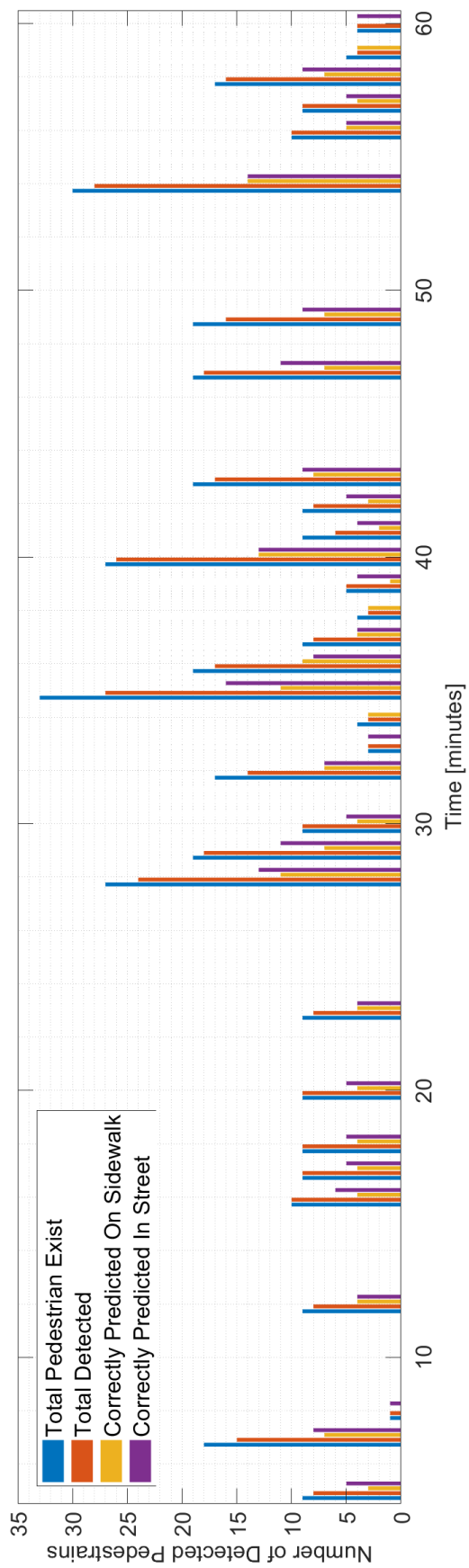


Figure 16. The effect of simultaneous transmission by pedestrians on the classification accuracy.

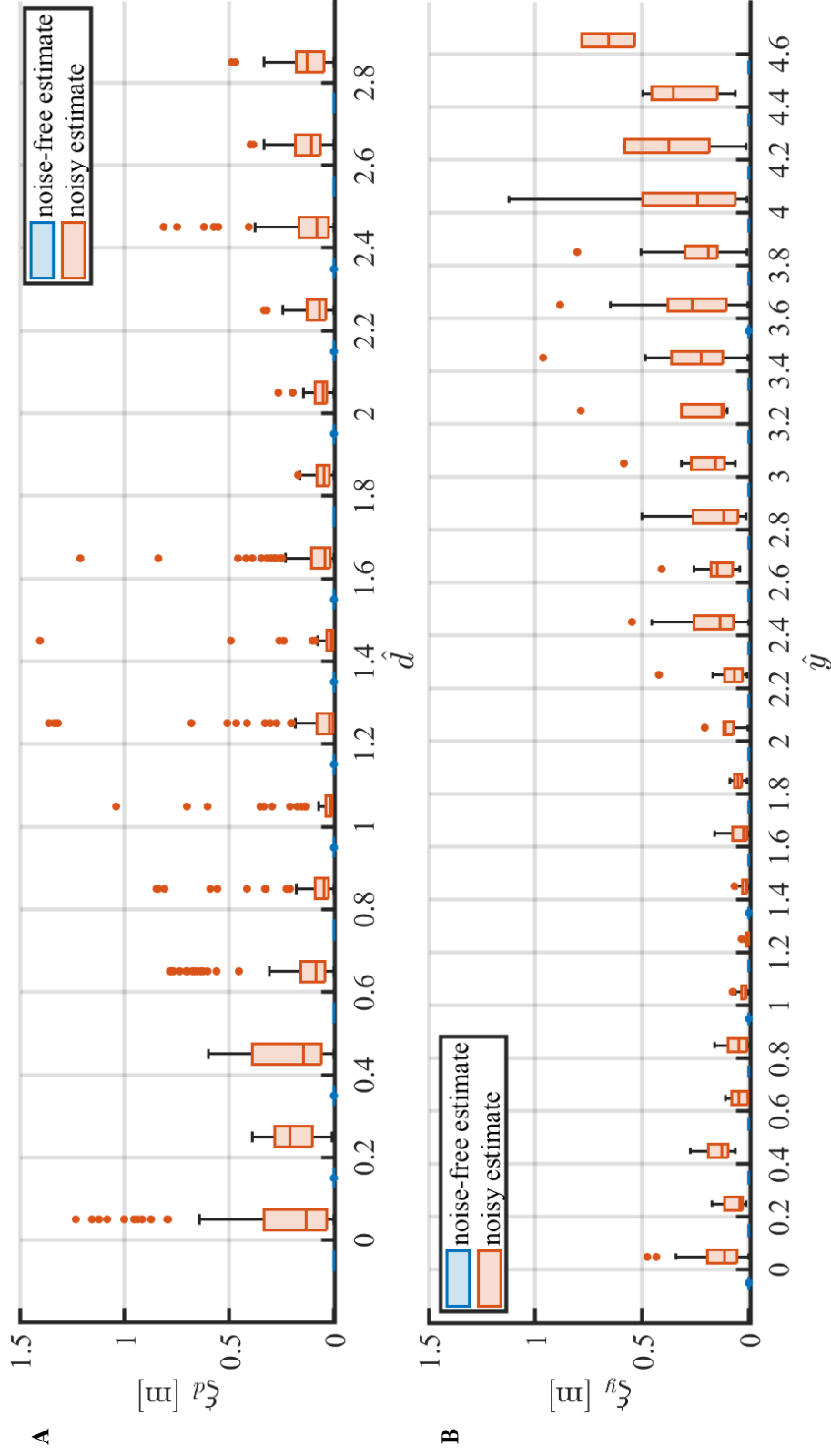


Figure 17. Distribution of localization error against the actual location (A) ξ_d against \hat{d} (B) ξ_y against \hat{y}

3.7.5 Accuracy of Crossing Speed Estimation

Figure 18A shows the Empirical Distribution Cumulative Function (ECDF) of the actual speeds, that are retrieved from SUMO, and the speeds that we estimate in noise-free and lastly, the speed estimate in noisy mode. The results showed that the noise affects the speed estimation as we can see from the difference between the actual and noisy estimates in the figure. In addition, we noticed that the difference between the actual and noise-free estimates is due to the change of the crossing cohort size, and this happens only when a new pedestrian joins the cohort. We show in Figure 18B the ECDF after removing the samples where a new pedestrian joins the cohort. As it can be seen in the figure, the difference between the estimated speed and the actual speed is lower when the cohort size is fixed.

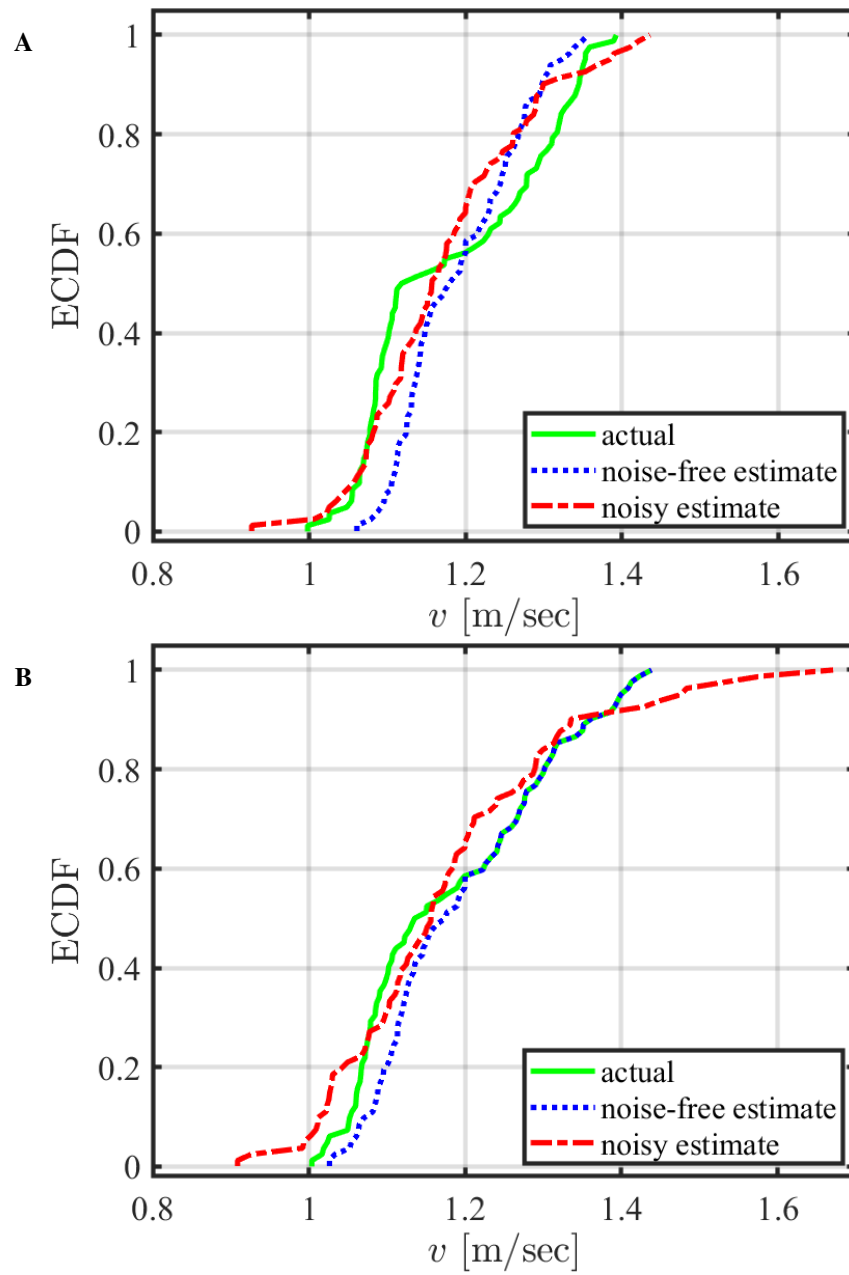


Figure 18. Distribution of localization error against the actual location (A) Dynamic Cohort Size
(B) Fixed Cohort Size

3.7.6 Accuracy of the Remaining Time to Cross

Figure 19A shows the ECDF of the average crossing time for each pedestrian in the street. We calculated the actual remaining crossing time based on the actual speed that is retrieved from SUMO. As the noise affects the speed, it also affects the remaining crossing time as we show in the figure. We noticed also that the difference between the actual and noise-free estimation is due to the change of the crossing cohort size, and this happens only the first time a new signal is detected in the crossing cohort. We show in Figure 19B the ECDF after removing the samples where a new pedestrian joins the cohort. As can be seen in the figure, the difference between noise-free estimate and the actual time to cross is lower.

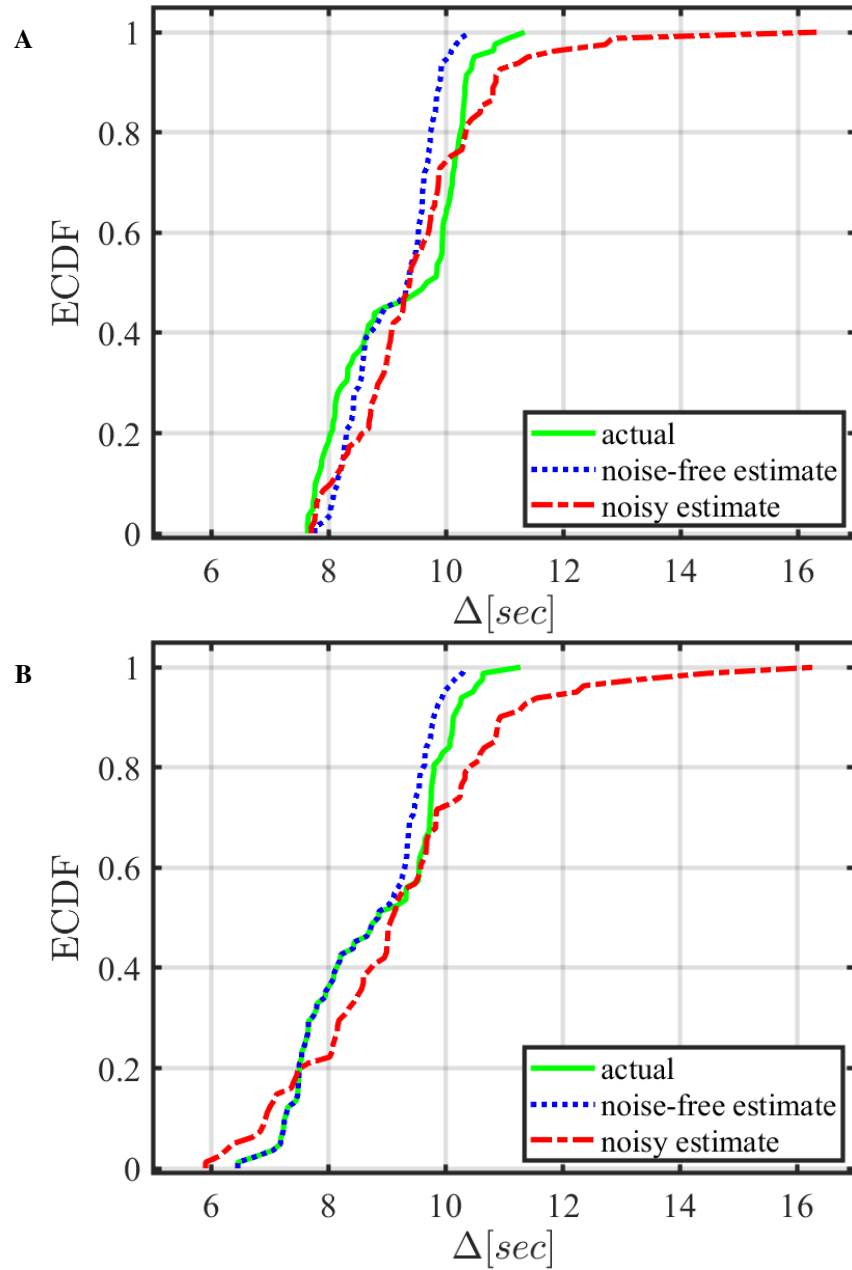


Figure 19. ECDF of remaining crossing time. (A) Dynamic Cohort Size (B) Fixed Cohort Size

3.7.7 Accuracy of Safety Zone Size

Figure 20 shows the ECDF for the propagation distance estimation averaged for each pedestrian in the dynamic and fixed cohort sizes. We noticed that the difference between the actual and noise-free estimate is less in the fixed cohort size. The difference between them increases based on the error of Δ estimation.

To justify the difference between the actual and estimated propagation distance, we measured the relative error of estimating Δ and D in noise-free mode for fixed size cohort compared to their actual values where the *relative error* = *actual value* – *estimated value*.

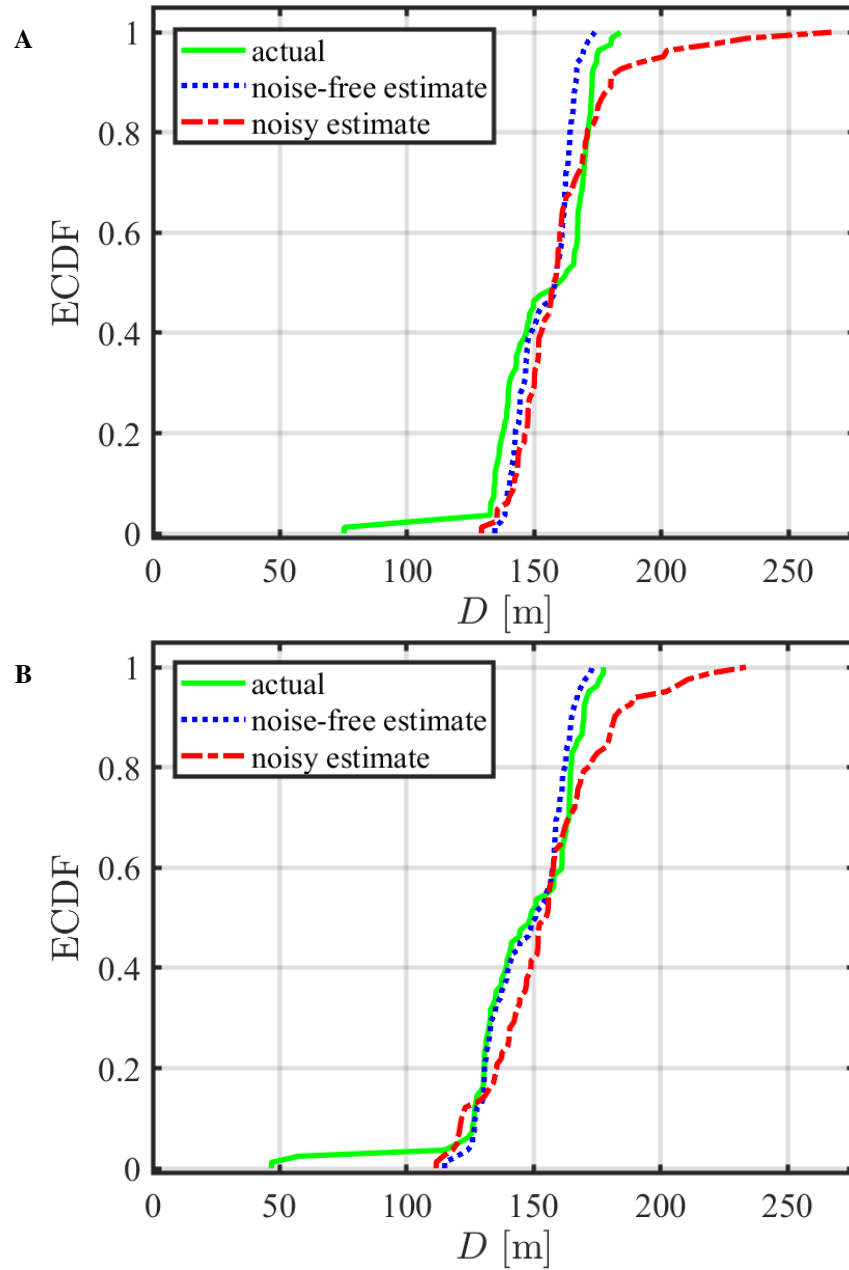


Figure 20. ECDF of propagation distance. (A) Dynamic Cohort Size (B) Fixed Cohort Size

The results showed that there is a high correlation between the relative error of estimating Δ and D as we show in Figure 21. The figure also shows that the majority of Δ errors are less than 3 seconds and cause about additional 40 meters of D . We see a high error in D since each ± 1 second of error in Δ is multiplied by the car's speed and the added r , so this second produces about ± 15 meters of D error. If the error is positive then ADOPT estimates a larger safety zone and the pedestrian is safe. Indeed, the risk may increase if the estimation is less than needed.

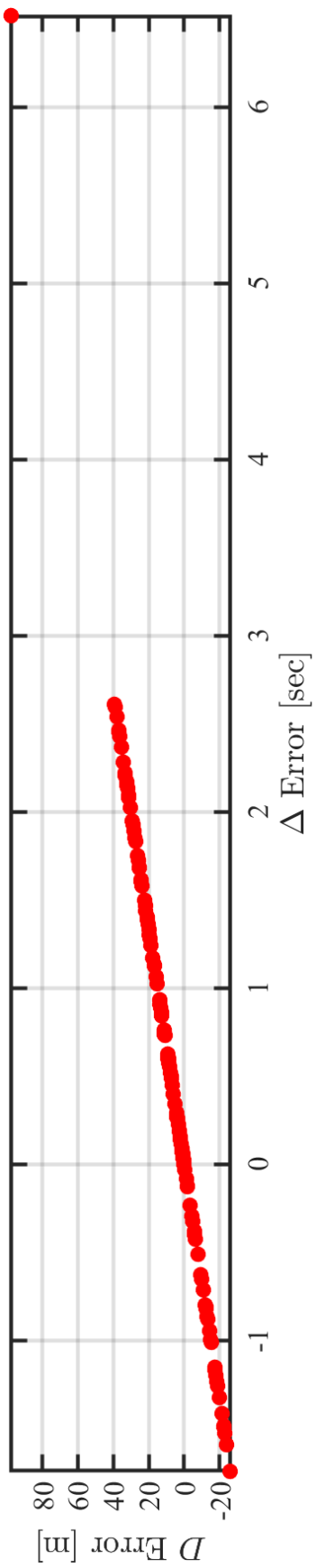


Figure 21. Correlation between the estimation error of D and Δ

In conclusion, the accuracy of the ADOPT classification depends on the amount of RSS noise that affects the $c(\Gamma)$ values near the edge of the sidewalk. For localization, the accuracy of ADOPT depends on the RSS noise and the distance of the pedestrian from the transceiver receiving the strongest signals. ADOPT accuracy in estimating the speed, remaining crossing time and Safety Zone size depends on the noise and changes in cohort size.

3.7.8 Evaluation of Occluded Pedestrian Protection

To evaluate the performance of ADOPT as an end-to-end system to protect occluded crossing pedestrians, we calculated the speed of the approaching car upon reaching the pedestrian crossing area. We assumed that the driver or the autonomous vehicle react to the "Caution" message promptly upon receiving it from the ADOPT app running in the car.

Referring to Figure 22, the approaching cars generated in SUMO adopt the new speed v_{safe} upon receiving the "Caution" messages as they approach the crossing pedestrians. We observed and aggregated the speeds at every 13-meters of car-to-pedestrians distances. As it can be seen also in the figure, the cars start maintaining their safe speeds gradually while they are approaching the crossing pedestrians which allows a smooth speed reduction without the need for a sudden stop. To compare the speed reduction caused by ADOPT with the speed of cars without ADOPT, we plotted their cruising speeds $v_{cruising}$ from SUMO in the same figure. We called it $v_{cruising}$ since SUMO cars do not maintain a fixed speed while moving, and also each car has its own speed random distribution with a determined maximum speed equal to the street's speed limit v_{max} .

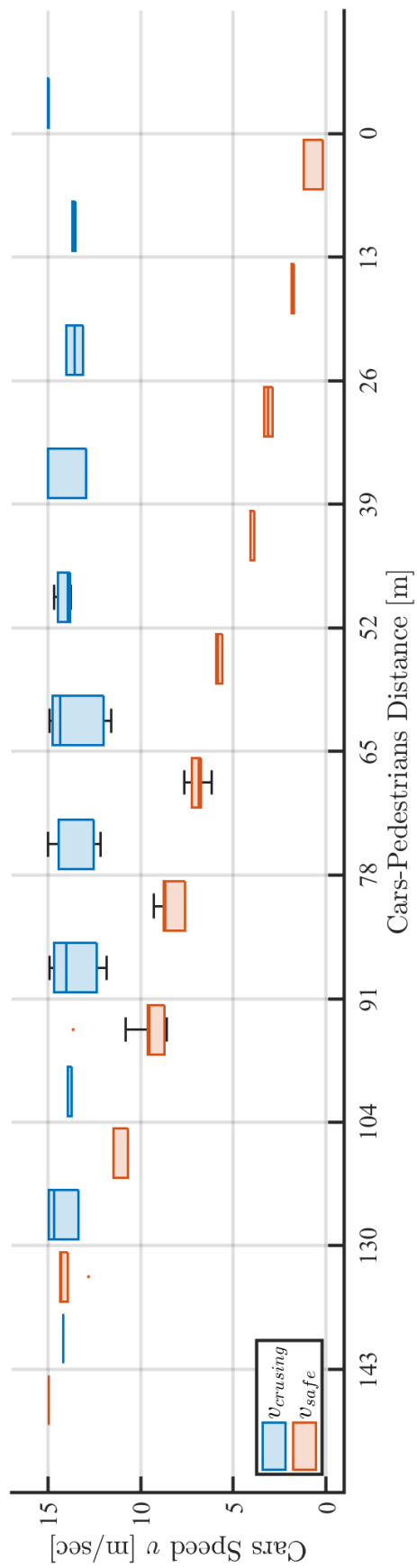


Figure 22. All approaching cars maintained safe speeds upon receiving the "Caution" message from ADOPT while they keep their cruising speeds without ADOPT "Caution" messages.

In the following, we show some examples from the simulation of approaching cars receiving the ADOPT "Caution" message and changing their speed accordingly. In Figure 23A, the approaching car with speed v_{max} receives a "Caution" message at location C and time $s1$ for a pedestrian crossing at location $L1$. The car reduces its speed to v_{safe} as a response to the alert message. We noticed that the car may intersect slightly before $(L1, e1)$ due to the error in estimating d and the crossing time Δ . In another example Figure 23B, the car receives another "Caution" message at location C' as a new pedestrian joins the cohort from the same location of L , and finishes crossing at $e2 > e1$. In this case, the car finds that the new speed (denoted by $v_{safe'}$) is lower than v_{safe} , so it adopts the new speed $v_{safe'}$ to avoid the collision. The expected reaction of the approaching car is to reduce its speed because the crossing time now becomes longer as a new pedestrian joins the cohort.

In a more complex example, cars report pedestrians at different locations $L1$ and $L2$ as in Figure 23C. When the car receives a new "Caution" message at time $s2$ and location C' , it calculates the new speed and finds that it is less than its current speed because $L2$ is closer than $L1$. Thus, it adopts the new speed $v_{safe'}$ until the pedestrian finishes crossing. In conclusion, approaching cars were able to maintain low speeds to avoid collision with the occluded crossing pedestrian accurately and in a timely manner based on the "Caution" messages received from ADOPT. This shows that ADOPT works end-to-end to effectively protect crossing pedestrians.

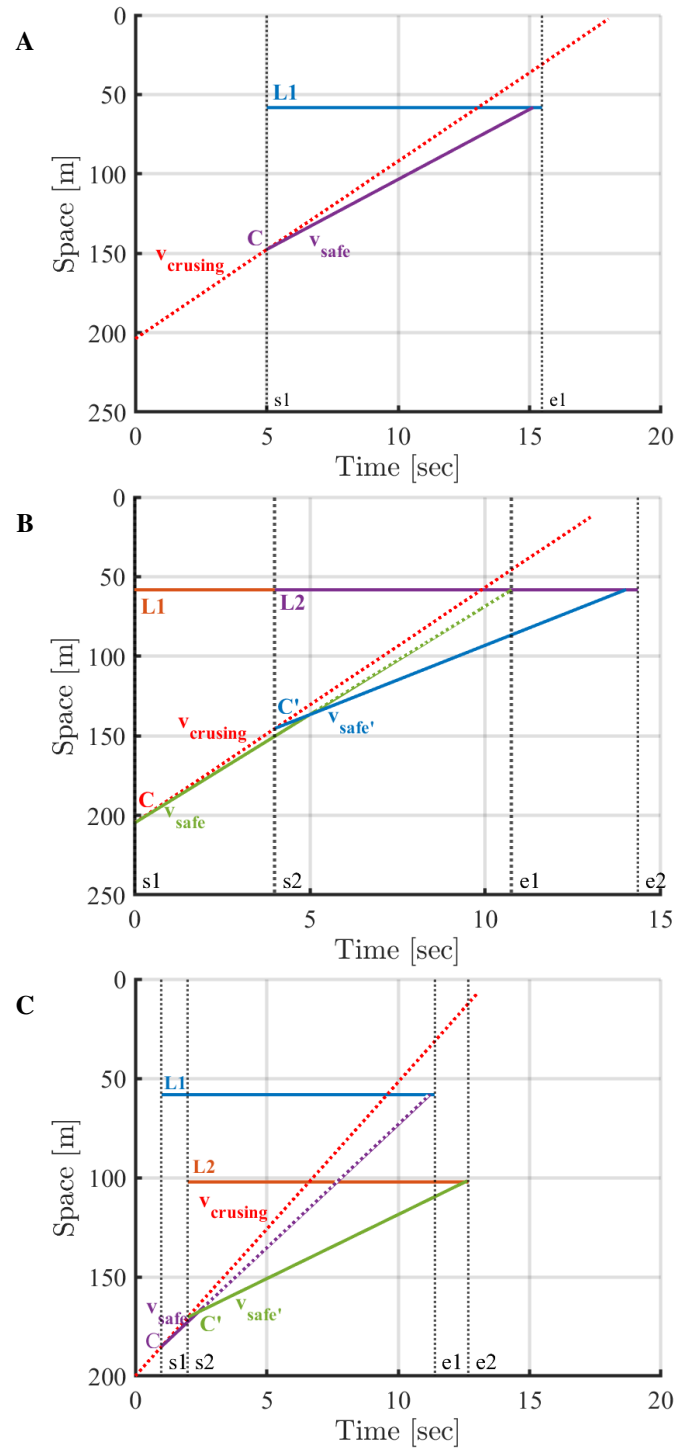


Figure 23. Moving vehicle reduces its speed upon receiving "Caution" message from ADOPT in many cases. (A) One pedestrian crossing the street. (B) Multiple pedestrians crossing the street at the same location. (C) Multiple pedestrians are crossing the street at different locations.

3.7.9 The Effect of Number of Transmitting Pedestrians on the Detection Rate

Although we assumed that the detection rate is 100%, that is all the transmitting pedestrians are detected at each second based on the sampling rate of the transceivers, we assessed the ability of the transceiver to detect all the transmitting pedestrians at each second when the sampling rate is 50 sample per second. Figure 24 shows that the transceiver may miss 0 pedestrians transmitting at the same second until there are more than 7 pedestrians, then the missing rate increases. These calculation are based on the estimated number of clear transmissions in Equation 15.

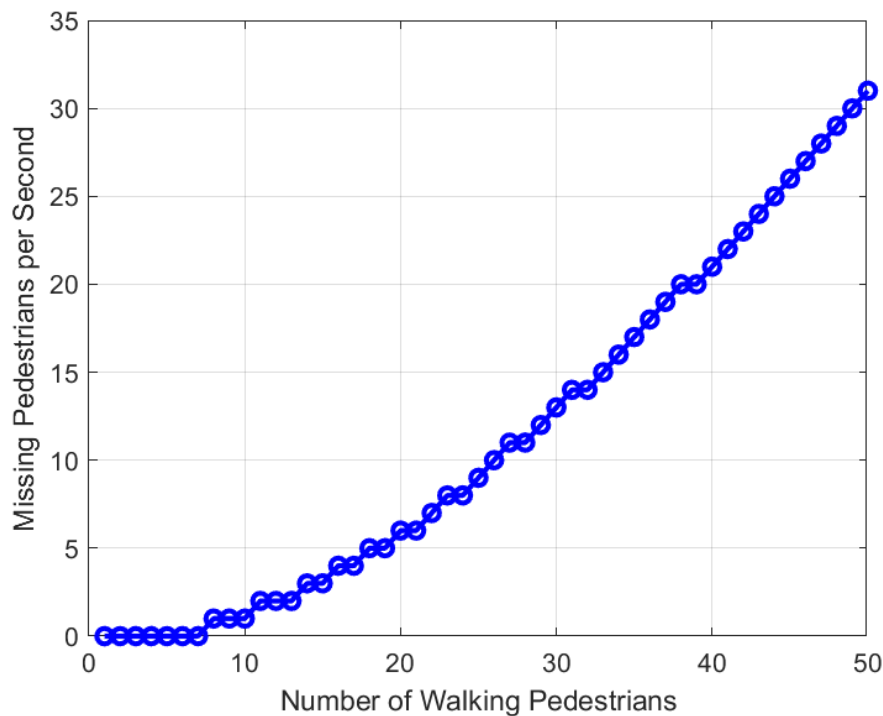


Figure 24. The expected number of missing pedestrians versus the number of transmitting pedestrians around the transceiver if sampling rate is 50 Hz.

In addition, we have investigated the various sampling rates that can accommodate 100 pedestrians who send signals at the same time. The sampling rate is adjustable feature in the transceiver and can be determined by the data rate of the transceiver. In Figure 25 shows the possible number pedestrians that can be detected each second if they transmit signals at the same time using different values of sampling rates.

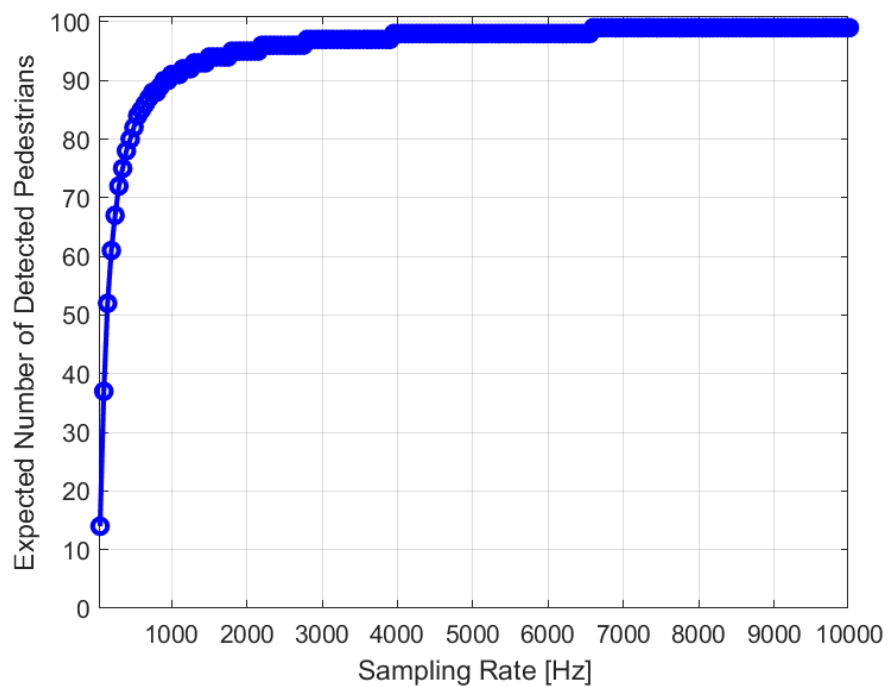


Figure 25. The expected number of detected pedestrians versus several sampling rates if there are 100 pedestrians transmitting at the same second.

3.7.10 The Time Performance of ADOPT Calculations

To estimate the processing time on a low-specification microcontroller, we measured the processing time of the process that we perform in ADOPT simulation in the parked car side on device A (Intel Core i7-155U PC). Then, we calculated the ratio between device A and device B (TMS320F280039C Microcontroller) from Texas Instruments [85]. After that, we calculated the ratio between device A specifications and device B specifications, then multiplied the ratio by the processing time from device A. Table 7 summarizes the specifications of both devices.

Table 7. Specifications and calculated ratios for Device A and Device B

Specification	Device A (Intel Core i7-155U PC)	Device B (TMS320F280039C Microcontroller)	Calculated Ratio
CPU Speed	1.7 GHz	0.120 GHz (120 MHz)	14.17
Number of Cores	10	1	10
RAM Speed	3200 MHz	100 MHz	32
RAM Size	16 GB	0.384 GB	41.67

Figure 26 illustrates the average processing time for different calculation processes in ADOPT. The processes include calculating δ_{RX} , y , d , v , Δ , and D with the classification computation. "Total" bar represents the overall average processing time for all calculation tasks combined. These results show the approximated processing time for ADOPT which is expected to be very low.

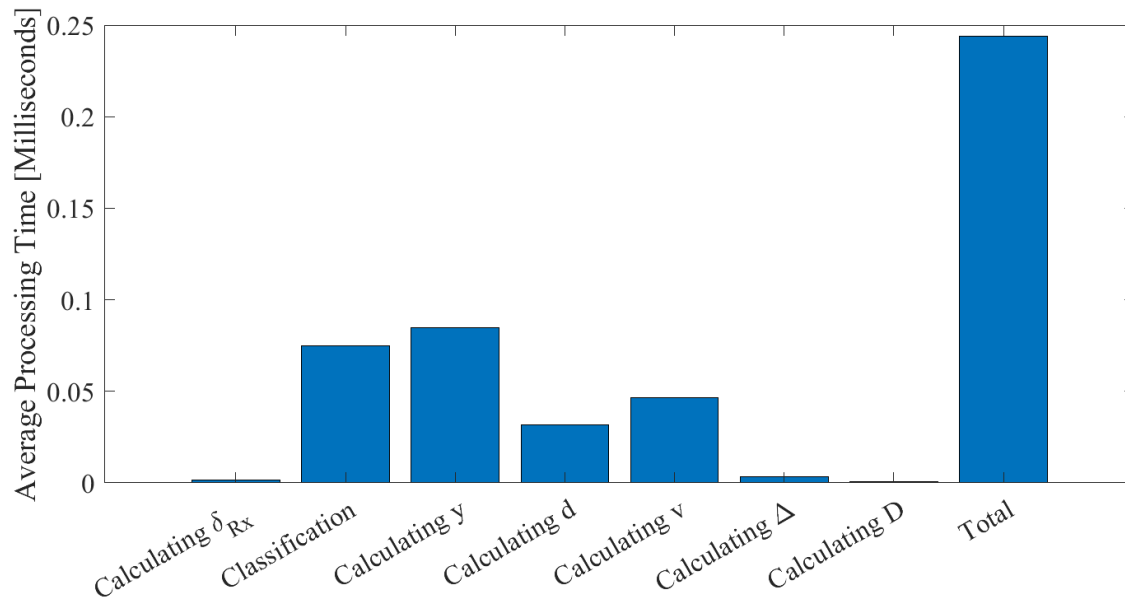


Figure 26. The average processing time for different ADOPT calculations and the total of combined processes.

3.8 CONCLUDING REMARKS

The common philosophy of all pedestrian detection approaches that we are aware of is that this task should be undertaken by the moving cars themselves. In a sharp departure from this philosophy, we proposed to employ cars parked along the sidewalk to detect and protect crossing pedestrians.

In support of this goal, we have proposed ADOPT: a system for Alerting Drivers to Occluded Pedestrian Traffic. ADOPT lays the theoretical foundations of a system that uses the on-board resources of parked cars to:

- Detect the presence of a group of crossing pedestrians – a crossing cohort;
- Predict the time the last member of the cohort takes to cross the street;

- Send alert messages to those approaching cars that may reach the crossing area while pedestrians are still in the street;
- Show how approaching cars can adjust their speed to avoid crashing into crossing pedestrians.

Importantly, in ADOPT communications occur over very short distances and at very low power. Our extensive simulations using SUMO-generated pedestrian and car traffic have shown the effectiveness of ADOPT in detecting and protecting crossing pedestrians.

In spite of this, there are a number of topics that need more work:

- First, it is important to consider cars that are not parked parallel to the sidewalk, e.g., cars that are parked at an angle;
- Second, we will investigate the problem of information overload. The problem arises when the (human) driver of an approaching car is alerted to the presence of various crossing cohorts. We are planning to design an app that minimized the information overload and, consequently, driver distraction;
- Third, it is of interest to optimize the process of disseminating alert messages as a function of the residual crossing time. In the current work “All clear” messages informing approaching cars that the cohort has finished crossing are not used. Incorporating them into ADOPT is targeted for future work;
- Fourth, it is important to investigate the additional fuel consumption, if any, attributable to ADOPT. We conjecture that ADOPT does not result in increased fuel consumption. Along

the same line of thought, it is important to investigate the effect of ADOPT on pollution and gas emissions;

- Fifth, in this dissertation, we have assumed that the sidewalk is modeled by a straight line. However, in many cases, the geometry of the street is vastly different, with curvilinear sidewalks prevailing. Naturally, this general geometry of the sidewalk presents more opportunities for occluded pedestrian traffic. It is important to extend ADOPT to handle gracefully this general scenario;
- Last, but certainly not least, security and privacy are very important and are getting active attention as discussed in the next section.

3.8.1 Security and Privacy in ADOPT

ADOPT involves two types of wireless communications: V2P and V2V. In the following, we discuss the security aspects of our communication types.

- Pedestrian-to-parked vehicle communications: In the pedestrian detection and localization process, the system reads transmitted signals and makes decisions based solely on the signal strength and not on the identity of the pedestrians. These decisions are based on anonymous received signal strengths that do not require unique identifiers. Also, ADOPT detects and localizes pedestrians in short-range communications that do not require transmitting the pedestrians' private data. With the proposed mechanism of pedestrian localization, ADOPT preserves pedestrians' privacy and security. In spite of this, we may consider a potential attack that may be mounted against ADOPT such as a Denial of Service (DoS) attack. In this attack, a group of pedestrians may stomp their feet on the ground to activate the system.

Our approach to pedestrian classification can distinguish if the signal is coming from the sidewalk or the street. If this group of people is generating signals from the street, they are at risk and the system should notify approaching cars regardless of their intent.

- **Parked vehicle to approaching vehicle communication:** This type of communication involves known security threats in V2V communications [8]. However, the short-range communication used in our system should allow the use of frequency hopping [56] to prevent attackers from sniffing or injecting fake information into V2V network. Moreover, short-range V2V communications have their security advantages [68] that are not present in long-range V2V communications. It is of great interest to develop security primitives that leverage the type of short-range communications that are used throughout the system [84].

CHAPTER 4

EVALUATING THE ENERGY DEMAND MODEL FOR ESTIMATING FUEL CONSUMPTION AND CO₂ EMISSIONS

In this chapter, we aim to answer the second research question **RQ2**: Can we accurately estimate the instantaneous fuel consumption and CO₂ emissions using the energy demand model?. Evaluating the energy demand model using publicly available data will enable us to apply it directly to our user-defined driving cycles, as we will show in Chapter 5.

In this chapter, we first evaluate the fuel consumption and CO₂ emission estimates produced by the energy demand model and to compare them to official measurements published by the EPA. Moreover, we demonstrate the ability of the energy demand model to be generalized to various driving cycles, including user-defined driving cycles and a variety of car models.

We describe our methodology in Section 4.1. Our results and sensitivity analysis are presented in Section 4.2. Finally, Section 4.3 offers concluding remarks and outlines directions for future research.

4.1 METHODOLOGY

The main goal of this section is to discuss, in some detail, the methodology followed for conducting this study.

4.1.1 Instantaneous Energy Demand Model

The energy demand model is a physics-based model that estimates the energy required to move

a car from point to point through a driving cycle. It takes as input the speed profile and the car specifications that affect the tractive force. The complexity of the energy demand model might vary depending on the number of input parameters. The selection of the energy-demand model depends on the availability of data to input into the model. In this work, the simple version of the energy demand model that was used by Jones [35] is used to estimate the instantaneous energy demand.

In the i -th second of the driving cycle, the instantaneous energy demand E_i (in *Joules*) can be estimated based on the car's dynamics as follows:

$$E_i = \begin{cases} m a_i v_i + f_0 v_i + f_2 v_i^3, & \text{for } a \geq 0 \\ 0, & \text{for } a < 0 \end{cases} \quad (30)$$

where m is the mass of the car in kilograms kg , a_i is the average acceleration of the car in the i -th second (in m/sec^2), and v_i is the current speed in m/sec . The model also uses f_0 , and f_2 that are the rolling resistance and the aerodynamic drag, respectively. These parameters play important role in the car movement. These terms represent the forces that the car needs to overcome while moving [26].

In accordance with other workers in [13], [26], [35] it is assumed that the energy demand during deceleration is zero since the engine does not provide power to the wheels while decelerating (i.e., negative acceleration). Similarly, the energy demand during idling (i.e., when speed is zero) is assumed to be zero as the car shuts down the engine if it stops for more than a few seconds, following the stop-start mechanism [31]. It is also assumed that this model is applied to conventional vehicles, where the energy used to overcome the inertia of the vehicle while braking is lost as heat due to friction.

It follows that the total instantaneous energy demand, E_{inst} , of the car in the interval $[0, T]$ is calculated as:

$$E_{inst} = \sum_{i=0}^T E_i \quad (31)$$

where T is the total number of seconds in the driving cycle of interest.

4.1.2 Estimating Fuel Consumption

The energy demand resulting from the calculations of Equation 30 can be used to obtain the amount of fuel expended to satisfy that demand. However, this equation only estimates the energy demand to overcome the road load and the mass forces (also called Energy to the Wheels) while a large amount of fuel is expended on the working of the internal parts of the car (i.e., the powertrain).

The fuel energy expended can be calculated knowing η , which is the efficiency of the powertrain to convert the fuel into mechanical energy to move the car. Once η is obtained, the fuel consumption can be estimated theoretically by the following formula that we adopt from Thomas [88]:

$$E_{Fuel} = \frac{E_{inst}}{\eta}, \quad (32)$$

where E_{Fuel} is an estimate of the expended fuel energy in *Joules*.

4.1.3 Determining η -- the Powertrain Efficiency

In his early work, Jones [35] used $\eta = 0.17$ as this value was determined by dividing the energy demand by the fuel energy that was measured experimentally. Due to advances in the car industry, the efficiency of cars to convert fuel into mechanical energy has increased [62], [88]. Therefore, an updated value for η is needed to estimate fuel consumption accurately. This value can be determined knowing the specifications of the car engine [13], [26]. Although these specifications

are not directly available to researchers in most cases, straightforward alternative approaches can be used to determine the value of η . In this study, the following approaches are applied:

- *Constant efficiency*: The simplest way to obtain updated values for η is to use the constant values reported by the EPA in [93]. The values [0.20, 0.16] are used for the urban driving cycle and [0.30, 0.25] for the highway cycle. Here, each pair represents the upper limit and the mean of the upper and lower limits of the percentage of fuel energy that is delivered to the wheels to move gasoline-fueled cars from the total expended energy;
- *Estimating the efficiency*: Another approach is to estimate the powertrain efficiency, as described by Jones [35] and Thomas [88]. This can be achieved by dividing the estimated energy demand by the measured fuel consumption. This value is chosen assuming that the measured fuel is known and can be obtained from the EPA datasets.

Specifically, the instantaneous efficiency η_i can be estimated from the instantaneous fuel consumption data provided by Argonne National Lab (ANL) [7] by employing the following formula as described in [88]:

$$\eta_i = \frac{E_i}{E_{Fuel_i}}, \quad (33)$$

where E_{Fuel_i} is the instantaneous fuel energy expended. E_{Fuel_i} is obtained by converting the fuel consumption from gallons [gal] to Joules, where 1 gal of fuel releases 120000000 Joules of energy. It is worth mentioning here that this value uses the measured (actual) fuel consumption. Although the results will be accurate, they may not be reliable, given that the actual data is used in the estimation process. This value is assumed to be the actual efficiency of the car, and it is beneficial to get some idea about the powertrain's efficiency;

- *Predicting the instantaneous efficiency:* The value of η can be predicted given that the instantaneous fuel consumption and energy demand for some cars are available and can be accessed. To predict the value of η using instantaneous data, a linear regression model is designed in this work using instantaneous test data for CAMRY XLE 2018 [7]. The model uses instantaneous speed and acceleration as predictors and produces instantaneous efficiency. Those two parameters were chosen because they are the only available data for predicting the value of the other cars. Data preprocessing is applied to eliminate idling and deceleration intervals prior to training. The linear regression model is designed assuming a linear relationship between the predictors and the instantaneous efficiency that is calculated using Equation 30. The trained model is used on other cars to predict their instantaneous powertrain efficiency η_i . It should be noted here that, as the model is trained only on one car's data, so it may not be sufficient to be applied to other cars.

4.1.4 Estimating CO2 Emissions

Extended EPA tests [94] have revealed that CO₂ emissions are highly correlated with the fuel consumed. Based on this, CO₂ emissions in grams per *KJoules* can be estimated given the expended fuel energy E_{Fuel} based on the EPA-prescribed formula in [94], which estimates the CO₂ as follows:

$$\text{CO}_2 = E_{Fuel} \times \text{Carbon Content} \times \text{Oxidation Fraction} \times \left(\frac{44}{12} \right), \quad (34)$$

where the Carbon Content is 0.0196 grams/Kilojoules and the Oxidation Fraction is 0.99, and the value $\frac{44}{12}$ is the molecular mass of CO₂.

The estimated CO₂ emissions are then compared with the emissions reported in [91] to eval-

uate how well the energy estimated by the energy demand model can be used to estimate these emissions. Furthermore, EPA CO₂ emissions are calculated by inserting the fuel energy measured by EPA E_{Fuel} in Equation 34.

4.1.5 Data Collection and Preprocessing

The purpose of this section is to provide a detailed illustration of the data collection to be used in the study. Figure 27 provides a summary of the data collection and the various processing steps involved.

The car specifications are first obtained from EPA Test Car Data files [91]. The speed profiles of the selected driving cycles are obtained from the EPA Dynamometer Driving Schedule [92]. The measured fuel consumption for those driving cycles is obtained from EPA test car and ANL data, which are then used to evaluate the estimations from the energy demand model.

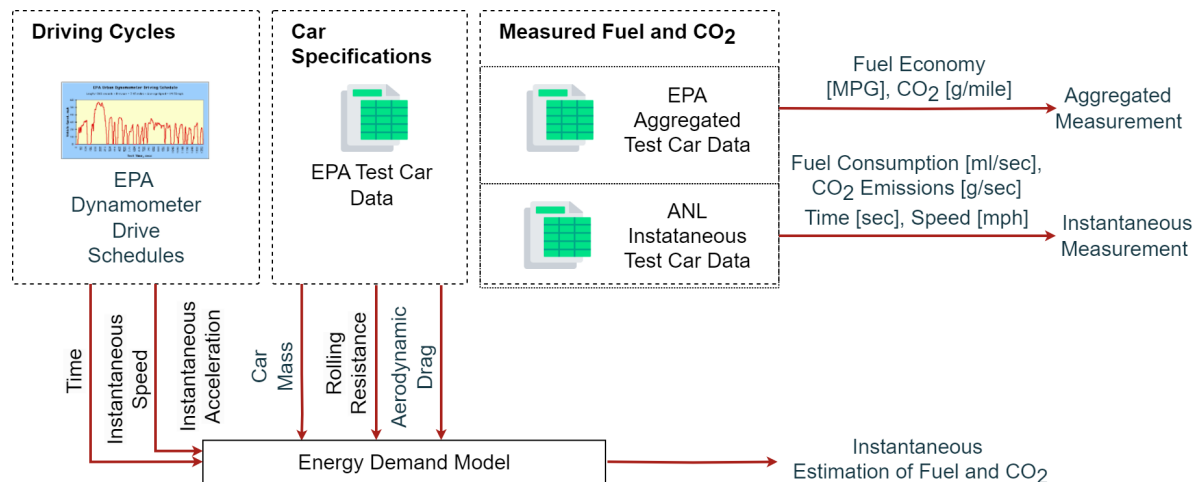


Figure 27. An illustration of our methodology to obtain the required data for the estimation and the evaluation processes.

Driving cycles

We used the energy demand model to estimate instantaneous (i.e., second-by-second) fuel consumption. Therefore, instantaneous speed and acceleration data of the car is required to estimate its energy demand. The speed profile is obtained from EPA Dynamometer Drive Schedules [92]. These schedules contain the time steps in seconds and the speed of the car in miles per hour (mph) during the test, and the acceleration is derived from the recorded speed. To evaluate the energy demand model, two driving cycles were selected. The first driving cycle is the EPA Urban Dynamometer Driving Schedule (UDDS), which represents the city driving conditions. The second cycle is the Highway Fuel Economy Driving Schedule (HWFET) which mimics highway driving conditions. The speed profile of the test car in both driving cycles is shown in Figure 28. Additional details about the selected driving cycles are shown in Table 8.

Table 8. Driving cycles details.

Cycle	Type	Average Speed	Distance	Duration
UDDS	City	19.59 mph	7.45 miles	1369 s
HWFET	Highway	48.3 mph	10.26 miles	765 s

To extract the required data from [91] files in a way that suits the selected driving cycles, the *TestCategory* field values 'FTP' and 'HWY' were chosen for UDDS and HWFET driving cycles, respectively.

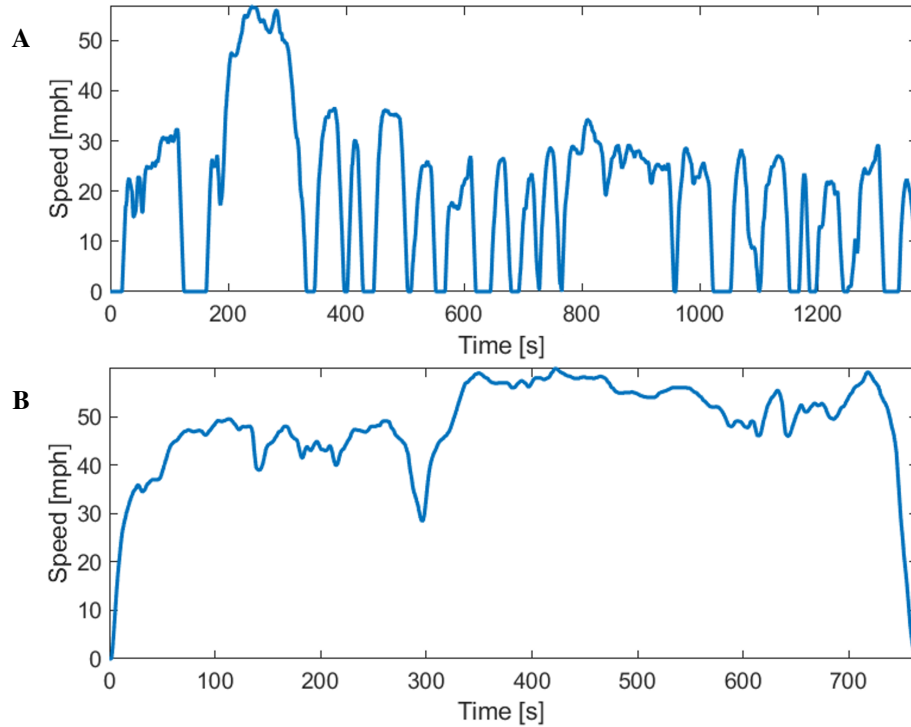


Figure 28. Speed profile for the driving cycles used. (A) UDDS cycle. (B) HWFET cycle.

Car specifications

As the energy demand model requires the car specifications to estimate its energy demand, these specifications have to be obtained from a publicly available dataset. Specifically, [91] provides data files that include test car specifications and the fuel consumed during laboratory tests for specific driving cycles. The data extracted is for the year 2023 test car list data. The car specifications obtained from this file are: the rolling resistance force f_0 (the unit used is Newton [nt]), the aerodynamic drag force f_2 (the unit used is Newton per mile per second squared [nt/mps^2]), and the mass in kilograms [kg]. The required unit conversions are done to ensure compliance with the energy demand model in Equation 30. These specifications are the inputs to the energy demand model.

Initially, several cars are randomly selected for the evaluation to ensure that the data used for the evaluation is free of errors or missing entries. Table 9 shows the list of selected cars and their specifications that are entered to the energy demand model. To further evaluate the energy demand model on a larger set of cars with their different specifications, all cars in the dataset will be included.

Table 9. Car specifications as obtained from EPA test car data (with unit conversion).

Car Model	Type	Mass [kg]	f_0 [nt]	f_2 [nt/mps ²]
Volkswagen Jetta	Car	1473.923	91.9	0.37
CHEVROLET MALIBU	Car	1587.302	135.5	0.46
HONDA ACCORD	Car	1643.991	188.2	0.55
TOYOTA CAMRY XLE/XSE	Car	1700.68	144.7	0.38
BMW 330i Sedan	Car	1757.37	198.4	0.42
Ford Edge	Truck	2040.816	142.2	0.59

Measured fuel consumption and CO₂ emissions data

The measured fuel and CO₂ emissions are obtained from the instantaneous dataset provided by ANL and the aggregated dataset provided by EPA.

- *Instantaneous measurement:* The instantaneous test car dataset provided by ANL [7] is used to evaluate the accuracy of the energy demand model estimates. At the time of writing

this work, the latest available instantaneous sedan data from ANL is for TOYOTA CAMRY XLE/XSE 2018 and HONDA ACCORD LX 2018. The obtained instantaneous fuel consumption is measured in gallons per second [gal/sec]. The dataset also includes the instantaneous CO₂ emissions during the laboratory tests, measured in milligrams per second [mg/s]. Additional steps are taken for unit conversion. Furthermore, additional preprocessing is required to synchronize the data provided. In the dataset, the data are sampled every 0.1 seconds, while the dynamometer test speed profile is sampled every second. Therefore, the measured data is down-sampled by choosing the nearest sample time in the speed profile entries.

- *Aggregated measurement:* For obtaining the measured fuel consumption during the laboratory test cycles, EPA provides aggregated fuel economy FE of existing cars in miles per gallon [mpg] in [91]. EPA test car files specify the fuel type that is used in the test. Additional steps are taken to convert [mpg] to the total gallons spent during the driving cycle as follows:

$$F_{Measured} = \frac{1}{FE} \times d, \quad (35)$$

where d is the total distance (in miles) traveled during the driving cycle.

The dataset also includes the aggregated CO₂ emissions during the laboratory tests measured in grams per mile [g/mi]. Again, additional steps are taken for unit conversion.

4.2 RESULTS AND ANALYSIS

In this section, the energy demand model is evaluated to demonstrate its accuracy in estimating fuel consumption and, consequently, the CO₂ emissions based on the speed profile for the selected

driving cycles and several car specifications. The energy demand model is evaluated using the selected values of η described in Section 4.1.3.

4.2.1 Overall Results

- *Constant Efficiency* $\eta = 1$: This value is chosen assuming that all the expended fuel is converted to mechanical energy to move the car through the driving cycle and that the powertrain loss is zero. While unrealistic, this value is chosen to assess the amount of the estimated energy compared to the measured energy. This value produced large differences in most cases. This is expected because, as indicated by EPA [93], a large amount of fuel that is not considered in the energy demand model is lost in the internal parts of the engine;
- *Constant Efficiency* $\eta = [0.20, 0.16]$ and $\eta = [0.3, 0.25]$: These values are chosen to represent the percentage of fuel energy that is delivered to the wheels to move gasoline-fueled cars as described in Section 4.1.3. $[0.20, 0.16]$ are better aligned with the EPA measurements for city driving cycle, and $[0.3, 0.25]$ are better aligned with the highway driving cycle;
- *Estimated η* : The estimated values of η for individual cars as described in Section 4.1.3 were applied here to estimate fuel consumption. These values were used in the evaluation, assuming that the actual fuel consumption is known. The estimated values of η for the selected cars are shown in Table 10;

The results show that the lowest errors in fuel estimation resulted from using these values. However, these results are not reliable because actual measurements were used to estimate fuel consumption and CO₂.

Table 10. Estimated η for the selected cars.

	Volkswagen	CHEVROLET	HONDA	TOYOTA	BMW	Ford
	Jetta	MALIBU	ACCORD	CAMRY XLE/XSE	330i Sedan	Edge
UDDS Estimated η	0.2056	0.21261	0.25574	0.21599	0.220750	0.18871
HWFET Estimated η	0.23079	0.2357	0.30457	0.24099	0.25763	0.22747

- *Predicted η* : Based on the designed linear regression model in Section 4.1.3, the mean of predicted values of η for TOYOTA CAMRY XLE 2018 is 0.20609 for the UDDS driving cycle and 0.30613 for the HWFET driving cycle. These values are close to the values reported by the EPA [93]. These values produced an accurate instantaneous estimate even though they were obtained by training the model on TOYOTA CAMRY XLE 2018. This indicates that the predicted instantaneous efficiency was able to estimate the fuel consumption and CO₂ accurately. However, this approach requires training on several cars, and obtaining the instantaneous data which are not always available.

4.2.2 Estimating Fuel Consumption Using Instantaneous ANL Data

The energy demand model is evaluated using instantaneous ANL data for TOYOTA CAMRY XLE 2018 and Honda Accord LX 2018. Figure 29 shows the instantaneous estimate for TOYOTA CAMRY XLE using the chosen values of η . The figure shows that in both driving cycles, the energy demand model was able to capture the changes in fuel consumption based on the changes in car dynamics, except during deceleration and idling, regardless of the used value of η .

The root mean square error (RMSE) was used to quantify the error of estimating the instanta-

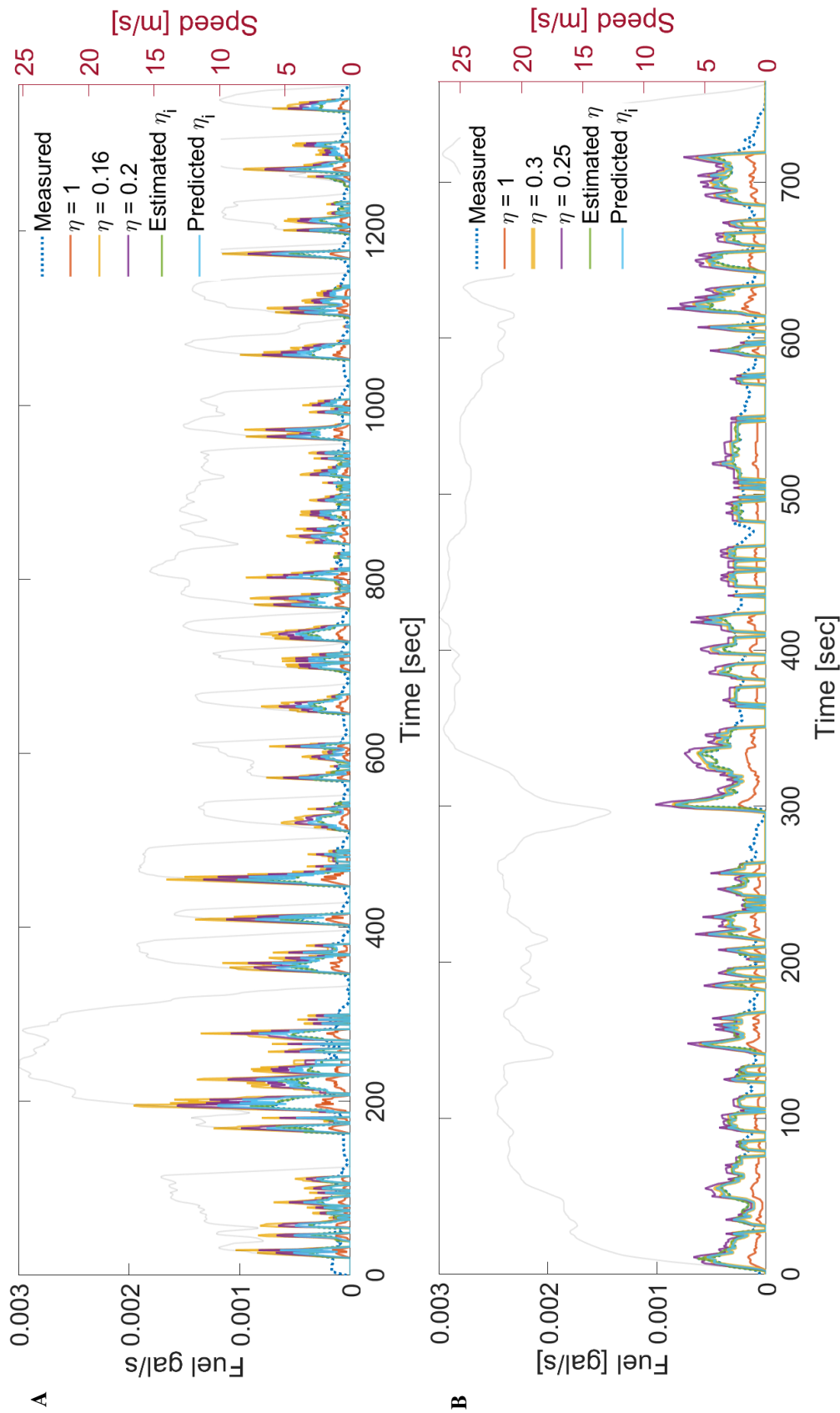


Figure 29. Instantaneous fuel consumption for CAMRY XLE/XSE estimated using several values of η . (A) UDSS cycle. (B) HWFET cycle.

neous fuel consumption and CO₂ emissions. The formula for the RMSE of fuel consumption is:

$$RMSE_{Fuel} = \sqrt{\frac{\sum_{i=1}^N (F_{i_{Measured}} - F_{i_{Estimated}})^2}{N}}, \quad (36)$$

where $F_{i_{Measured}}$ and $F_{i_{Estimated}}$ are, respectively, the measured and estimated fuel consumption in second i , and N is the total number of data samples. As it mentioned above, $F_{i_{Measured}}$ is obtained from the ANL dataset. Table 11 shows that the $RMSE_{Fuel}$ for both cars in both driving cycles is high when $\eta = 1$, and low when using the selected $\eta = 0.16$ and 0.20 . Both values can be used to accurately estimate instantaneous fuel consumption.

Table 11. $RMSE_{Fuel}$ [gal/sec] for the selected cars.

Car Model	Cycle	$\eta = 1$	$\eta = 0.16$	$\eta = 0.20$	Estimated η_i	Predicted η_i
ACCORD	UDDS	0.0001346	0.0001885	0.0001282	0.0000588	0.0000840
	HWFET	0.0002002	0.0001121	0.0001268	0.0001057	0.0001118
CAMRY	UDDS	0.0001427	0.0002063	0.0001401	0.0000599	0.0000904
	HWFET	0.0001961	0.0001178	0.0001417	0.0001042	0.0001165

For CO₂ emission estimation error, the instantaneous estimate is obtained using Equation 34 and was compared with the instantaneous measurements from ANL. Figure 30 shows the instantaneous CO₂ emissions measured by ANL and our estimated results. The figure shows that the instantaneous CO₂ emissions were captured quite accurately by using the estimated fuel energy.

$RMSE_{CO_2}$ is also calculated as

$$RMSE_{CO_2} = \sqrt{\frac{\sum_{i=1}^N (CO_{2i_{Measured}} - CO_{2i_{Estimated}})^2}{N}}, \quad (37)$$

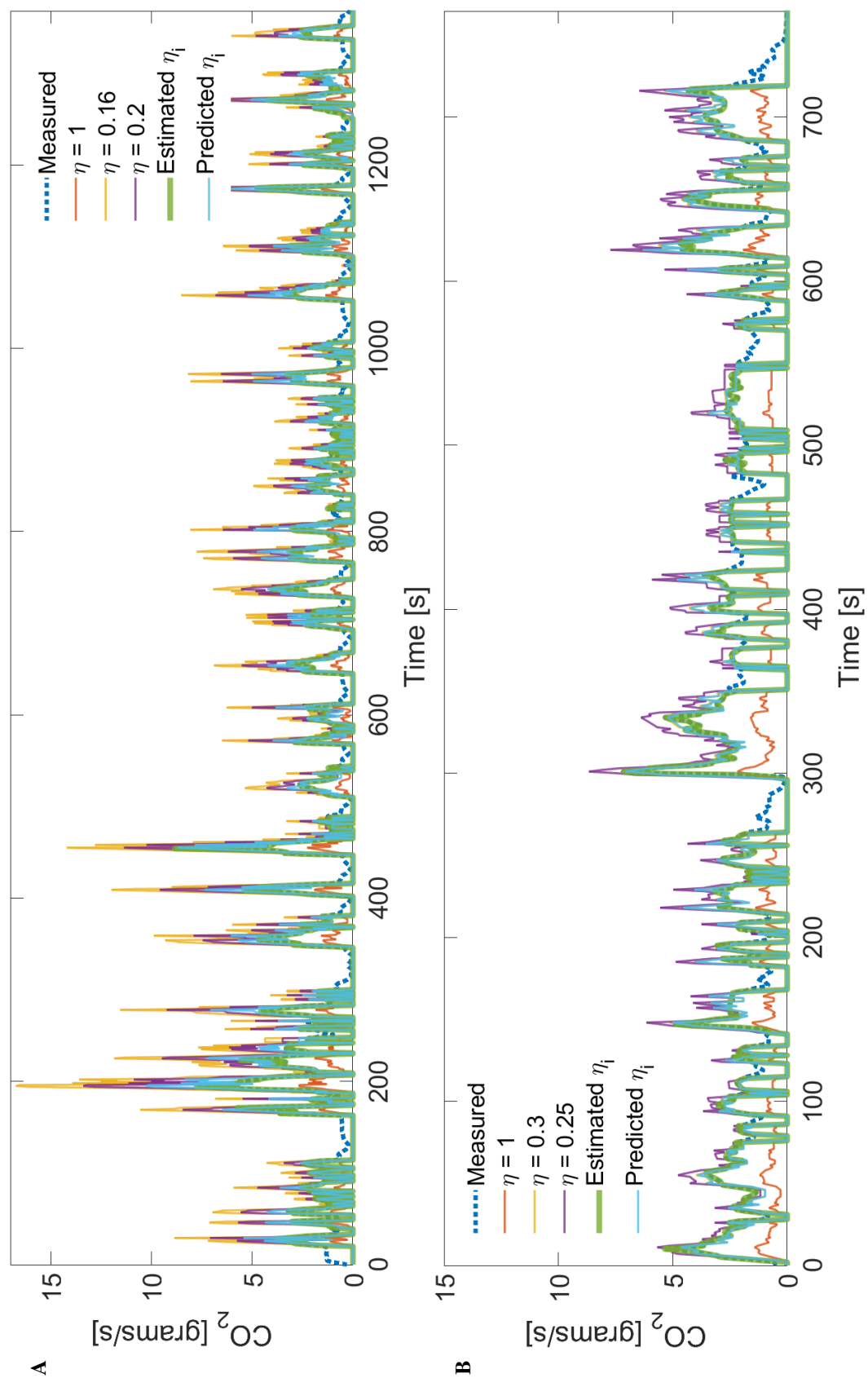


Figure 30. Instantaneous CO₂ emissions for TOYOTA CAMRY XLE/XSE estimated using several values for η . (A) UDDS cycle. (B)

HWFET cycle.

where $CO_{2i_{Measured}}$ and $CO_{2i_{Estimated}}$ are, respectively, the measured and estimated fuel consumption in second i , and N is the total number of data samples. The results shown in Table 12 confirm the accuracy of the energy demand model in estimating CO_2 emissions, as the RMSE is very low. Not surprisingly, when $\eta = 1$, the error is high because the powertrain loss was not considered. However, the errors are reasonably low when using the constant, estimated and predicted efficiency values for each driving cycle.

Table 12. $RMSE_{CO_2}$ [grams/sec] for the selected cars.

Car Model	Cycle	$\eta = 1$	$\eta = 0.16$	$\eta = 0.20$	Estimated η_i	Predicted η_i
ACCORD	UDDS	1.219	1.560	1.058	0.526	0.712
	HWFET	1.301	1.713	1.163	0.523	0.775
CAMRY	UDDS	1.809	0.999	1.084	0.946	1.000
	HWFET	1.716	1.014	1.202	0.905	1.005

4.2.3 Estimating Fuel Consumption Using Aggregated EPA Data of Selected Cars

Figure 31 shows the estimated total fuel consumed at the end of each driving cycle for the selected cars. Selecting $\eta = 1$ results in a very low accuracy compared to EPA measurements. It can be seen from the figure the ability of the model to accurately estimate the total instantaneous fuel consumption when $\eta = 0.2$ for UDDS and $\eta = 0.3$ in HWFET compared to EPA measurements.

The energy demand model is also able to capture the variety of car specifications as fuel consumption increases as the mass of the car increases. It can be seen also that selecting $\eta = 0.16$

resulted in a lower accuracy in the estimation of fuel consumption compared to the EPA measurements in UDDS.

For the estimate of CO₂ shown in the same figure, as the CO₂ emissions are highly correlated with the expended energy, it can be seen the same effect of the choice of η on the accuracy of the estimate.

Furthermore, the effect of individual values of η are not generalized to all cars. For example, it can be seen from the UDDS data in the same figure, that $\eta = 0.2$ has produced an accurate estimate for most selected cars except for ACCORD.

To measure the accuracy of the estimate, the Root Squared Error is used for the fuel consumption estimate (RSE_{Fuel}) in [gal/mile] is used where it is defined as follows:

$$RSE_{Fuel} = \sqrt{(F_{measured} - F_{estimated})^2}, \quad (38)$$

where $F_{measured}$ and $F_{estimated}$ are, respectively, the measured fuel consumption obtained from EPA data and the estimated fuel using the energy demand model.

Table 13 shows the RSE_{Fuel} of each selected car based on each selected value of η . The mean of RSE_{Fuel} for each car is also evaluated to assess the average accuracy. As can be seen in the table, the highest error was produced by not considering the powertrain loss, that is, when $\eta = 1$. The estimated η produced the lowest error, but this value can not be used as it was explained above. The constant values of η produced acceptable errors among all cars.

For measuring the accuracy of estimating the CO₂ emissions, the root mean square error is also used. It is calculated as follows:

$$RSE_{CO_2} = \sqrt{(CO_{2measured} - CO_{2estimated})^2}, \quad (39)$$

where $CO_{2measured}$ and $CO_{2estimated}$ are, respectively, the measured CO₂ obtained from EPA

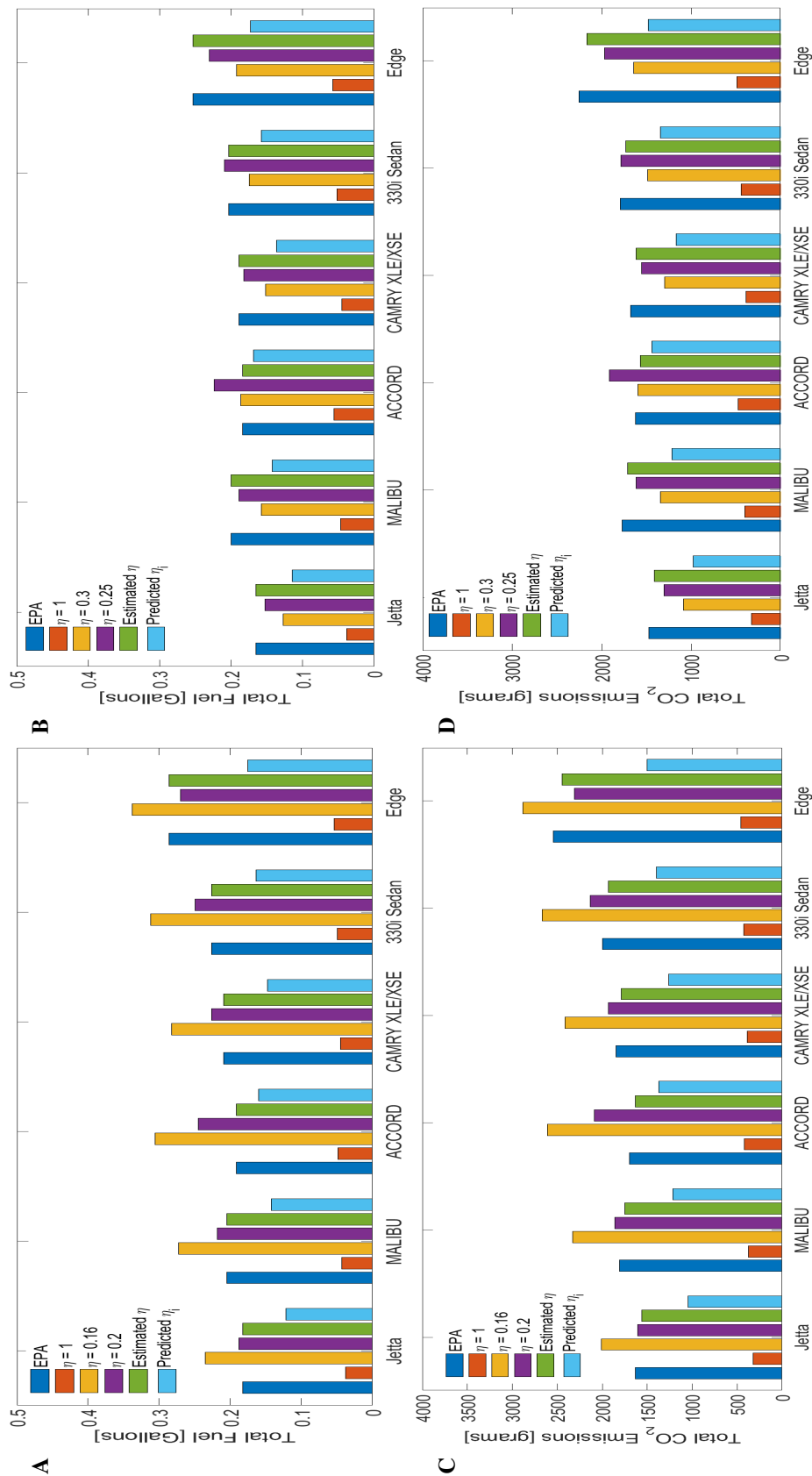


Figure 31. Total fuel consumption and CO₂ for selected cars using several values for η . (A) UDDS cycle. (B) UDDS cycle. (C) HWFET cycle. (D) HWFET cycle.

Table 13. RSE_{Fuel} [gal/mile] of the selected cars.

Car Model	Cycle	$\eta = 1$	$\eta = 0.2$	$\eta = 0.16$	Estimated η	Predicted η_i
Volkswagen Jetta	UDDS	0.014191	0.005048	0.000468	0.000031	0.005954
	HWFET	0.012432	0.003749	0.001268	0.000028	0.004980
CHEVROLET MALIBU	UDDS	0.015771	0.006536	0.001225	0.000035	0.006155
	HWFET	0.014963	0.004221	0.001152	0.000034	0.005717
HONDA ACCORD	UDDS	0.013913	0.011126	0.005164	0.000033	0.003040
	HWFET	0.012493	0.000242	0.003880	0.000032	0.001503
TOYOTA CAMRY XLE/XSE	UDDS	0.016012	0.007095	0.001594	0.000036	0.006048
	HWFET	0.014010	0.003655	0.000697	0.000032	0.005111
BMW 330i Sedan	UDDS	0.017221	0.008334	0.002249	0.000039	0.006119
	HWFET	0.014737	0.002832	0.000570	0.000035	0.004481
Ford Edge	UDDS	0.022686	0.004957	0.001625	0.000049	0.010825
	HWFET	0.019130	0.006017	0.002270	0.000044	0.007857
Mean RSE_{Fuel}	UDDS	0.016632	0.007183	0.002054	0.000037	0.006357
	HWFET	0.014628	0.003453	0.001639	0.000034	0.004941

data and the estimated CO_2 using the energy demand model. Table 14 shows the RSE_{CO_2} of each selected car based on each selected value of η . The mean of RSE_{CO_2} per car is also calculated to measure the mean of errors per car. As can be seen in the table, the highest error was produced by not considering any powertrain loss, that is when $\eta = 1$. The estimated η produced a high error across all cars. The constant values of η produced acceptable errors across all cars. Although the predicted value of η produced a slightly higher error, the error is not significantly high, compared to other values.

Table 14. RSE_{CO_2} [grams/mile] of the selected cars.

Car Model	Cycle	$\eta = 1$	$\eta = 0.2$	$\eta = 0.16$	Estimated η	Predicted η_i
Volkswagen Jetta	UDDS	175.87	50.56	3.35	9.23	78.92
	HWFET	112.17	37.89	16.67	6.07	48.42
CHEVROLET MALIBU	UDDS	192.79	69.74	7.23	7.60	79.62
	HWFET	133.83	41.94	15.68	6.13	54.73
HONDA ACCORD	UDDS	171.76	122.92	52.76	8.41	43.79
	HWFET	112.09	3.16	27.97	5.49	18.08
TOYOTA CAMRY XLE/XSE	UDDS	196.42	75.54	10.78	8.39	79.15
	HWFET	125.54	36.96	11.65	5.97	49.42
BMW 330i Sedan	UDDS	210.72	90.04	18.43	8.50	80.05
	HWFET	131.35	29.52	0.43	5.60	43.63
Ford Edge	UDDS	280.03	45.29	32.17	13.62	140.44
	HWFET	171.93	59.76	27.72	8.67	75.50
Mean RSE_{CO_2}	UDDS	204.60	75.68	20.79	9.29	83.66
	HWFET	131.15	34.87	16.69	6.32	48.30

4.2.4 Estimating Fuel Consumption Using Aggregated EPA Data for all Cars

To expand the evaluation on various cars, the energy demand model was applied on all the cars listed in the dataset. The distribution of RSE_{Fuel} based on each η value is shown in Figure 32. The results proved that $\eta = 0.2$ for the UDDS driving cycle and $\eta = 0.3$ for the WHFET driving cycle are the best values that represent the powertrain efficiency and can be used in the fuel consumption estimation model, resulting in a lower error.

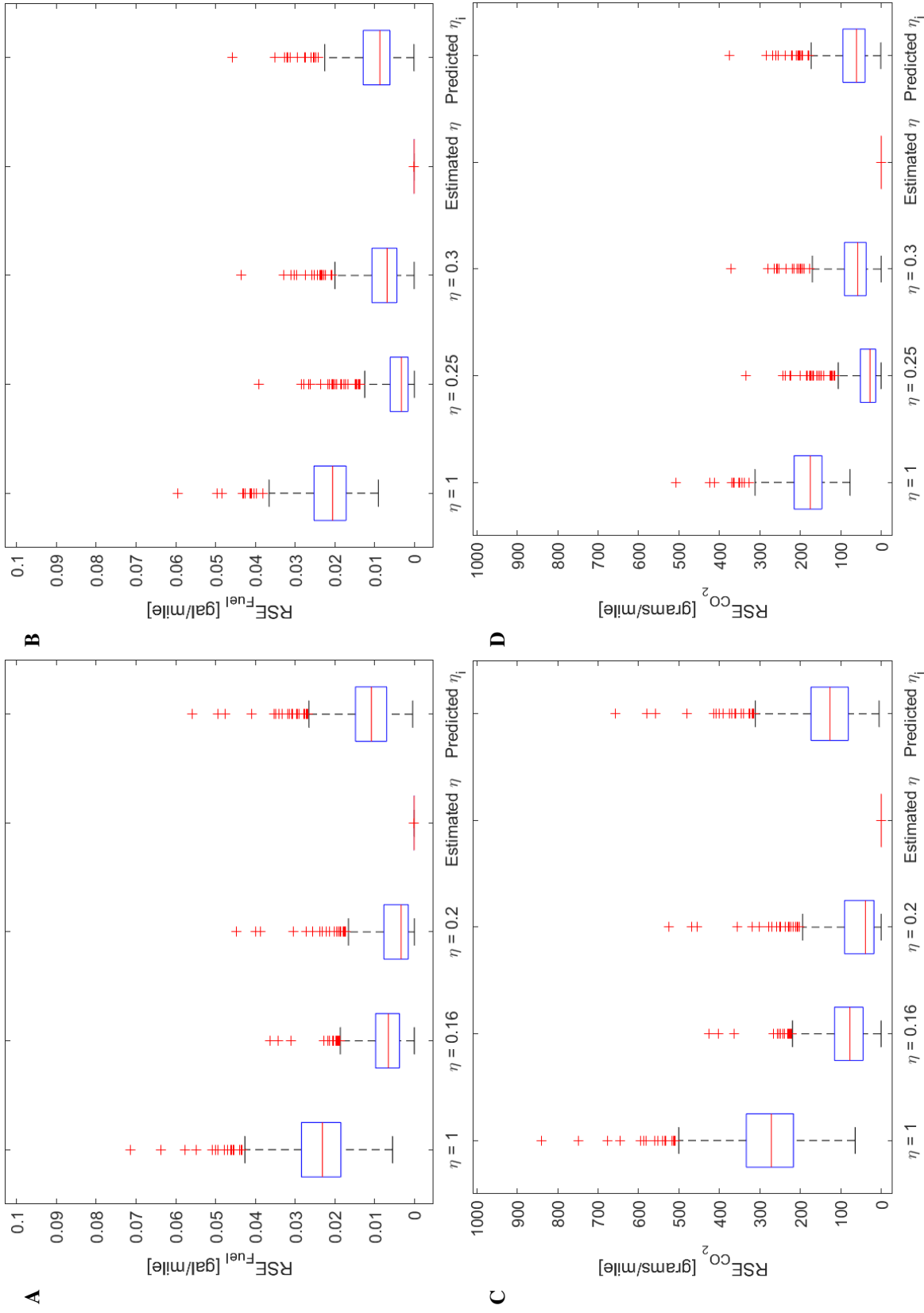


Figure 32. RSS_{Fuel} and RSS_{CO_2} for all cars under various values of η . (A) UDSS cycle. (B) HWFET cycle. (C) UDSS cycle. (D) HWFET cycle.

HWFET cycle.

Overall, our results show that the energy demand model is effective in estimating fuel consumption and CO₂ emissions for user-defined driving cycles, depending on the selection of the correct efficiency value. The efficiency values obtained from [93] for gasoline cars showed the best performance among the other values. In addition, the small estimation errors in both driving cycles indicate that the model can be generalized to estimate fuel consumption for arbitrary driving cycle. From the result, if the driving cycle is expected to have significant changes in speed, as in the UDDS driving cycle, then $\eta = 0.16$ or $\eta = 0.2$ could generate accurate estimates. On the other hand, if the speed changes are insignificant, as in the HWFET driving cycle, then $\eta = 0.3$ or $\eta = 0.25$ could generate accurate estimates. The low errors among all cars also indicate that the energy demand model can be applied using different car specifications as long as the correct efficiency of the car is properly selected.

4.2.5 Comparing the Energy Demand Model with the Engine-Specific Model

In this section, the estimation of fuel consumption using the energy demand model is compared with the fuel consumption estimated using known engine-specific efficiency as used by Chaim and Shmerling [13] which used the UN / ECE Extra-Urban Driving Cycle (EUDC) to evaluate their model. Since EUDC does not include aggressive deceleration and idle periods, the average efficiency of the highway driving cycle calculated in [88] for the year 2011 ($\eta = 0.17$) is used in the energy demand model. The speed profile of EUDC is obtained from [92]. The specifications for similar cars that were selected in [13] were obtained from [91] for the year 2011. The selected cars and their specifications are listed in Table 15 compared to the specifications that were used in [13].

Figure 33 shows that choosing $\eta = 0.27$ to calculate fuel consumption in the EUDC cycle

results in a close estimate when the model uses engine-specific efficiency. The result of both models is also compared with the EPA highway fuel consumption¹. It can be seen here that the energy demand model with $\eta = 0.27$ produced a closer estimate to the EPA measurements than [13].

Table 15. Comparisons of car specifications used in this study and in [13].

Car Model	Horse Power [kW]		Mass [kg]	
	EPA	[13]	EPA	[13]
YARIS	79.0	73.1	1190.5	1005.0
GENESIS COUPE	156.6	157.3	1700.7	1570.0
CAMRY	199.9	196.9	1757.4	1570.0

4.2.6 Sensitivity Analysis

A sensitivity analysis study was conducted on the instantaneous and aggregated data to explore how the parameters used in the model affect the estimation error RSE_{Fuel} . For the instantaneous parameters, (i.e., the *speed* and *acceleration*) is explored on the instantaneous ANL data. This analysis is performed by choosing $\eta = 0.2$ for the UDDS driving cycle and $\eta = 0.3$ for the WH-FET driving cycle. The correlation was measured by calculating the Pearson correlation coefficient. Figure 34 shows a low Pearson correlation between the *speed* and *acceleration* values and the RSE_{Fuel} , which shows the lack of significant correlation between these parameters and the es-

¹The fuel consumption was adjusted to the distance traveled in the EUDC cycle

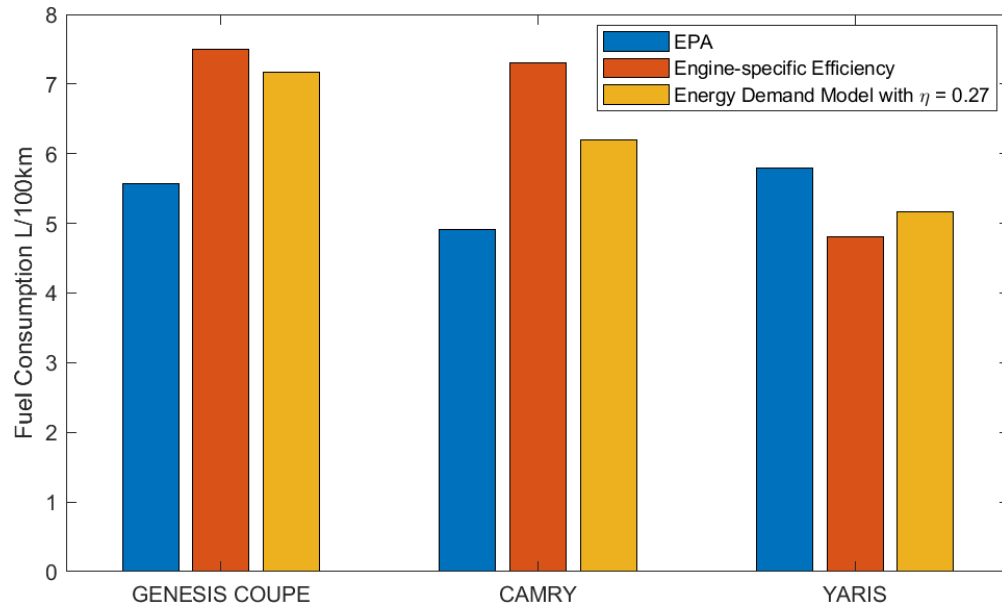


Figure 33. Results of applying the energy demand model on EUDC driving cycle compared with engine-specific model used in [13].

timination errors. The figures also show that disregarding idling (i.e., speed = 0) and decelerating (i.e., acceleration < 0) instances does not contribute significantly to the model inaccuracy.

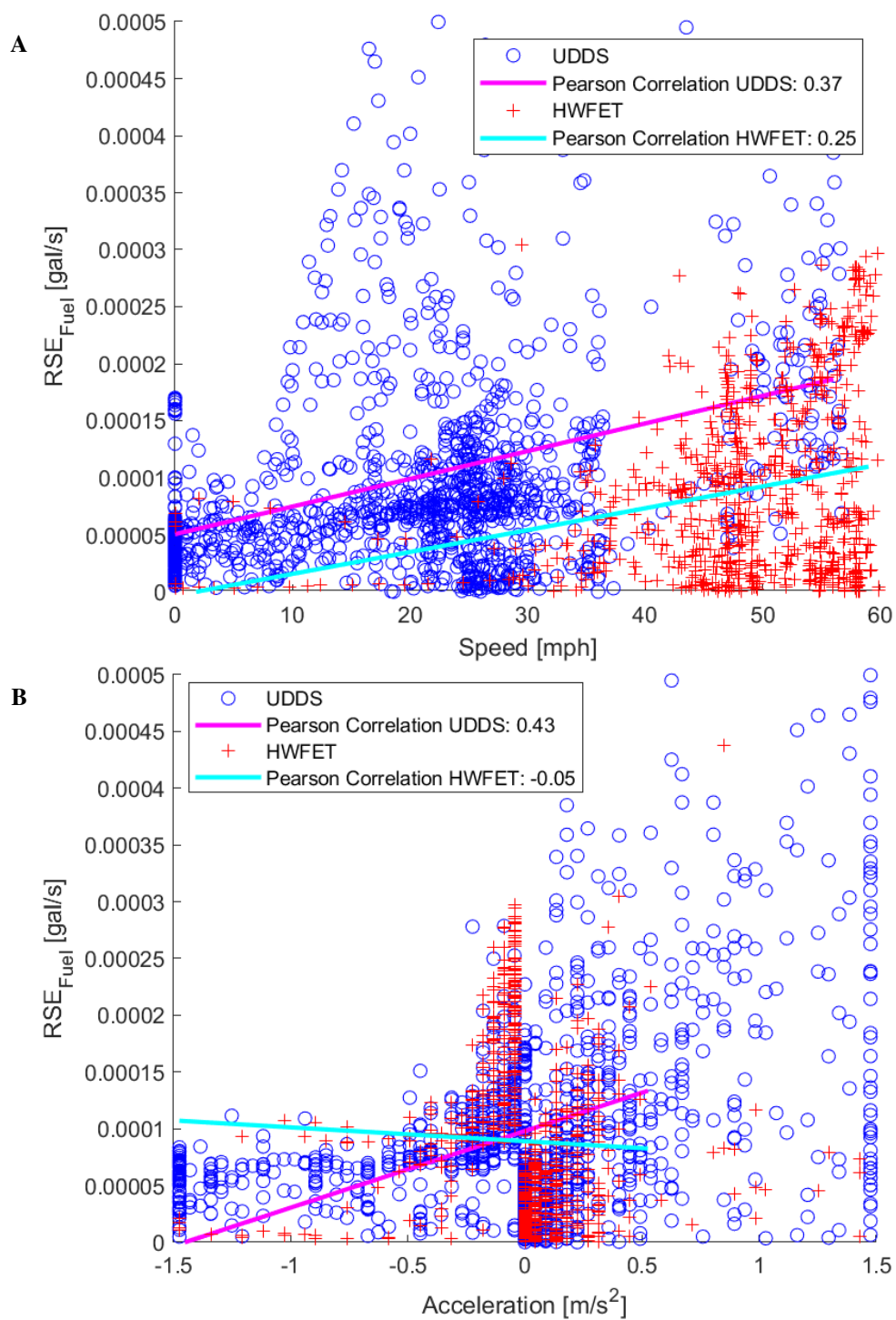


Figure 34. Sensitivity analysis of RSS_{Fuel} against used parameters from EPA and ANL instantaneous data. (A) v_i . (B) a_i .

Next, the correlation between the parameters $mass, f_0$ and f_2 and RSE_{Fuel} are investigated in the aggregated data. Figure 35 shows a low Pearson correlation between the $mass, f_0$ and f_2 and the RSE_{Fuel} . This indicates a lack of significant correlation between these parameters and the model inaccuracy.

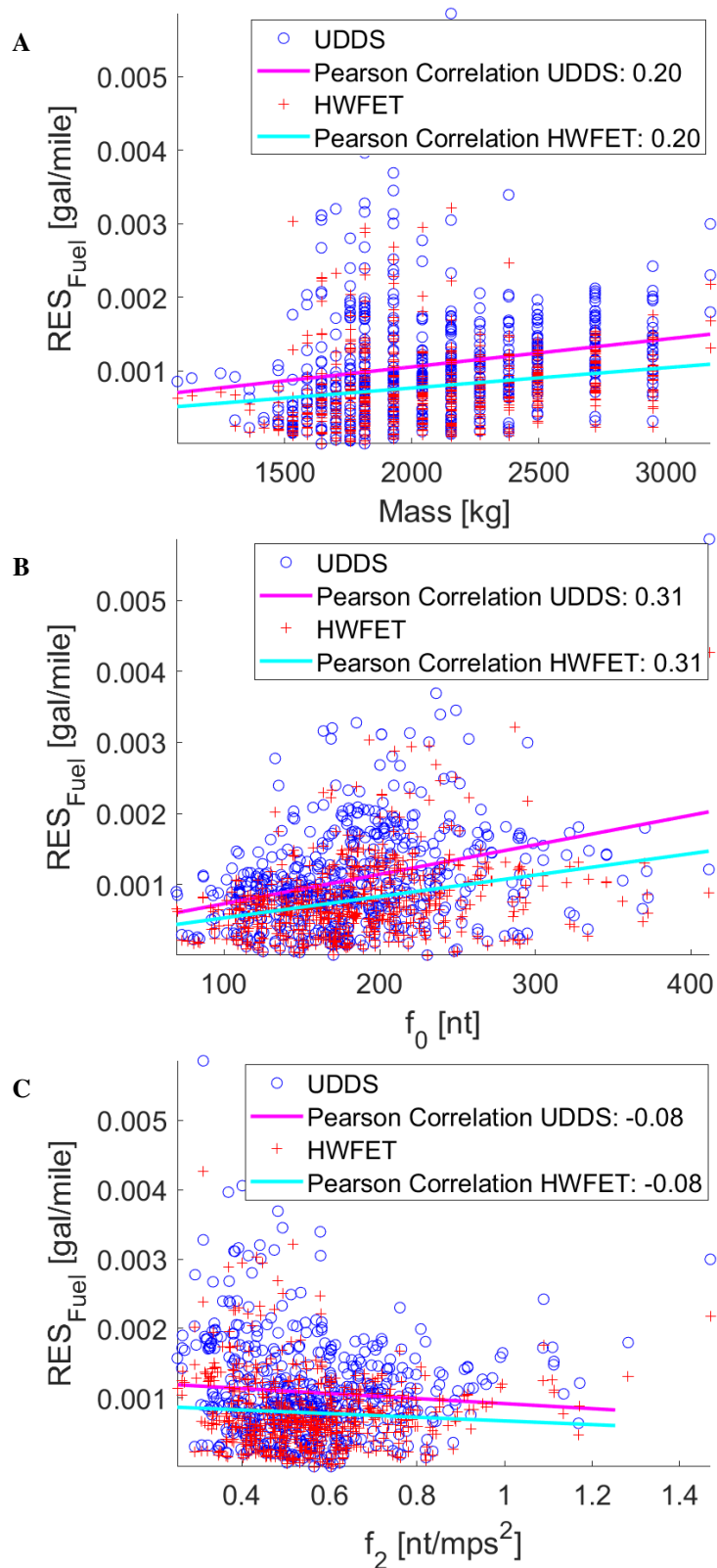


Figure 35. Sensitivity analysis of RSS_{Fuel} against used parameters from EPA aggregated data. (A) Mass of the car. (B) f_0 . (C) f_2 .

4.3 CONCLUDING REMARKS

We provided an empirical evaluation of the energy demand model in relation to its ability to accurately estimate fuel consumption and CO₂ emissions. The first main contribution of this work was to evaluate the fuel consumption and CO₂ emission estimates produced by the energy demand model and compare them to official measurements published by the EPA. Our second main contribution was to demonstrate the ability of the energy demand model to be generalized to various driving cycles, including user-defined driving cycles and a variety of car models. We also provided a simple approach for cross-disciplinary researchers to implement the model directly, given publicly available data related to car specifications. By applying the model to the EPA dynamometer driving cycles, the results showed that the model can be generalized to a large class of user-defined driving cycles. The accuracy of the estimation varied slightly across different car models.

In spite of these encouraging results, additional investigations are required to explore the effect of car specifications on the efficiency of converting fuel into tractive energy to ensure its accuracy across different car models. This aspect is left for future work. The evaluation study showed that when using the EPA's publicly available powertrain efficiencies, the energy demand model produced results that are fairly close to those that the EPA reported for fuel economy and CO₂ emissions. This indicates that the model can be used to estimate fuel and CO₂ for any user-defined driving cycles, provided the correct powertrain efficiency value is used.

CHAPTER 5

REDUCING THE ENVIRONMENTAL IMPACT OF CROSSING PEDESTRIANS

In this chapter, we aim to answer our third research question: **RQ3**: Can the alert messages about crossing pedestrians reduce the environmental impact of midblock crossing?. In Section 5.1, we briefly revisit the energy demand model and show how we use it to estimate the instantaneous fuel consumption and use its output to estimate the CO₂ emissions for our driving cycle. Next, in Section 5.2, we explain the alert system model. Then, we explain the speed reduction schemes in Section 5.3. Next, we present the simulation model and show the results of our proposed schemes in Section 5.4. Finally, we conclude this chapter in Section 5.5.

5.1 FUEL CONSUMPTION AND EMISSION ESTIMATION MODEL

The physics-based energy demand model was used by Jones [35] to estimate the energy required to move a car from point to point through a driving cycle. The model takes as inputs the speed profile and car specifications that influence the tractive force. We employed the model to estimate fuel consumption based on the instantaneous energy demand using the following Equation [88]:

$$E_{Fuel} = \frac{E_{inst}}{\eta},$$

where E_{Fuel} is the estimation of the total expended fuel energy in *Joules* and η refers to the efficiency of the engine in converting fuel into a tractive power. the total instantaneous energy

demand on the car in the interval $[0, T]$ is calculated as follows:

$$E_{inst} = \sum_{i=0}^T m a_i v_i + f_0 v_i + f_2 v_i^3,$$

where i is the time unit (i.e., one second), m is the mass of the car in kg , a_i is the current acceleration of the car in m/sec^2 and v_i is the current speed in m/sec . f_0, f_2 are the rolling resistance and aerodynamic drag of the car, respectively. These terms represent the forces that a car must overcome while moving [26]. As stated by US Environmental Protection Agency (EPA)[93], only 12% to 30% of the fuel goes to the wheel of the car. We assume that the power demand during deceleration is zero because the engine does not provide power to the wheels while braking. Similarly, the power demand during idling is zero as the car shuts off the engine if it stops for more than a few seconds [31].

To estimate the CO_2 emissions, we use the EPA formula [94]:

$$CO_2 = E_{Fuel} \times \text{Carbon Content} \times \text{Oxidation Fraction} \times \left(\frac{44}{12} \right),$$

CO_2 emissions are highly correlated with the fuel consumed. Based on this, the CO_2 emissions in grams per $KJoules$ can be estimated based on the expended fuel energy E_{Fuel} . The Carbon Content equals to $0.0196 g/KJ$ and the Oxidation Fraction equals to 0.99 and the value $\frac{44}{12}$ is the molecular mass of CO_2 divided by the atomic mass of carbon.

5.2 THE ALERT SYSTEM MODEL

We assume a system that can reliably detect pedestrians crossing the midblock and that sends alert messages to approaching cars, as illustrated in Figure 36. For example, approaching cars may receive, through V2I communications, alert messages from a street monitoring system that uses cameras as proposed by Noh and Yeo [53]. It may also receive, through V2V communications, alert

messages from cars parked along the curb that detect crossing pedestrians as proposed by Alali, Olariu, and Jain [4]. Similarly, the approaching cars may receive alert messages from other approaching cars through V2V Ngo, Fang, and Wang [51]. Finally, cars may receive alert messages from pedestrian hand-held or wearable devices through Vehicle-to-Pedestrian (V2P) communications as proposed by Tahmasbi-Sarvestani, Nourkhiz Mahjoub, Fallah, Moradi-Pari, and Abuchaar [83].

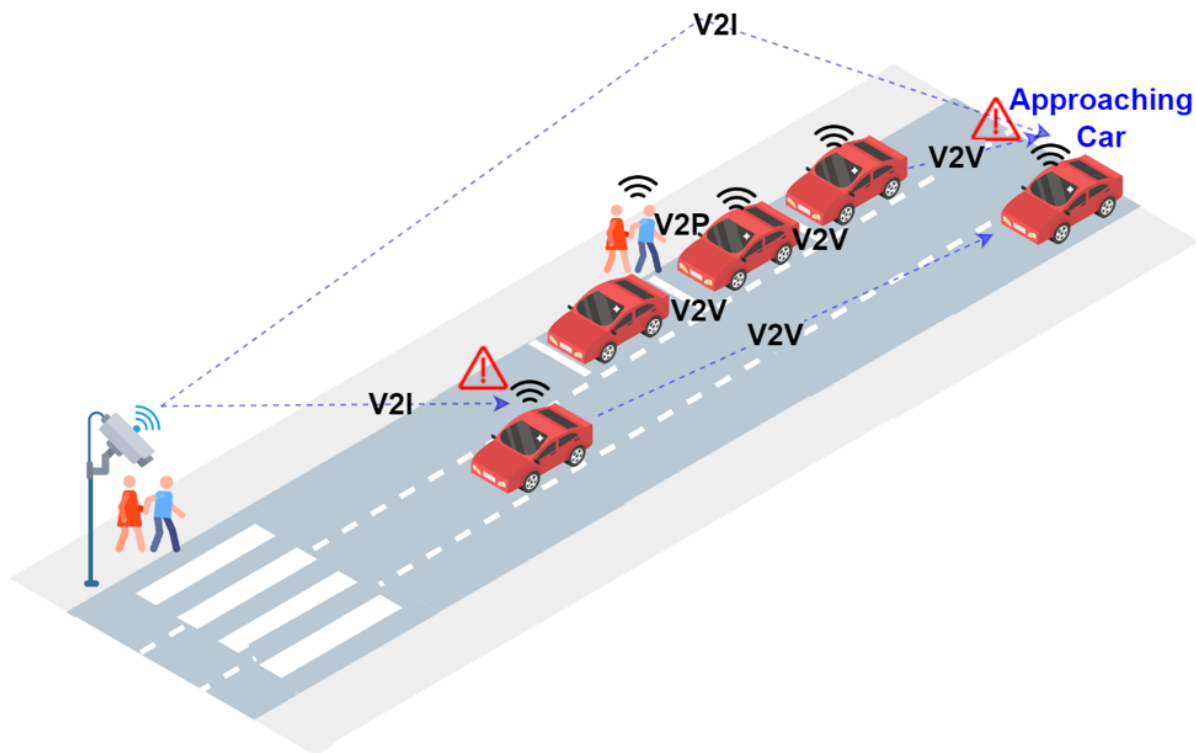


Figure 36. A generic alert system model.

We assume that alert messages include the location of the crossing and the speed of the pedestrians. Using a digital map, the car determines the width of the street. With this information, the

car can determine the remaining crossing time and the speed it should maintain to avoid colliding with the pedestrians, as we illustrate in Section 5.3.

5.3 SPEED REDUCTION SCHEMES

Assume that at time s_1 an approaching car at location C_1 receives the first alert message containing location L_1 for the crossing cohort and the remaining crossing time, which indicates that the crossing will be over at time e_1 . Using the time-space diagram shown in Figure 37, the car can calculate the maximum safe speed as:

$$v_{safe_i} = \min \left\{ v_{safe_{i-1}}, \frac{L_i - C_i}{e_i - s_i} \right\}, \quad (40)$$

where i is the alert message number. v_{safe_i} is the safe speed determined using the information included in the received message number i . If the received message is the first message, then v_{safe_i} is equal to the street speed limit v_{max} .

Now, let us assume that after a while and before the car reaches the crossing location L_1 of the first crossing, it receives another message about a cohort crosses at different location L_2 , as we show in Figure 38.

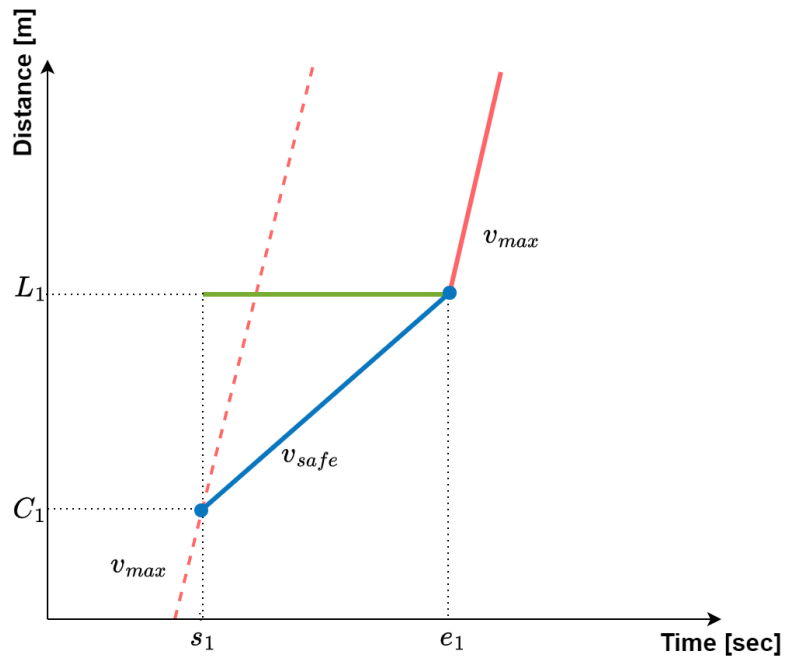


Figure 37. Trajectory of a car receiving one alert message about midblock crossing

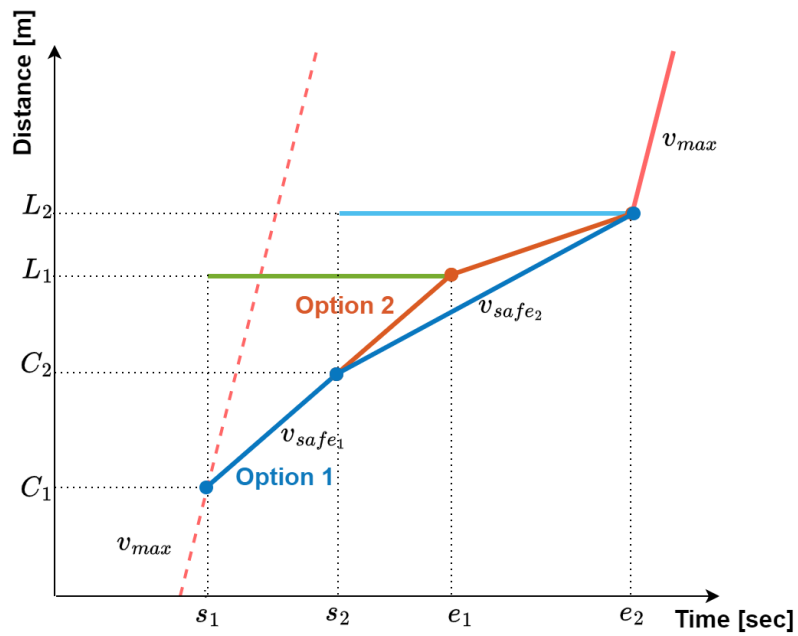


Figure 38. Trajectory of a car receiving two alert messages about midblock crossing

When the car receives the alert 2, it checks whether there is a previous alert 1 affects its speed. If no alert was received, the car reduces its speed immediately according to the calculated crossing time. On the other hand, if there is a previous alert, the car will check if the location of the current crossing pedestrian L_2 is closer than that of the previous pedestrian location L_1 . If it is closer, then the car would choose between the two options, which represent our proposed schemes, Option 1 or Option 2, as explained below:

- **Option 1: Immediate deceleration** This option is illustrated in Figure 38. In this option, the car at location C_2 responds immediately to the second message by reducing its speed. We note here that this option would also prevent collisions with pedestrians at location L_1 without the need to stop at L_1 . Indeed, when the car reaches the crossing area, it can resume a normal speed equal to the speed limit v_{max} .
- **Option 2: Deferred deceleration:** This option represents the second scheme we propose in this work. This option is depicted in Figure 38. In this option, after the car reduces its speed for crossing at location L_1 , when it is at location C_2 it receives the second message about cohort crossing at location L_2 . When the car compares the new safe speed v_{safe_2} with its current speed v_{safe_1} , it finds that v_{safe_1} is lower. Therefore, it may choose not to respond to this message and maintain its current speed until it reaches the crossing at L_1 . When it passes the area, it will reduce its speed according to the remaining crossing time for the cohort at location L_2 .

These two proposed schemes can be compared with other trajectories that can be taken when the car does not notice the pedestrian in advance. We call this trajectory (Sudden Stop) where there are midblock crossings, but the car does not receive any information beforehand, and alternatively

it notices the pedestrian near the crossing location and stops suddenly. Note that the (Sudden Stop) trajectory is similar to a trajectory that would be taken by an aggressive driver who does not adhere to the alert message.

All of these trajectories can be compared to a baseline trajectory when there are no midblock crossing pedestrians. We call this trajectory (No Peds.) which stands for No Pedestrians.

It is important to determine the possible scenarios that may occur when there are several simultaneous crossings at several locations, and an approaching car receives alert messages. This also enables an accurate evaluation of the effectiveness of each reaction in reducing the environmental impacts. Therefore, we designed six possible scenarios for three pedestrians crossing at the same speed (i.e., they had the same crossing time) at three different locations L1, L2, and L3. In each scenario, the order of starting crossing changes at each location. Figure 39 shows six scenarios with their expected reactions.

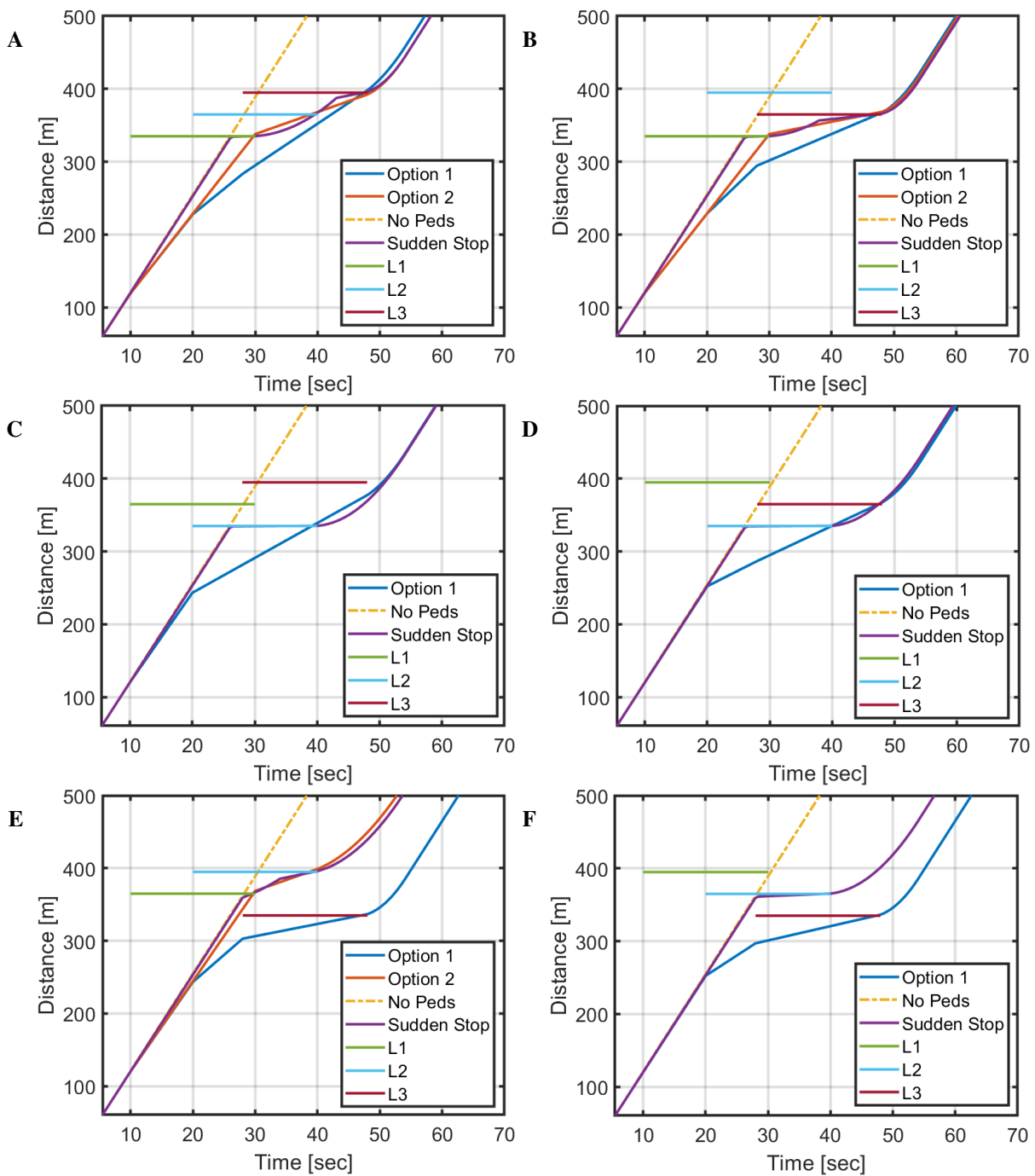


Figure 39. Evaluated scenarios of vehicle trajectory when receiving three alert messages. (A)

Scenario 1. (B) Scenario 2. (C) Scenario 3. (D) Scenario 4. (E) Scenario 5. (F) Scenario 6.

In scenarios 3, 4 and 6, (Figures 39C, 39D, and 39F), the only option for the car to avoid collisions with pedestrians without staying idle is immediate deceleration (that is, Option 1). This is the only available option, given that the second alert location is closer to the car than the first alert.

In **Scenario 3**, the car receives the message at time 10 about a pedestrian/cohort crosses at location L_1 , the car calculates the safe speed v_{safe_1} and finds that it is equal to the speed limit, so it continues cruising at the same speed. Note that even if the car does not reduce its speed, it will avoid the collision with the pedestrian without the need to stop at the crossing location. At time 20, the car receives a second alert for a crossing at location L_2 . Now, because the location is closer than L_1 and v_{safe_2} is less than the current speed v_{safe_1} , the car immediately reduces its speed to v_{safe_2} . When the third crossing starts at location L_3 which is farther away from L_2 , the car calculates v_{safe_3} which, this time, is larger than the current speed, so it keeps the minimum which is the current speed v_{safe_2} . When it reaches L_2 , its speed can be increased to v_{safe_2} if it is less than the speed limit. In **Scenario 4**, crossing at location L_1 starts first, and the car receives the first alert, but as in Scenario 3, this does not affect the current speed because the safe speed now is similar to the speed limit. At time 20, crossing at a closer location L_2 starts, which makes the car reduce its speed to avoid the collision. At time 28, a crossing starts at location L_3 , but it has no effect this time because $v_{safe_2} = v_{safe_3}$. In **Scenario 6**, the car does not reduce its speed for crossing at L_1 , but it does so when crossing at location L_2 starts. Again, when L_3 has a crossing, the car reduces its speed to avoid the collision.

On the other hand, a second option is available to the car to defer the deceleration in Scenarios 1,2 and 5 (Figures 39A, 39B, and 39E). This is actually because the second alert is for crossing at location farther away than the location of the first alert. In **Scenario 1**, the car receives the message

at time 10 about a pedestrian/cohort crosses at location L_1 , the car calculates the safe speed and finds that it is less than the speed limit v_{max} ; thus, it reduces its speed to v_{safe1} . Then, when a crossing starts at location L_2 which is farther away from L_1 , it receives the second alert. Now, as the car calculates its v_{safe2} and finds that it is less than the current speed v_{safe1} , so it has now two options: either to decelerate immediately to reach v_{safe2} or to continue on v_{safe1} until it reaches L_1 crossing then decelerates for the second alert. When the third crossing starts at location L_3 , the car calculates v_{safe3} which, this time, is less than the current speed (for both options), but ,again, since L_3 is farther than L_2 , it has now the two options. Similarly, in **Scenario 2**, crossing at location L_1 starts first, and the car receives the first alert, then crossing starts at L_2 , so the car has the two options. However, when crossing at L_3 starts, the car must reduce its speed immediately without having a second option because L_3 is closer than L_2 . In **Scenario 5**, the car does not reduce its speed for L_1 crossing as it can avoid the collision even it maintains the speed limit. Again, when crossing at further location L_2 starts, it has the two options. However, when the third crossing at location L_3 starts, it affects Option 1 and forces the car to reduce its speed immediately.

In the following, we explain the possible rational reactions of an approaching car when it receives an alert message to a crossing cohort at one location, and after awhile, it receives another message of a pedestrian crossing at the same or another location. We examine two cases that may occur in the street while pedestrians cross the midblock.

In this case, the car receives a second alert message about cohort crossing at a location that is different from the first one.

5.4 SIMULATION AND RESULTS

5.4.1 Simulation Model

To generate cars traffic, we utilize Simulation of Urban MObility (SUMO) [46], a microscopic simulation modeling vehicles and pedestrian mobility. In the simulation, we created a one way street with two lanes for on-street parking in the right-hand of the street and a left-hand lane for moving cars.

For generating pedestrian traffic, and because we have specific scenarios we aim to study, we determine fixed locations of pedestrian crossing with fixed speed. We chose the minimum speed of crossing midblock reported in [20] to assure safety of pedestrians. We assume that each time a car approaches those determined locations, there is a pedestrian crosses the street at the same time, and it receives a message once the pedestrian starts crossing. To achieve this, we disable the randomness in pedestrian generation in SUMO to prove the effectiveness of our schemes. The parameters of the simulation are as follows: street length = 500 meters [m], street width = 13 [m], street speed limit = 30 [mph] 13.4 [m/s], pedestrian speed = 0.67 [m/s], crossing time = 20 [s].

We implemented our proposed schemes on two car models from year 2023 data provided by [91]. The first car is the sedan TOYOTA CAMRY LE/SE has mass = 1644 kilogram, $f_0 = 113.82$ newton and $f_2 = 0.36 \text{ newton} \times \frac{\text{second}^2}{\text{meter}^2}$. The second car is the SUV TOYOTA HIGHLANDER that has mass = 2040.8 kg, $f_0 = 139.7$ newton and $f_2 = 0.56 \text{ newton} \times \frac{\text{second}^2}{\text{meter}^2}$. According to the EPA data, CAMRY LE/SE consumes less fuel and emit less CO₂ than HIGHLANDER in city driving cycles.

5.4.2 Simulation Results

In this section, we provide an evaluation of the proposed schemes in terms of reducing fuel consumption and CO₂ emissions using the two cars. Additionally, we prove that receiving informative messages about midblock pedestrians in a timely manner through V2V communications reduces the environmental impacts associated with midblock crossing. We compare the fuel consumed during the trips in Option 1 and Option 2 in all the assumed scenarios with the additional trajectories (No Peds.) and and (Sudden Stop). Figure 39 shows the six scenarios along with the additional generated trajectories for comparison. We evaluate the fuel consumed and the emitted CO₂ for the four trajectories in each scenario.

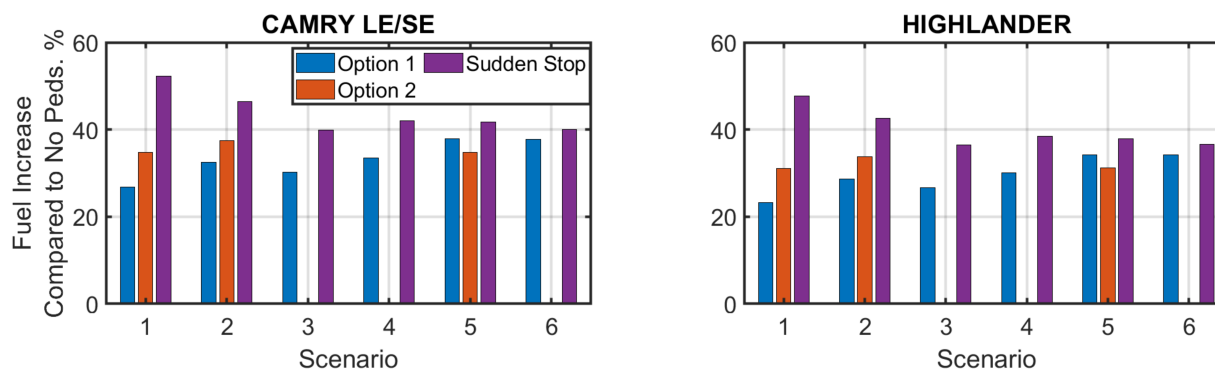


Figure 40. The increase of fuel consumed for all the trajectories compared to no pedestrian trajectory in all scenarios

We measured the increase percentage of fuel as a result of midblock crossing compared to the case when there are no pedestrian (No Peds.). Figure 40 and Figure 41 show that accommodating pedestrians in all scenarios increases the fuel consumption and emissions compared to the case

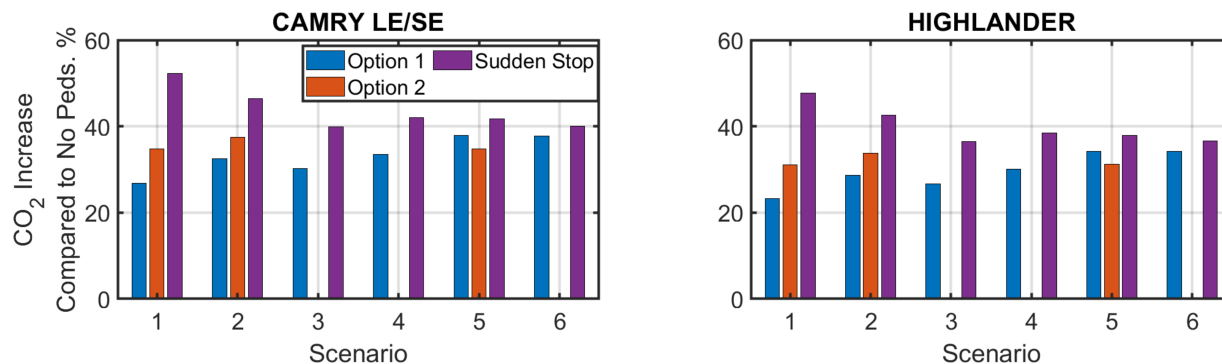


Figure 41. The increase of emitted CO₂ for all the trajectories compared to no pedestrian trajectory in all scenarios

where there are no pedestrians (No Peds.). However, receiving timely informative messages that allow the car to maintain a safe speed consumes less fuel and emits less CO₂ than the Sudden Stop. This is because when the car maintains a lower speed in advance until the pedestrians finish crossing, it consumes less fuel and consequently emits less CO₂. Conversely, when the car does not have timely information and suddenly stops at the crossing location, and later resume its normal speed after passing it, it consumes more fuel because of the higher speed and acceleration phases.

The reduction of fuel consumption and CO₂ emissions in the proposed schemes is shown in Figure 42 and Figure 43, respectively. The reduction of Option 1 and Option 2 were compared with the (Sudden Stop) trajectory. As can be seen, the reduction in fuel consumption is higher in the two options. We can also see that Scenario 1 has the highest fuel and emission reduction. This shows the effectiveness of the proposed schemes in this case. While in the other scenarios, as new information about pedestrian crossing at a closer location may require consuming more fuel as the time allowed to reduce the speed is less than in Scenario 1.

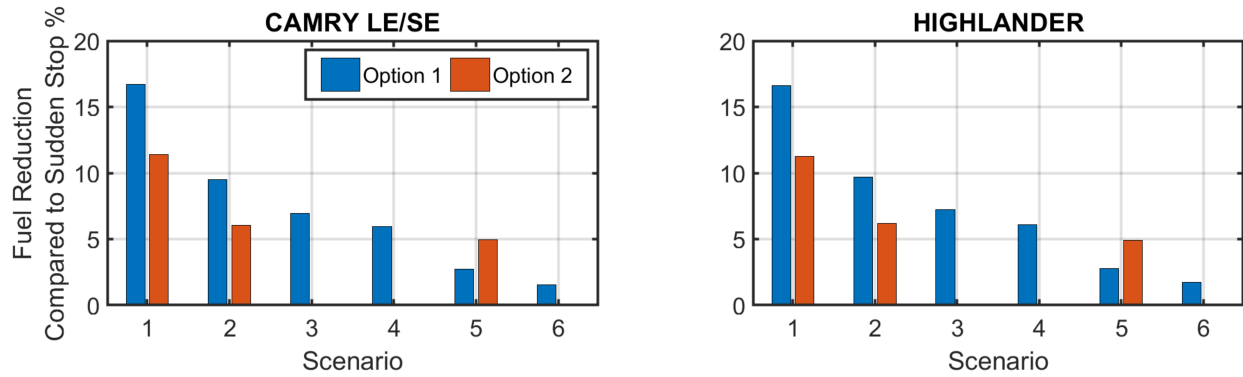


Figure 42. The reduction of fuel consumed for all the trajectories compared to sudden stop trajectory in all scenarios

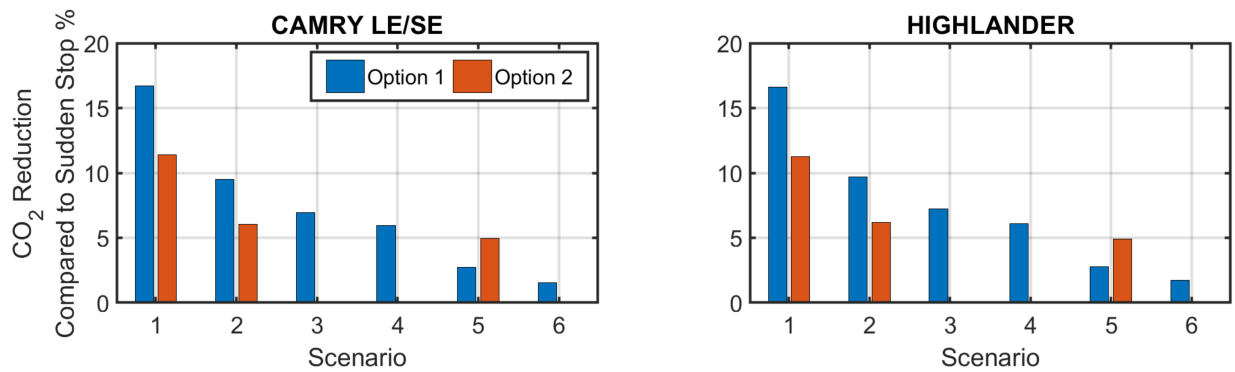


Figure 43. The reduction of emitted CO₂ for all the trajectories compared to sudden stop trajectory in all scenarios.

To discuss the results in detail, we show duration of driving modes (acceleration, deceleration, cruising and idling) for all the trajectories in all the scenarios in Table. 16. This data is applicable to the two cars since the speed profile is the same for both. From Table. 16, we see that in Scenario 1 the two options consumed less fuel than sudden stop because in both trajectories the car maintained a lower speed than sudden stop. Another reason is that in sudden stop, and because the car does not have adequate information in advance, it tries to resume its normal speed after it passes the crossing location. This causes an increase in the acceleration duration, which consumes more fuel. This was also applied to the other scenarios.

Table 16. Speed statistics and duration of driving modes in the evaluated scenarios

Scenario	Trajectory	Speed		Acceleration	Deceleration	Cruising		Idling
		μ [mph]	σ			Duration [seconds]	Duration [seconds]	
1	Option 1	23.934	7.3384	7	1.5	85	0	
	Option 2	23.6805	8.9587	7	1.5	86	0	
	No Peds	29.9982	1.07E-14	0	0	74.5	0	
	Sudden Stop	23.6799	10.386	20.5	2.5	71.5	4.5	
2	Option 1	23.2338	8.824	7	1.5	87.5	0	
	Option 2	23.1714	10.0558	7	1.5	88	0	
	No Peds	29.9982	1.07E-14	0	0	74.5	0	
	Sudden Stop	23.0918	11.3951	16	2.5	78.5	13.5	
3	Option 1	23.4776	8.6753	7	1.5	86.5	0	
	Option 2	23.4776	8.6753	7	1.5	86.5	0	
	No Peds	29.9982	1.07E-14	0	0	74.5	0	
	Sudden Stop	23.4451	11.3236	15.5	2	77.5	14	

Table 16. Speed statistics and duration of driving modes in the evaluated scenarios (Continued)

Scenario	Trajectory	Speed		Acceleration Duration [seconds]	Deceleration Duration [seconds]	Cruising Duration [seconds]	Idling Duration [seconds]
		μ [mph]	σ				
4	Option 1	23.2619	9.4685	7	1.5	87.5	0
	Option 2	23.2619	9.4685	7	1.5	87.5	0
	No Peds	29.9982	1.07E-14	0	0	74.5	0
	Sudden Stop	23.3836	11.337	15	2.5	78	14
5	Option 1	22.6306	10.6188	7	2	90	0
	Option 2	25.1097	8.0688	15	1.5	72.5	0
	No Peds	29.9982	1.07E-14	0	0	74.5	0
	Sudden Stop	24.8747	8.9741	19.5	1.5	69	0
6	Option 1	22.5959	10.7654	7	1.5	90	0
	Option 2	22.5959	10.7654	7	1.5	90	0
	No Peds	29.9982	1.07E-14	0	0	74.5	0
	Sudden Stop	24.0758	10.6726	15.5	2	75.5	11.5

We conclude that receiving advance information about midblock crossing allows the car to reduce the fuel consumption by up to 16.7% over Sudden Stop and on average 7.4% for both options. Specifically, immediate deceleration reduced about 7.3507% from Sudden Stop and deferred deceleration reduced 7.4511% on average. This conclusion applies to CAMRY data, and we achieved approximately similar reduction for the HIGHLANDER model. As the CO₂ emission are highly correlated with fuel consumption, emissions were reduced correspondingly. It is worth mentioning that neither of the schemes affected the average speed for the whole trip which means that our scheme did not increase trip time.

5.5 CONCLUDING REMARKS

Our main contribution was to propose schemes that mitigate the environmental impacts (increased fuel consumption and CO₂ emissions) of pedestrian midblock crossing by leveraging information about the location and expected duration of the crossing. We evaluated the impact of car decisions on fuel consumption and emissions by exploring potential trajectories that cars can take as a result of messages received. Our extensive simulations showed that the timely dissemination of pedestrian crossing information to approaching vehicles can reduce fuel consumption and emissions by up to 16.7% of the fuel consumed during a sudden driver reaction.

CHAPTER 6

CONCLUSION

We recognize the challenges that need to be overcome in order to achieve improved occluded pedestrian safety at midblock while reducing fuel consumption and CO₂ emissions. In this dissertation, we made contributions to fill the following research gaps: 1) Although parked cars are one of the major causes of pedestrian occlusion, they have not been leveraged to support occluded pedestrian detection; 2) Researchers interested in the environment and transportation need an accurate and straightforward model to estimate fuel consumption for their driving cycles and car specifications; and 3) Reducing fuel consumption due to midblock pedestrian accommodation has not been investigated in pedestrian safety systems. These gaps drive us to ask our main research question: Can we utilize parked cars to protect occluded pedestrians and reduce the environmental impact of accommodating pedestrians? This question is divided into three questions to be addressed in separate chapters in this dissertation. The three questions are: **RQ1:** Can we utilize parked cars to protect occluded pedestrians and alert approaching cars?; **RQ2:** Can we accurately estimate the instantaneous fuel consumption and CO₂ emissions using the energy demand model?; and **RQ3:** Can the alert messages about crossing pedestrians reduce the environmental impact of midblock crossing?

We addressed **RQ1** in Chapter 3 where we proposed ADOPT: a system to employ cars parked along the sidewalk to detect and protect crossing pedestrians. In ADOPT, we laid the theoretical foundations to enlist parked cars to protect occluded pedestrians at midblock. With the parked cars, we were able to: 1) Detect crossing pedestrians using short-range and low-power resources;

2) Provide a binary classification for pedestrians using only their radio frequency noise; 3) Accommodate several pedestrians at the same time; 4) Alert approaching cars promptly so they can avoid collision with the pedestrians without the need to stop. Our extensive simulations using SUMO-generated pedestrian and car traffic have shown the effectiveness of ADOPT in detecting and protecting crossing pedestrians. All these tasks were achieved using low-power and low-range communication resources.

Then, we addressed the second research question **RQ2** in Chapter 4 where we provided an empirical evaluation of the energy demand model in relation to its ability to accurately estimate fuel consumption and CO₂ emissions. We evaluated the fuel consumption and CO₂ emission estimates produced by the energy demand model and to compare them to official measurements published by the EPA. Furthermore, we demonstrated the ability of the energy demand model to be generalized to various driving cycles, including user-defined driving cycles and a variety of car models. The work provided a simple approach for cross-disciplinary researchers to implement the model directly, given publicly available data related to car specifications. By applying the model to the EPA dynamometer driving cycles, the results showed that the model can be generalized to a large class of user-defined driving cycles. The accuracy of the estimation varied slightly across different car models. The evaluation study showed that when using the EPA's publicly available powertrain efficiencies, the energy demand model produced results that are fairly close to those that the EPA reported for fuel economy and CO₂ emissions. This indicates that the model can be used to accurately estimate fuel and CO₂ for any user-defined driving cycles, provided the correct powertrain efficiency value is used.

Lastly, we addressed our third research question **RQ3** in Chapter 5 where we proposed speed reduction schemes that mitigate the environmental impacts (increased fuel consumption and CO₂

emissions) of pedestrian midblock crossing by leveraging information about the location and expected duration of the crossing that were sent by parked cars in a timely manner. We evaluated the impact of car decisions on fuel consumption and emissions by exploring potential trajectories that cars can take as a result of messages received. Our extensive simulations showed that timely dissemination of the information about pedestrian crossing at midblock to approaching vehicles can reduce fuel consumption and emissions by up to 16.7% of the fuel consumed if the car suddenly stops at the crossing area.

6.1 CONTRIBUTION

In the following, we revisit the key contributions of this dissertation:

1. Providing the theoretical foundations of a low-power and infrastructure-free occluded pedestrian detection system (Chapter 3);
2. Introducing a novel criterion for the *binary* classification of pedestrians as “on the sidewalk” or “in the street” (Chapter 3);
3. Offers a scheme for estimating the expected time it takes a crossing cohort to clear the street(Chapter 3);
4. Providing an algorithm that allows approaching cars to adjust their speed dynamically, given several simultaneous crossing locations (Chapter 3);
5. Estimating fuel consumption and CO₂ emissions for driving cycles resulting by adopting ADOPT suggested speed using more realistic parameters (Chapter 3);
6. Providing a scheme for cars to choose the speed that reduces the elevated fuel consumption

- and CO₂ emissions while avoiding colliding with pedestrians (Chapter 3);
7. Applying the energy demand model for fuel consumption estimation, including instantaneous and average speed for user-defined driving cycles;
 8. Comparing the computed fuel consumption with real-world data of several driving cycles and evaluating the accuracy of the energy demand approach (Chapter 4);
 9. Providing a simple approach for cross-disciplinary researchers to implement the model directly, given publicly available data related to car specifications (Chapter 4);
 10. Providing schemes to reduce speed appropriately based on alert messages sent to approaching cars along the street about midblock crossing. The proposed scheme showed a reduction in fuel consumption and CO₂ compared to sudden reaction (Chapter 5).

6.2 LIMITATIONS AND FUTURE WORK

We identified several limitations in our work that can be addressed in future research. Below, we outline potential improvements for various sections of this dissertation:

In Chapter 3, our system currently sends alert messages only backward, where each parked car alerts the car behind it. This constraint should be relaxed to allow messages to be sent forward, warning approaching cars from the opposite direction. Additionally, our pedestrian classification and localization algorithms assume that the car is parked in parallel to the sidewalk. If the car is not parked parallel, the accuracy of these algorithms decreases. Future work should address this issue. Another limitation is the potential for information overload when multiple pedestrians cross near parked cars simultaneously. This can distract human drivers. We plan to design an app to

minimize this information overload and reduce driver distraction. Furthermore, we assumed the sidewalk is modeled by a straight line. However, streets often have curvilinear sidewalks, which can obscure pedestrian traffic. Extending ADOPT to handle these general sidewalk geometries is essential. The social impacts of ADOPT also need evaluation. It is crucial to assess ADOPT's effect on car traffic flow and manage pedestrian and car traffic based on their density. Additionally, we need to study whether ADOPT encourages jaywalking by making pedestrians feel safer.

Another possible extension to ADOPT system involves using parked cars to alert pedestrians about approaching vehicles, potentially protecting midblock crossing pedestrians without disrupting traffic flow. Another research direction involves equipping cars with low-power transceivers to sense RF noise from other cars. This could enable parked cars to report available parking spots in real time to a central system, providing valuable information to drivers.

In Chapter 4, further investigation is needed to explore how car specifications affect the efficiency of converting fuel into tractive energy, ensuring accuracy across different car models.

Lastly, in Chapter 5, additional research is required to understand the impact of distances between crossing areas on fuel consumption and emissions. Additionally, the simulation needs to be expanded to include a wider range of pedestrian speeds and varied environmental variables such as car traffic density.

REFERENCES

- [1] S. Abdelhamid, H. S. Hassanein, and G. Takahara, "Vehicle as a resource (VaaR)," *IEEE Network*, vol. 29, no. 1, pp. 12–17, 2015.
- [2] H. Achour and A. G. Olabi, "Driving cycle developments and their impacts on energy consumption of transportation," *Journal of Cleaner Production*, vol. 112, pp. 1778–1788, 2016. [Online]. Available: <https://doi.org/10.1016/j.jclepro.2015.08.007>.
- [3] K. Ahn, "Microscopic fuel consumption and emission modeling," Ph.D. dissertation, Virginia Tech, 1998.
- [4] A. Alali, S. Olariu, and S. Jain, "ADOPT: a system for alerting drivers to occluded pedestrian traffic," *Vehicular Communications*, vol. 41, p. 100601, 2023, ISSN: 2214-2096. DOI: <https://doi.org/10.1016/j.vehcom.2023.100601>. [Online]. Available: <https://www.sciencedirect.com/science/article/pii/S2214209623000311>.
- [5] M. Aljohani, S. Olariu, A. Alali, and S. Jain, "A survey of parking solutions for smart cities," *IEEE Trans. Intell. Transp. Syst.*, vol. 23, no. 8, pp. 10012–10029, Aug. 2022.
- [6] M. Alsabaan, K. Naik, and T. Khalifa, "Optimization of fuel cost and emissions using V2V communications," *IEEE Trans. Intell. Transp. Syst.*, vol. 14, no. 3, pp. 1449–1461, Sep. 2013. [Online]. Available: <http://dx.doi.org/10.1109/TITS.2013.2262175>.
- [7] Argonne National Lab, *Conventional vehicle testing*, <https://www.anl.gov/taps/conventional-vehicle-testing>, Accessed: December 5, 2023, 2023.

- [8] M. Arif, G. Wang, Z. A. Bhuiyan, T. Wang, and J. Chen, "A survey on security attacks in VANETs: Communication, applications and challenges," *Vehicular Communications*, vol. 19, p. 100 179, Oct. 2019.
- [9] R. Bak and M. Kiec, "Influence of midblock pedestrian crossings on urban street capacity," *Transportation research record*, vol. 2316, no. 1, pp. 76–83, Jan. 2012. [Online]. Available: <https://doi.org/10.3141/2316-09>.
- [10] A. Ben Khalifa, I. Alouani, M. A. Mahjoub, and A. Rivenq, "A novel multi-view pedestrian detection database for collaborative intelligent transportation systems," *Future Gener. Comput. Syst.*, vol. 113, pp. 506–527, Dec. 2020.
- [11] R. D. Brehar, M. P. Muresan, T. Marița, C.-C. Vancea, M. Negru, and S. Nedevschi, "Pedestrian Street-Cross action recognition in monocular far infrared sequences," *IEEE Access*, vol. 9, pp. 74 302–74 324, 2021.
- [12] W. Bronzi, R. Frank, G. Castignani, and T. Engel, "Bluetooth low energy for inter-vehicular communications," in *2014 IEEE Vehicular Networking Conference (VNC)*, Dec. 2014, pp. 215–221.
- [13] M. Chaim and E. Shmerling, "A model for vehicle fuel consumption estimation at urban operating conditions," *International Journal of Mechanics*, vol. 7, pp. 18–23, 2013. [Online]. Available: <https://api.semanticscholar.org/CorpusID:204922990>.
- [14] Z. Chen and X. Huang, "Pedestrian detection for autonomous vehicle using Multi-Spectral cameras," *IEEE Transactions on Intelligent Vehicles*, vol. 4, no. 2, pp. 211–219, Jun. 2019.

- [15] T. Combs, L. Sandt, M. Clamann, and N. McDonald, "Automated vehicles and pedestrian safety: Exploring the promise and limits of pedestrian detection," *American journal of preventive medicine*, vol. 56, no. 1, pp. 1–7, 2019.
- [16] G. De Nicolao, A. Ferrara, and L. Giacomini, "Onboard Sensor-Based collision risk assessment to improve pedestrians' safety," *IEEE Trans. Veh. Technol.*, vol. 56, no. 5, pp. 2405–2413, Sep. 2007.
- [17] K. Dhondge, S. Song, B.-Y. Choi, and H. Park, "WiFiHonk: Smartphone-Based beacon stuffed WiFi Car2X-Communication system for vulnerable road user safety," in *2014 IEEE 79th Vehicular Technology Conference (VTC Spring)*, May 2014, pp. 1–5.
- [18] D. Eckhoff, C. Sommer, R. German, and F. Dressler, "Cooperative awareness at low vehicle densities: How parked cars can help see through buildings," in *2011 IEEE Global Telecommunications Conference - GLOBECOM 2011*, Dec. 2011, pp. 1–6.
- [19] S. El Hamdani, N. Benamar, and M. Younis, "Pedestrian support in intelligent transportation systems: Challenges, solutions and open issues," *Transp. Res. Part C: Emerg. Technol.*, vol. 121, p. 102 856, Dec. 2020.
- [20] A. Forde and J. Daniel, "Pedestrian walking speed at un-signalized midblock crosswalk and its impact on urban street segment performance," *Journal of Traffic and Transportation Engineering (English Edition)*, vol. 8, no. 1, pp. 57–69, Feb. 2021. [Online]. Available: <https://www.sciencedirect.com/science/article/pii/S209575641830415X>.
- [21] J. H. Gawron, G. A. Keoleian, R. D. De Kleine, T. J. Wallington, and H. C. Kim, "Life cycle assessment of connected and automated vehicles: Sensing and computing subsystem and vehicle level effects," in *Environmental science & technology*, vol. 52, no. 5, pp. 3249–

- 3256, Mar. 2018. [Online]. Available: <http://dx.doi.org/10.1021/acs.est.7b04576>.
- [22] S. Gilroy, E. Jones, and M. Glavin, “Overcoming occlusion in the automotive environment—a review,” *IEEE Trans. Intell. Transp. Syst.*, vol. 22, no. 1, pp. 23–35, 2019.
- [23] Governors Highway Safety Association, *Pedestrian traffic fatalities by state: 2023 preliminary data*, Accessed: 2024-06-22, 2024. [Online]. Available: <https://www.ghsa.org/resources/Pedestrians24>.
- [24] O. Grembek, A. Kurzhanskiy, A. Medury, P. Varaiya, and M. Yu, “Making intersections safer with I2V communication,” *Transp. Res. Part C: Emerg. Technol.*, vol. 102, pp. 396–410, May 2019.
- [25] W. M. Griggs, R. Verago, J. Naoum-Sawaya, R. H. Ordóñez-Hurtado, R. Gilmore, and R. N. Shorten, “Localizing missing entities using parked vehicles: An RFID-Based system,” *IEEE Internet of Things Journal*, vol. 5, no. 5, pp. 4018–4030, Oct. 2018. [Online]. Available: <https://doi.org/10.1109/JIOT.2018.2864590>.
- [26] L. Guzzella, A. Sciarretta, *et al.*, *Vehicle propulsion systems*. Springer, 2007, vol. 1.
- [27] Y. He, C. Zhu, and X.-C. Yin, “Occluded pedestrian detection via Distribution-Based Mutual-Supervised feature learning,” *IEEE Trans. Intell. Transp. Syst.*, pp. 1–16, 2021.
- [28] P.-F. Ho and J.-C. Chen, “WiSafe: Wi-Fi pedestrian collision avoidance system,” *IEEE Trans. Veh. Technol.*, vol. 66, no. 6, pp. 4564–4578, Jun. 2017.
- [29] HopeRF, *RFM75 Datasheet*, <https://www.hoperf.com/modules/2.4g/index.html>, Accessed: 2024-05-29.

- [30] Q. Huang, Y. Mei, W. Wang, and Q. Zhang, "Toward Battery-Free wearable devices: The synergy between two feet," *ACM Trans. Cyber-Phys. Syst.*, vol. 2, no. 3, pp. 1–18, Jun. 2018.
- [31] S. Huff, S. Davis, R. Boundy, and R. Gibson, "Auto stop-start fuel consumption benefits," in *SAE Technical Paper*, 2023, p. 0346. DOI: 10.4271/2023-01-0346. [Online]. Available: <https://doi.org/10.4271/2023-01-0346>.
- [32] T. Hunsanon, N. Kronprasert, A. Upayokin, and P. Songchitruksa, "Control strategy for vehicular and pedestrian midblock crossing movements," *Transportation Research Procedia*, vol. 25, pp. 1672–1689, 2017, World Conference on Transport Research - WCTR 2016 Shanghai. 10-15 July 2016, ISSN: 2352-1465. DOI: <https://doi.org/10.1016/j.trpro.2017.05.124>. [Online]. Available: <https://www.sciencedirect.com/science/article/pii/S2352146517304155>.
- [33] M. Islam, M. Rahman, M. Chowdhury, G. Comert, E. D. Sood, and A. Apon, "Vision-Based personal safety messages (PSMs) generation for connected vehicles," *IEEE Trans. Veh. Technol.*, vol. 69, no. 9, pp. 9402–9416, Sep. 2020.
- [34] P. Jokic and M. Magno, "Powering smart wearable systems with flexible solar energy harvesting," in *2017 IEEE International Symposium on Circuits and Systems (ISCAS)*, IEEE, May 2017, pp. 1–4. [Online]. Available: <http://dx.doi.org/10.1109/ISCAS.2017.8050615>.
- [35] R. Jones, "Quantitative effects of acceleration rate on fuel consumption," Environmental Protection Agency, Ann Arbor, MI (USA), Tech. Rep. EPA-AA-SDSB-80-06 Tech Rpt. Apr. 1980. [Online]. Available: <https://trid.trb.org/view/155653>.

- [36] A. Kabil, K. Rabieh, F. Kaleem, and M. A. Azer, "Vehicle to pedestrian systems: Survey, challenges and recent trends," *IEEE Access*, pp. 1–1, 2022. [Online]. Available: <http://dx.doi.org/10.1109/ACCESS.2022.3224772>.
- [37] R. Kabir, S. M. Remias, J. Waddell, and D. Zhu, "Time-series fuel consumption prediction assessing delay impacts on energy using vehicular trajectory," *Transportation Research Part D: Transport and Environment*, vol. 117, p. 103 678, 2023, ISSN: 1361-9209. DOI: <https://doi.org/10.1016/j.trd.2023.103678>. [Online]. Available: <https://www.sciencedirect.com/science/article/pii/S1361920923000755>.
- [38] R. Koppa, *Human factors*, N. R. C. Traffic Flow Theory Transportation Research Board Monograph, Ed., 2003.
- [39] S. K. Kwon, E. Hyun, J.-H. Lee, J. Lee, and S. H. Son, "A Low-Complexity scheme for partially occluded pedestrian detection using LIDAR-RADAR sensor fusion," in *2016 IEEE 22nd International Conference on Embedded and Real-Time Computing Systems and Applications (RTCSA)*, Aug. 2016, pp. 104–104.
- [40] T. Larson, A. Wyman, D. S. Hurwitz, M. Dorado, S. Quayle, and S. Shetler, "Evaluation of dynamic passive pedestrian detection," *Transportation Research Interdisciplinary Perspectives*, vol. 8, p. 100 268, Nov. 2020.
- [41] X. Li and J.-Q. Sun, "Effect of interactions between vehicles and pedestrians on fuel consumption and emissions," *Physica A: Statistical Mechanics and its Applications*, vol. 416, pp. 661–675, Dec. 2014. [Online]. Available: <https://www.sciencedirect.com/science/article/pii/S0378437114007869>.

- [42] X. Li and Y.-J. Wu, "Real-time estimation of pedestrian volume at button-activated mid-block crosswalks using traffic controller event-based data," *Transp. Res. Part C: Emerg. Technol.*, vol. 122, p. 102 876, Jan. 2021.
- [43] N. Liu, M. Liu, W. Lou, G. Chen, and J. Cao, "PVA in VANETs: Stopped cars are not silent," in *2011 Proceedings IEEE INFOCOM*, Apr. 2011, pp. 431–435.
- [44] Y. T. Lo and S. Lee, *Antenna Handbook: theory, applications, and design*. Springer Science & Business Media, 2013.
- [45] S. W. Loke, "Cooperative automated vehicles: A review of opportunities and challenges in socially intelligent vehicles beyond networking," *IEEE Transactions on Intelligent Vehicles*, vol. 4, no. 4, pp. 509–518, Dec. 2019.
- [46] P. A. Lopez, M. Behrisch, L. Bieker-Walz, J. Erdmann, Y.-P. Flötteröd, R. Hilbrich, L. Lücken, J. Rummel, P. Wagner, and E. Wießner, "Microscopic traffic simulation using SUMO," in *The 21st IEEE International Conference on Intelligent Transportation Systems*, 2018, pp. 2575–2582.
- [47] Y. Lu, X. Xu, C. Ding, and G. Lu, "A speed control method at successive signalized intersections under connected vehicles environment," *IEEE Intelligent Transportation Systems Magazine*, vol. 11, no. 3, pp. 117–128, 2019. [Online]. Available: <http://dx.doi.org/10.1109/MITS.2019.2919638>.
- [48] I. Mahdinia, A. J. Khattak, and A. Mohsena Haque, "How effective are pedestrian crash prevention systems in improving pedestrian safety? harnessing large-scale experimental data," *Accid. Anal. Prev.*, vol. 171, p. 106 669, Jun. 2022.

- [49] P. Merdrignac, O. Shagdar, and F. Nashashibi, "Fusion of perception and V2P communication systems for the safety of vulnerable road users," *IEEE Trans. Intell. Transp. Syst.*, vol. 18, no. 7, pp. 1740–1751, Jul. 2017.
- [50] National Highway Traffic Safety Administration, *Countermeasures that work: Pedestrian safety*, Accessed: 2024-06-22, 2023. [Online]. Available: <https://www.nhtsa.gov/book/countermeasures-that-work/pedestrian-safety>.
- [51] H. Ngo, H. Fang, and H. Wang, "Cooperative perception with V2V communication for autonomous vehicles," *IEEE Trans. Veh. Technol.*, pp. 1–10, 2023. [Online]. Available: <http://dx.doi.org/10.1109/TVT.2023.3264020>.
- [52] C. Ning, L. Menglu, Y. Hao, S. Xueping, and L. Yunhong, "Survey of pedestrian detection with occlusion," *Complex & Intelligent Systems*, vol. 7, no. 1, pp. 577–587, Feb. 2021.
- [53] B. Noh and H. Yeo, "A novel method of predictive collision risk area estimation for proactive pedestrian accident prevention system in urban surveillance infrastructure," *Transportation research part C: emerging technologies*, vol. 137, p. 103 570, 2022.
- [54] B. Noh and H. Yeo, "A novel method of predictive collision risk area estimation for proactive pedestrian accident prevention system in urban surveillance infrastructure," *Transportation Research Part C: Emerging Technologies*, vol. 137, p. 103 570, 2022.
- [55] Nordic Semiconductor, *nRF24L01+ Datasheet*, <https://www.nordicsemi.com/Products/Low-power-short-range-wireless/nRF24-series>, Accessed: 2024-05-29.
- [56] S. Olariu, A. Wadaa, L. Wilson, and M. Eltoweissy, "Wireless sensor networks: Leveraging the virtual infrastructure," *IEEE Netw.*, vol. 18, no. 4, pp. 51–56, Jul. 2004.

- [57] S. Olariu and M. C. Weigle, Eds., *Vehicular Networks: From Theory to Practice*. CRC Press/Taylor & Francis, Mar. 2009.
- [58] A. Páez-Montoro, M. García-Valderas, E. Olías-Ruíz, and C. López-Ongil, “Solar energy harvesting to improve capabilities of wearable devices,” en, *Sensors*, vol. 22, no. 10, May 2022. [Online]. Available: <http://dx.doi.org/10.3390/s22103950>.
- [59] A. Palffy, J. F. P. Kooij, and D. M. Gavrilă, “Occlusion aware sensor fusion for early crossing pedestrian detection,” in *2019 IEEE Intelligent Vehicles Symposium (IV)*, Jun. 2019, pp. 1768–1774.
- [60] A. Palffy, J. F. P. Kooij, and D. M. Gavrilă, “Detecting darting out pedestrians with occlusion aware sensor fusion of radar and stereo camera,” *IEEE Transactions on Intelligent Vehicles*, vol. 8, no. 2, pp. 1459–1472, Feb. 2023. [Online]. Available: <http://dx.doi.org/10.1109/TIV.2022.3220435>.
- [61] Y. Pang, J. Xie, M. H. Khan, R. M. Anwer, F. S. Khan, and L. Shao, “Mask-guided attention network for occluded pedestrian detection,” in *Proceedings of the IEEE/CVF international conference on computer vision*, 2019, pp. 4967–4975.
- [62] N. A. Patankar, J. Lin, and T. N. Patankar, “Mileage efficiency of cars,” *Cleaner Engineering and Technology*, vol. 4, p. 100 240, Oct. 2021. [Online]. Available: <https://www.sciencedirect.com/science/article/pii/S2666790821002007>.
- [63] F. Pereira, H. Sampaio, R. Chaves, R. Correia, M. Luís, S. Sargento, M. Jordão, L. Almeida, C. Senna, A. S. R. Oliveira, *et al.*, “When backscatter communication meets vehicular networks: Boosting crosswalk awareness,” *IEEE Access*, vol. 8, pp. 34 507–34 521, 2020.

- [64] J. R. Pérez Cruz, N. Lakouari, J. C. Pérez Sansalvador, and J. L. Zapotecatl López, “Effect of interactions between vehicles and mid-block crosswalks on traffic flow and CO₂ emission,” *Applied Sciences*, vol. 11, no. 24, 2021, ISSN: 2076-3417. [Online]. Available: <https://www.mdpi.com/2076-3417/11/24/11794>.
- [65] H. Perugu, “Emission modelling of light-duty vehicles in india using the revamped VSP-based MOVES model: The case study of hyderabad,” *Transportation Research Part D: Transport and Environment*, vol. 68, pp. 150–163, Mar. 2019. [Online]. Available: <https://www.sciencedirect.com/science/article/pii/S1361920917301104>.
- [66] P. K. D. Pramanik, N. Sinhababu, B. Mukherjee, S. Padmanaban, A. Maity, B. K. Upadhyaya, J. B. Holm-Nielsen, and P. Choudhury, “Power consumption analysis, measurement, management, and issues: A State-of-the-Art review of smartphone battery and energy usage,” *IEEE Access*, vol. 7, pp. 182 113–182 172, 2019. [Online]. Available: <http://dx.doi.org/10.1109/ACCESS.2019.2958684>.
- [67] H. A. Rakha, K. Ahn, K. Moran, B. Saerens, and E. V. den Bulck, “Virginia Tech comprehensive power-based fuel consumption model: Model development and testing,” *Transportation Research Part D: Transport and Environment*, vol. 16, no. 7, pp. 492–503, 2011, ISSN: 1361-9209. DOI: <https://doi.org/10.1016/j.trd.2011.05.008>. [Online]. Available: <https://www.sciencedirect.com/science/article/pii/S1361920911000782>.
- [68] D. B. Rawat, B. B. Bista, G. Yan, and S. Olariu, “Vehicle-to-Vehicle connectivity and communication framework for vehicular Ad-Hoc networks,” in *2014 8-th International Conference on Complex, Intelligent and Software Intensive Systems*, Jul. 2014, pp. 44–49.

- [69] D. Sam, C. Velanganni, and T. E. Evangelin, "A vehicle control system using a time synchronized hybrid vanet to reduce road accidents caused by human error," *Vehicular Communications*, vol. 6, pp. 17–28, 2016.
- [70] A. Sarker, C. Qiu, and H. Shen, "Connectivity maintenance for Next-Generation decentralized vehicle platoon networks," *IEEE/ACM Trans. Netw.*, vol. 28, no. 4, pp. 1449–1462, Aug. 2020.
- [71] S. Seneviratne, Y. Hu, T. Nguyen, G. Lan, S. Khalifa, K. Thilakarathna, M. Hassan, and A. Seneviratne, "A survey of wearable devices and challenges," *IEEE Communications Surveys Tutorials*, vol. 19, no. 4, pp. 2573–2620, 2017.
- [72] P. Sewalkar and J. Seitz, "Vehicle-to-Pedestrian communication for vulnerable road users: Survey, design considerations, and challenges," *Sensors*, vol. 19, no. 2, Jan. 2019.
- [73] M. S. Shahriar, A. K. Kale, and K. Chang, "Cooperative pedestrian safety framework using 5G-NR V2P communications," in *2023 Fourteenth International Conference on Ubiquitous and Future Networks (ICUFN)*, ieeexplore.ieee.org, Jul. 2023, pp. 8–11. [Online]. Available: <http://dx.doi.org/10.1109/ICUFN57995.2023.10199945>.
- [74] S. Shaw, Y. Hou, W. Zhong, Q. Sun, T. Guan, and L. Su, "Instantaneous fuel consumption estimation using smartphones," in *2019 IEEE 90th Vehicular Technology Conference (VTC2019-Fall)*, IEEE, 2019, pp. 1–6. DOI: 10.1109/VTCFall.2019.8891261.
- [75] I. El-Shawarby, K. Ahn, and H. Rakha, "Comparative field evaluation of vehicle cruise speed and acceleration level impacts on hot stabilized emissions," *Transportation Research Part D: Transport and Environment*, vol. 10, no. 1, pp. 13–30, Jan. 2005. [Online]. Available: <https://www.sciencedirect.com/science/article/pii/S1361920904000604>.

- [76] C. Sommer, D. Eckhoff, and F. Dressler, "IVC in cities: Signal attenuation by buildings and how parked cars can improve the situation," *IEEE Trans. Mob. Comput.*, vol. 13, no. 8, pp. 1733–1745, Aug. 2014.
- [77] I. Soto, M. Calderon, O. Amador, and M. Urueña, "A survey on road safety and traffic efficiency vehicular applications based on C-V2X technologies," *Vehicular Communications*, vol. 33, p. 100428, Jan. 2022. [Online]. Available: <https://www.sciencedirect.com/science/article/pii/S2214209621000978>.
- [78] Standard, ISO, "Road vehicles—Controller Area Network (CAN) – part 1: Data link layer and physical signalling," *ISO*, vol. 11898, p. 1, 2003.
- [79] T. Stoyanova, F. Kerasiotis, K. Efstathiou, and G. Papadopoulos, "Modeling of the RSS uncertainty for RSS-Based outdoor localization and tracking applications in wireless sensor networks," in *2010 Fourth International Conference on Sensor Technologies and Applications*, ieeexplore.ieee.org, Jul. 2010, pp. 45–50.
- [80] T. Stoyanova, F. Kerasiotis, and G. Papadopoulos, "RSS-based outdoor localization with wireless sensor networks in practice," in *Technological Breakthroughs in Modern Wireless Sensor Applications*, IGI Global, 2015, pp. 225–256.
- [81] P. Sun and A. Boukerche, "A novel Internet-of-Vehicles assisted collaborative low-visible pedestrian detection approach," in *GLOBECOM 2020 - 2020 IEEE Global Communications Conference*, Dec. 2020, pp. 1–6.
- [82] P. Sun and A. Boukerche, "Challenges and potential solutions for designing a practical pedestrian detection framework for supporting autonomous driving," in *Proc. 18th ACM*

- Symposium on Mobility Management and Wireless Access (MobiWac'20)*, Alicante, Spain, Nov. 2020, pp. 75–82.
- [83] A. Tahmasbi-Sarvestani, H. Nourkhiz Mahjoub, Y. P. Fallah, E. Moradi-Pari, and O. Abuchaar, “Implementation and evaluation of a cooperative vehicle-to-pedestrian safety application,” *IEEE Intelligent Transportation Systems Magazine*, vol. 9, no. 4, pp. 62–75, 2017.
- [84] S. El-Tawab, A. Alhafdhi, D. Treeumnuk, D. C. Popescu, and S. Olariu, “Physical layer aspects of information exchange in the NOTICE architecture,” *IEEE Intelligent Transportation Systems Magazine*, vol. 7, no. 1, pp. 8–18, 2015.
- [85] Texas Instruments, *Launchxl-f280039c*, Accessed: 2024-05-31, 2024. [Online]. Available: <https://www.ti.com/tool/LAUNCHXL-F280039C>.
- [86] Texas Instruments, *CC2500 Datasheet*, <https://www.ti.com/product/CC2500>, Accessed: 2024-05-29.
- [87] H. O. Tezcan, M. Elmorssy, and G. Aksoy, “Pedestrian crossing behavior at midblock crosswalks,” *J. Safety Res.*, vol. 71, pp. 49–57, Dec. 2019.
- [88] J. Thomas, “Drive cycle powertrain efficiencies and trends derived from EPA vehicle dynamometer results,” *SAE International Journal of Passenger Cars-Mechanical Systems*, vol. 7, no. 2014-01-2562, pp. 1374–1384, 2014. DOI: <https://doi.org/10.4271/2014-01-2562>.
- [89] O. K. Tonguz and W. Viriyasitavat, “Cars as roadside units: A self-organizing network solution,” *IEEE Communications Magazine*, vol. 51, no. 12, pp. 112–120, 2013.

- [90] United States Department of Energy and United States Environmental Protection Agency, *EPA Test Car List Definitions*, <https://www.epa.gov/sites/default/files/2016-07/documents/test-car-list-definitions.pdf>, Accessed: May 7, 2024, United States Environmental Protection Agency, 2016.
- [91] United States Department of Energy and United States Environmental Protection Agency, *Data for cars used in testing fuel economy*, <https://www.epa.gov/compliance-and-fuel-economy-data/data-cars-used-testing-fuel-economy>, Accessed: November 7, 2023, 2023.
- [92] United States Department of Energy and United States Environmental Protection Agency, *Dynamometer Drive Schedules*, <https://www.epa.gov/vehicle-and-fuel-emissions-testing/dynamometer-drive-schedules>, Accessed: November 7, 2023, 2023.
- [93] United States Department of Energy and United States Environmental Protection Agency, *Where the Energy Goes: Gasoline Vehicles*, Accessed 2024, United States Department of Energy and United States Environmental Protection Agency. [Online]. Available: <https://www.fueleconomy.gov/feg/atv.shtml> (visited on 02/18/2024).
- [94] United States Environmental Protection Agency, *MOVES2004 energy and emission inputs*, Office of Transportation and Air Quality, Washington, D.C., 2005. [Online]. Available: <https://nepis.epa.gov/Exe/ZyPURL.cgi?Dockkey=P1001DAQ.txt>.
- [95] United States Environmental Protection Agency, *Carbon pollution from transportation*, Accessed: 2024-06-20, 2024. [Online]. Available: <https://www.epa.gov/transportation-air-pollution-and-climate-change/carbon-pollution-transportation#:~:>

text=%E2%80%8BGreenhouse%20gas%20(GHG)%20emissions , contributor%20of%
20U.S.%20GHG%20emissions.

- [96] United States Environmental Protection Agency, *MOtor Vehicle Emission Simulator (MOVES)*, United States Environmental Protection Agency, Accessed 2024. [Online]. Available: <https://www.epa.gov/moves> (visited on 02/18/2024).
- [97] United States Government. “GPS accuracy - GPS.gov.” (Accessed: 2023-08-15), [Online]. Available: <https://www.gps.gov/systems/gps/performance/accuracy/>.
- [98] N. Wan, A. Vahidi, and A. Luckow, “Optimal speed advisory for connected vehicles in arterial roads and the impact on mixed traffic,” *Transportation Research Part C: Emerging Technologies*, vol. 69, pp. 548–563, Aug. 2016. [Online]. Available: <https://www.sciencedirect.com/science/article/pii/S0968090X16000292>.
- [99] D. Wang, W. Fu, Q. Song, and J. Zhou, “Potential risk assessment for safe driving of autonomous vehicles under occluded vision,” *en, Sci. Rep.*, vol. 12, no. 1, p. 4981, Mar. 2022. [Online]. Available: <http://dx.doi.org/10.1038/s41598-022-08810-z>.
- [100] H. Wang, L. Fu, Y. Zhou, and H. Li, “Modelling of the fuel consumption for passenger cars regarding driving characteristics,” *Transp. Res. Part D: Trans. Environ.*, vol. 13, no. 7, pp. 479–482, Oct. 2008. [Online]. Available: <https://www.sciencedirect.com/science/article/pii/S1361920908001041>.
- [101] M. I.-C. Wang, C. H.-P. Wen, and H. J. Chao, “Roadrunner+: An autonomous intersection management cooperating with connected autonomous vehicles and pedestrians with spillback considered,” *ACM Trans. Cyber-Phys. Syst.*, vol. 6, no. 1, pp. 1–29, Nov. 2021. [Online]. Available: <https://doi.org/10.1145/3488246>.

- [102] P. Wang, M. Zhou, and Z. Ding, "A VRU collision warning system with Kalman-Filter-Based positioning accuracy improvement," in *2021 IEEE International Conference on Information Communication and Software Engineering (ICICSE)*, Mar. 2021, pp. 191–198.
- [103] J. Weng, Q. Liang, G. Qiao, Z. Chen, and J. Rong, "Taxi fuel consumption and emissions estimation model based on the reconstruction of driving trajectory," *Advances in Mechanical Engineering*, vol. 9, no. 7, p. 1 687 814 017 708 708, Jul. 2017. [Online]. Available: <https://doi.org/10.1177/1687814017708708>.
- [104] T. Yoshizawa, D. Singelée, J. T. Muehlberg, S. Delbruel, A. Taherkordi, D. Hughes, and B. Preneel, "A survey of security and privacy issues in V2X communication systems," *ACM Comput. Surv.*, vol. 55, no. 9, pp. 1–36, Jan. 2023. [Online]. Available: <https://doi.org/10.1145/3558052>.
- [105] B.-Y. Yu, Z.-H. Wang, L. Ju, C. Zhang, Z.-G. Liu, L. Tao, and W.-B. Lu, "Flexible and wearable hybrid RF and solar energy harvesting system," *IEEE transactions on antennas and propagation*, vol. 70, no. 3, pp. 2223–2233, Mar. 2022. [Online]. Available: <http://dx.doi.org/10.1109/TAP.2021.3118814>.
- [106] L. Yue, M. Abdel-Aty, Y. Wu, O. Zheng, and J. Yuan, "In-depth approach for identifying crash causation patterns and its implications for pedestrian crash prevention," *J. Safety Res.*, vol. 73, pp. 119–132, 2020.
- [107] A. Zanella, "Best practice in RSS measurements and ranging," *IEEE Communications Surveys Tutorials*, vol. 18, no. 4, pp. 2662–2686, 2016.

- [108] C. Zhang, B. Zhou, G. Chen, and F. Chen, "Quantitative analysis of pedestrian safety at uncontrolled multi-lane mid-block crosswalks in China," *Accid. Anal. Prev.*, vol. 108, pp. 19–26, Nov. 2017.
- [109] M. Zhang, A. Brunoud, A. Lombard, Y. Mualla, A. Abbas-Turki, and A. Koukam, "Cooperative behaviors of connected autonomous vehicles and pedestrians to provide safe and efficient traffic in industrial sites," in *2022 IEEE International Conference on Systems, Man, and Cybernetics (SMC)*, Prague, Czech Republic: IEEE, Oct. 2022, pp. 2802–2807. [Online]. Available: <https://ieeexplore.ieee.org/abstract/document/9945188/>.
- [110] R. Zhang, L. Song, A. Jaiprakash, T. Talty, A. Alanazi, A. Alghafis, A. A. Biyabani, and Ozan Tonguz, "Using Ultra-Wideband technology in vehicles for infrastructure-free localization," in *2019 IEEE 5th World Forum on Internet of Things (WF-IoT)*, Apr. 2019, pp. 122–127.
- [111] S. Zhang, R. Benenson, M. Omran, J. Hosang, and B. Schiele, "How far are we from solving pedestrian detection?" In *Proceedings of the IEEE conference on computer vision and pattern recognition*, 2016, pp. 1259–1267.
- [112] S. Zhang, J. Yang, and B. Schiele, "Occluded pedestrian detection through guided attention in CNNs," in *Proceedings of the IEEE conference on Computer Vision and Pattern Recognition*, 2018, pp. 6995–7003.
- [113] S. Zhang, M. Abdel-Aty, Y. Wu, and O. Zheng, "Pedestrian crossing intention prediction at Red-Light using pose estimation," *IEEE Trans. Intell. Transp. Syst.*, pp. 1–9, 2021.
- [114] J. Zhao and Z. You, "A shoe-embedded piezoelectric energy harvester for wearable sensors," *Sensors*, vol. 14, no. 7, pp. 12 497–12 510, Jul. 2014.

- [115] J. Zhao, H. Xu, H. Liu, J. Wu, Y. Zheng, and D. Wu, "Detection and tracking of pedestrians and vehicles using roadside LiDAR sensors," *Transp. Res. Part C: Emerg. Technol.*, vol. 100, pp. 68–87, Mar. 2019.
- [116] C. Zhou, M. Yang, and J. Yuan, "Discriminative feature transformation for occluded pedestrian detection," in *Proceedings of the IEEE/CVF International Conference on Computer Vision*, 2019, pp. 9557–9566.
- [117] M. Zhou, H. Jin, and W. Wang, "A review of vehicle fuel consumption models to evaluate eco-driving and eco-routing," *Transp. Res. Part D: Trans. Environ.*, vol. 49, pp. 203–218, Dec. 2016. [Online]. Available: <https://www.sciencedirect.com/science/article/pii/S1361920916306009>.
- [118] Y. Zou, L. Bo, and Z. Li, "Recent progress in human body energy harvesting for smart bioelectronic system," *Fundamental Research*, vol. 1, no. 3, pp. 364–382, May 2021. [Online]. Available: <https://www.sciencedirect.com/science/article/pii/S2667325821000698>.

APPENDIX A

TIME-SPACE DIAGRAM OF A CROSSING COHORT

Let us turn our attention to the time-space diagram corresponding to a crossing cohort. Referring to Figure 44, imagine a crossing cohort at location L that starts crossing the street at time s_1 and clears the street by time e_1 . Since the “space” coordinate of the cohort does not change, the corresponding time-space diagram is captured by a horizontal line segment with endpoints (s_1, L) and (e_1, L) .

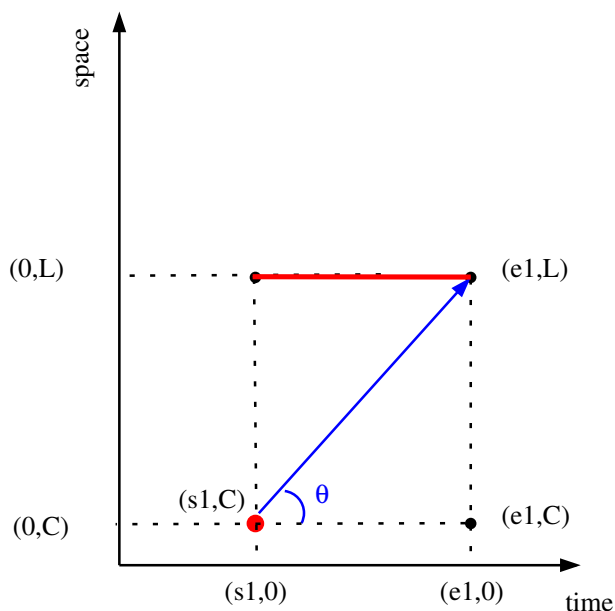


Figure 44. Illustrating the time-space diagram of a crossing pedestrian.

Now, consider an approaching car and assume that the coordinates of the car when it receives

the “Caution – pedestrian in the street” message are $(s1, C)$. What is the largest average speed that the approaching car should adopt to avoid crashing into the cohort? The answer is simple: the car should not reach the point $(0, L)$ while the crossing is in progress, namely in the time interval $[s1, e1)$. However, the car may reach $(0, L)$ at time $e1$, as by that time the cohort has finished crossing safely. Thus, using (1), the car should adopt the following *safe average speed*:

$$v_{safe} = \min \left\{ v_{max}, \frac{L - C}{e1 - s1} \right\} \quad (41)$$

where v_{max} is the speed limit on the road considered. Assuming that $\frac{L - C}{e1 - s1} \leq v_{max}$, this safe speed is visualized in Figure 44 as the slope of the blue segment connecting the points $(s1, C)$ and $(e1, L)$.

APPENDIX B

EPA TEST CAR DATA

Specific fields from EPA test car data were used in this work [91]. For additional clarification, Table 17 has a list of these fields and their usage in this work. It should be noted here that, to the best of our knowledge, there is only one file that contains the metadata for test car files [90]. Moreover, this file does not contain metadata for all the fields, so interpretation with a personal effort was performed to map the fields to the required data.

Table 17. List of used fields from EPA test car aggregated data and their usage.

Description	EPA Test Car Data		Usage in this work	
	Field Name	Unit	Parameter Name	Unit
Rolling Resistance Drag Force	TargetCoefAlbf	<i>lbf</i>	f_0	Newton [<i>nt</i>]
Aerodynamic Drag Force	TargetCoefClbfmph2	<i>lbf/mph²</i>	f_2	<i>nt/mps²</i>
Car Mass	EquivalentTestWeightlbs	<i>lbs</i>	<i>mass</i>	killograms [<i>kg</i>]
Fuel Economy	RND_ADJ_FE	miles per gallon [<i>mpg</i>]	<i>FE</i>	<i>mpg</i>
CO ₂ Emission	CO2gmi	gram per mile [<i>g/mile</i>]	$CO_{2Measured}$	<i>g/mile</i>

VITA

Abrar Abdulrahman Alali

Department of Computer Science

Old Dominion University

Norfolk, VA 23529

EDUCATION

2011-2013, Master of Science in Computer Science, California Lutheran University.

2001-2006, Bachelor of Science in Computer Science, Taibah University, Saudi Arabia.

PROFESSIONAL EXPERIENCE

2014-Present, Saudi Electronic University, Saudi Arabia.

PUBLICATIONS

1. Alali, A., Olariu, S. and Jain, S., ADOPT: A system for Alerting Drivers to Occluded Pedestrian Traffic. *Vehicular Communications*, 41, p.100601, 2023.
2. Aljohani, M., Olariu, S., Alali, A. and Jain, S., A survey of parking solutions for smart cities. *IEEE Transactions on Intelligent Transportation Systems*, 23(8), pp.10012-10029, 2021.

A complete list is available at: [scholar.google.com/citations?user = AqeiPcAAAAJ&hl = en](https://scholar.google.com/citations?user=AqeiPcAAAAJ&hl=en).